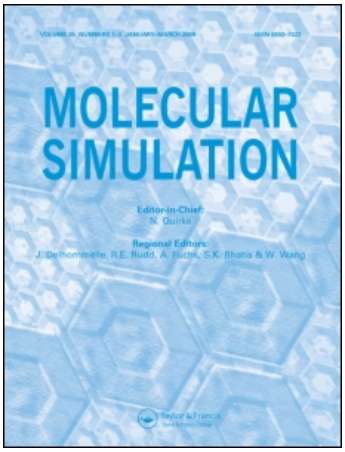

Molecular Simulation
Publication details, including instructions for authors and subscription information:
http://www.informaworld.com/smpp/title~content=t713644482

DL_POLY: Application to molecular simulation

W. Smith[a]; C. W. Yong[a]; P. M. Rodger[b]
[a] Computation Science and Engineering Department, C.L.R.C. Daresbury Laboratory, Daresbury, Warrington, UK [b] Department of Chemistry, University of Warwick, Coventry, UK

Online publication date: 26 October 2010

To cite this Article Smith, W. , Yong, C. W. and Rodger, P. M.(2002) 'DL_POLY: Application to molecular simulation', Molecular Simulation, 28: 5, 385 — 471
To link to this Article: DOI: 10.1080/08927020290018769
URL: http://dx.doi.org/10.1080/08927020290018769

Molecular Simulation, 2002 VOL. 28 (5), pp. 385–471

DL_POLY: APPLICATION TO MOLECULAR SIMULATION*

W. SMITH[a], C.W. YONG[a] and P.M. RODGER[b]

[a]*Computation Science and Engineering Department, C.L.R.C. Daresbury Laboratory, Daresbury, Warrington WA4 4AD, UK;* [b]*Department of Chemistry, University of Warwick, Coventry, UK*

DL_POLY is a general-purpose molecular dynamics simulation package, which was developed by Daresbury Laboratory in the mid-1990s for the molecular simulation community in the United Kingdom. The package now has a world-wide user base and applications in many areas of molecular simulation. In this article we briefly review the history and design of the package and highlight some recent applications in the areas of; liquids and solutions; spectroscopy; ionic solids; molecular crystals; polymers; glasses; membranes; proteins; solid and liquid interfaces; catalysis; liquid crystals; intercalation and clathrates; and novel systems. The strengths and weaknesses of the code and its future in the near term are also discussed.

Keywords: DL_POLY; Molecular dynamics; Partial radial distribution function; Nuclear magnetic resonance; Crystal structure; Diffusion; Catalysis; Spectroscopy; Interfaces; Liquids; Solutions; Polymers; Membranes; Proteins

INTRODUCTION

Background

DL_POLY was originally developed to meet the needs of the United Kingdom's *Collaborative Computational Project No*. 5 (CCP5) which, after 20 years existence, still represents the UK molecular simulation community [1]. The demand was for a general purpose package, which would exploit the parallel computers emerging in the 1990s and expand the application of molecular

*Invited article

ISSN 0892-7022 © 2002 Taylor & Francis Ltd
DOI: 10.1080/08927020290018769

simulation into areas of study, such as macromolecules, which were regarded as scientifically challenging. With funding from the UK's Science and Engineering Research Council, the package was developed at Daresbury Laboratory by W. Smith and T.R. Forester. The initial target machine was an Intel iPSC/860 with 64 processors, but the code was quickly adapted for other emerging platforms, such as the Cray T3D and T3E and IBM SP/2, where sometimes several hundred processors were available. From its initial release in 1994, over 640 licences have been taken out world-wide, so the code is clearly making an impact. The current version of the code, at the time of writing, is DL_POLY_2.13.

Design, Functionality and Performance

The DL_POLY code is broadly based on the *Replicated Data* (RD) parallelisation strategy [3–5] for distributed memory parallel computers. In this strategy, the simulated system is replicated on each processor, with equal sharing of the computational tasks between them. This offers a number of important advantages in a parallel molecular dynamics (MD) implementation. The most important of which is the relative ease with which complex molecular force-fields and structures may be incorporated. Familiar requirements such as the Verlet neighbour list [2,3] and the Ewald sum [2,5] may be easily and efficiently adapted. Another important advantage is that RD "collapses" trivially easily to run on a single processor, which means users may familiarise themselves with the software on local workstations before progressing seamlessly to more complex parallel architectures.

On the down side however, the high communication overhead associated with the RD strategy implies poor performance scaling with large numbers of processors [8]. Fortunately, this is offset by the trend towards larger simulated systems (in excess of 10,000 atoms), which improves the algorithmic efficiency, and advances in communication hardware, which has greatly increased communication speeds and reduced latency. Both of these have extended the working range of DL_POLY considerably. However, one important requirement—the SHAKE algorithm [9] for rigid bonds, is both difficult to implement with RD and performance limiting on large parallel computers, though it is reasonably efficient if relatively few processors are used [4,10]. The performance of DL_POLY on various parallel platforms is shown on the DL_POLY website [7] and it is clear from the examples shown that a high price can be paid if rigid bonds are an essential requirement. Guest has benchmarked the code on a wide variety of single processor workstations [12], and offers a clear guide to the best machines for DL_POLY execution.

A full description of the functional capabilities of DL_POLY is given in the DL_POLY User Manual, which may be viewed at (or obtained from) the DL_POLY website [7]. A useful short summary of an earlier release is given in Ref. [11]. Acceptable molecular models range from "free" atoms or ions, through flexible molecules (with or without constraint bonds), to semi-rigid and rigid molecules. Intramolecular forces include extensible bonds, valence angles, dihedral and improper dihedral terms, and inversion potentials. Many analytical forms are available for each. Likewise a broad range of non-bonded interatomic potentials is available. Electrostatic interactions may be handled by Ewald sum, Smooth Particle Mesh Ewald [13], Hautman-Klein-Ewald (for two-dimensional periodic systems) [14], Reaction Field [15] or assorted direct summation methods. The dynamical simulations may be performed in NVE (microcanonical), NVT (canonical) or NPT (isothermal–isobaric) ensembles, which, combined with the permitted varieties of molecular structure, give rise to over 30 different integration routines.

DL_POLY is highly portable. Written almost exclusively in FORTRAN (mostly F77 with some F90 features) it may be compiled on any UNIX platform. Multiprocessor implementations, whether on Symmetric Multiprocessor Platforms (SMPs), homogeneous distributed memory machines or PC clusters (so-called Beowulf systems) require the MPI (Message Passing Interface) library. At heart DL_POLY is a *distributed memory* application, so its performance on SMP systems should not be expected to be optimal. In addition, the relatively poor communication performance of many Beowulf systems does not provide for the best scaling behaviour at this time. On Cray T3E and SGI machines memory–memory message passing (SHMEM) facilities may be used, and are highly efficient.

An important benefit for users of DL_POLY is that the software is supplied as *source code*, which means it is directly amenable to user modification and verification. This has proved to be very advantageous to all parties. Many users of the code have made their own modifications to add extra functionality beyond the already extensive facilities. The software bugs that are inevitable in any large code have, on occasion, been identified by users and communicated to the software developers, to the considerable benefit of all. This openness is undoubtedly a great strength for any software package.

Availability

DL_POLY is available world-wide and free of charge to university based researchers. A licence may be downloaded from the DL_POLY website [7]. The

source code is transferred by FTP on receipt of the signed licence. (Interested commercial organisations should contact w.smith@dl.ac.uk.)

APPLICATIONS

Given that the potential range of DL_POLY applications is extremely broad, a comprehensive review of all areas is not practical, so the examples highlighted here are by no means exhaustive. However they do serve to show the versatility and power of DL_POLY when complemented by the ingenuity of its users, many of whom have been creative enough to apply or even extended the code in ways not anticipated by the initial authors.

Liquids and Solutions

DL_POLY enables the study of liquids of considerable complexity. Of interest is the structure of pure liquids and solutions of various kinds, mostly in water. The structure is most often described via Radial Distribution Functions (RDFs) or Angular Distribution Functions (ADFs) and frequently ties in with experimental investigations, particularly with Neutron Scattering (NS) experiments. Associated with these are thermodynamic issues, for which free energy and entropy are the main properties of interest. Also of interest are time dependent properties, of which diffusion (exemplified by the Mean Square Displacement (MSD) or Velocity Autocorrelation Function (VAF)) is the prime example. In solutions (including non-aqueous solutions) there is much interest in describing hydrogen bonding, and the issues of hydrophobicity and hydrophilicity and their influence on solvent structure are strong themes.

Also amenable to investigation by MD are some aspects of spectroscopy. Many spectroscopic experiments are concerned with species in solution and the influence of the solvent on the spectroscopic transition is manifest in the spectrum. MD thus provides a means to explore these effects and to learn more about the dynamical processes that underly them.

Structure and Dynamics

From its earliest origins MD has been used to augment experimental studies of liquids. A good example of this is in the interpretation of NS experiments. This approach is exemplified by Benmore and Loh's study of ethanol [16]. Isotopic substitution (deuterium for hydrogen) in the ethanol permitted the experimental

extraction of 10 partial radial distribution functions (PRDFs), with which the results of the simulation, based on the Jorgensen OPLS potential model [17], compared well. The results confirmed the presence of hydrogen bonding in the liquid, consistent with winding chain conformations.

A similar study was performed on methanol by Bianchi *et al.* [18]. A series of six simulations of liquid methanol, with different potentials and structural models for the molecule, were performed and compared with NS experiments employing H-D isotopic substitution. In all cases the system energy and total radial distribution were adequately reproduced, though diffusion was only correctly obtained in the model with explict (though non-interacting) methyl hydrogens. This result was ascribed to the more realistic molecular moment of inertia. PRDFs were consistent across the models but quantitative agreement with experiment was poor. The conclusion drawn was that these widely used models required more refinement to produce an accurate description.

The structure of dilute aqueous *n*-alcohol solutions (from methanol to butanol) was investigated by Fidler and Rodger [20] using the OPLS and TIP4P [19] potential models for the organic species and water, respectively. Interest focused on the structure of the water in the presence of hydrophilic (hydroxyl) and hydrophobic (alkane) groups, and the relative importance of these groups in determining the overall structure. Within a predefined "solvation sphere" three- and four-body order parameters were calculated, together with PRDFs, to quantify the water structure. Dynamical properties were determined from the sphere residence time, VAF, and Legendre orientational correlation (LOC) functions. The structural study revealed the alkane groups had no effect on the water structure (no clathrate formation), but the hydroxyl groups promoted a lowering of water–water coordination numbers nearby. The residence time for water near the hydroxyl (1.25 ps) was of order three times that near the alkyl groups. Differences in the water VAF functions for the different alcohols were interpreted as an inertial effect. The LOC functions were consistent with the presence of tetrahedral H-bonded water clusters, which could dissociate.

Hydrogen bonding in aqueous carbohydrate solutions has been studied by Astley *et al.* [21]. At issue was how to quantify the lifetime of a hydrogen bond (H-bond) in dynamical simulations where geometric criteria are to some degree arbitrary. The model system was a single α-D-glucose molecule in 248 water molecules, with the SPC water model [22] and a specifically developed carbohydrate model. The idealised model for the H-bond was defined as a (neutral) COH fragment paired with a water molecule, using the minimum of the three available O–H distances to distinguish between the donor and acceptor. Study of the COH–H_2O dimer energy distributions showed that the COH is a stronger donor than an acceptor, a result consistent with quantum chemistry

calculations. In a more detailed study of several geometric H-bond criteria (O–O distance and O–H–O bond angles) plus the donor–acceptor dimer energy (five parameters in all, as functions of time), revealed the difficulty in establishing a definition of the H-bond consistent across the criteria. To handle this difficulty a three-level energetic model was constructed. Firstly, a 25 ps rolling average the dimer energy was obtained. Analysis of the frequency histogram for the lowest dimer interaction energies permitted upper ($E_{\text{off}} = -0.7\,\text{kcal mol}^{-1}$) and lower ($E_{\text{on}} = -2.4\,\text{kcal mol}^{-1}$) energy criteria to be established, such that the H-bond was deemed to start when the dimer energy (E_{D}) was less than E_{on} and ended when E_{D} exceeded E_{off}. If E_{D} dropped below a third energy criterion ($-4.75\,\text{kcal mol}^{-1}$) the COH group was deemed to be the donor, and the acceptor otherwise. The authors subsequently showed that this model was fully consistent with the observed data and chemical intuition for H-bond occurrence.

Carver *et al.* [23] performed simulations of *N*-methylpyrrolidone (MeP) in dilute aqueous solution, to shed light on the molecular mechanisms underlying the antifreeze activity of pyrrolidone-ring containing polymers, such as polyvinylpyrrolidone (PVP). The MeP molecule has hydrophilic and hydrophobic regions and strongly influences the structure of liquid water in its vicinity. The series of simulations, which used CHARMM potentials [24] and SPC water, investigated both structural and dynamical effects. The PRDFs showed strong hydrogen bonding with the (hydrophilic) MeP oxygen, and a "partial clathrate cage" of water molecules around the hydrophobic methyl group. ADFs indicated the H-bonds point away from the methyl and form the H-bond network of the observed "cage". Angularly resolved PRDFs revealed up to four solvation shells of water around the MeP oxygen as well as the influence of the methyl group on the structure of the first solvation shell. The methyl group had up to three solvation shells and the structure was also influenced by the solute shape. H-bond network analysis indicated less structure overall in water in the presence of MeP. MSD calculations of bulk and MeP-solvated water molecules obtained lower diffusivity for solvated water. The mutual VAF of MeP and solvated water was strongly oscillatory, resulting from the strong hydrogen bonding between the water and MeP oxygen. Orientational time correlation functions revealed, as expected, that water rotation is slower in the MeP solvation shell and dipolar relaxation is strongly affected by the proximity of MeP oxygen. The power spectrum of the MeP VAFs had three strong peaks between 40–80 cm^{-1} which were thought to arise from the strong cage effects observed in this system.

A study of solvation ranging from the hydrophobic to hydrophilic regimes has been conducted by Lynden-Bell *et al.* [25] for a system composed of SPC/E water [26] and a Lennard–Jones (L–J) solute. Using extended system dynamics,

fictitious masses were assigned to the solute charge and diameter. The resulting system was equivalent to a real system with fixed mean charge and diameter. Free energy was obtained as a function of these variables from the associated distribution functions. A biasing potential was used to dampen statistical noise (i.e. restrict the parameters to within defined windows). The solvation free energy as a function of solute charge had a single maximum near zero charge (Fig. 1, top), where the solute was hydrophobic. However it was not symmetric, and peaked at a small positive charge. The molecular nature of water (as opposed to a continuum) was presented as the cause. The charge asymmetry was also apparent in the free energy variation with solute diameter (Fig. 1, bottom); a negative charge was more strongly stabilised than a positive charge of equal magnitude.

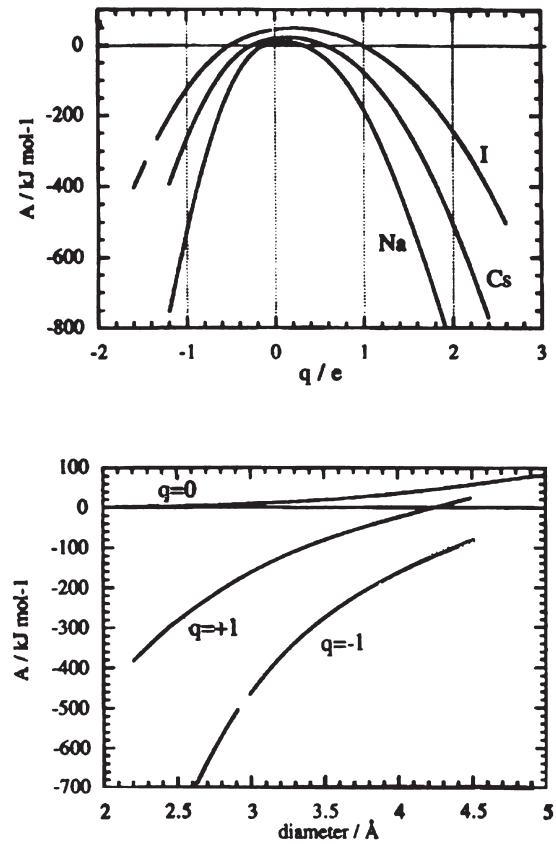

FIGURE 1 Ionic solvation free energies. Ionic solvation free energy as a function of ion charge (top) and size (bottom) obtained by extended system molecular dynamics. Free energy is maximum when the charge is slightly positive, and increases with ion diameter irrespective of charge. Fig. reprinted from Ref. [25] with the permission of the authors and the Journal of Chemical Physics.

Solvation free energy for neutral solutes increased slowly with solute diameter, indicating increased solvent order. Solvation entropy, as a function of charge, had a double maximum, with a minimum at small positive charge. The minimum corresponded to hydrophobic ordering. Increasing the charge magnitude disrupted the water H-bond network (structure breaking), with an increase in entropy, until at large positive or negative charges, entropy once again decreased due to ordering of the solvation shells. The solvation entropy as a function of solute diameter had a distinct maximum for both positive and negative ions, though again there was asymmetry with charge sign. The maximum signals a change from hydrophilic to hydrophobic ordering. For neutral solutes, entropy decreased with increasing solute diameter, as expected. Calculated solute-oxygen PRDFs showed that diminishing entropy of solvation was indicated by the weakening of the second peak, signifying a decrease in structural order.

The extended system method has also been applied by Lynden-Bell *et al.* to the issue of symmetry breaking in the polarisable I_3^- ion [27] in water. The extended system included the molecular dipole, as a function of which, the free energy of solvation was calculated. The free energy had a maximum for zero dipole. Comparison with quantum chemistry calculations of the polarisation energy as a function of the dipole magnitude led to the prediction that the I_3^- ion develops a spontaneous dipole in aqueous solution. As a consequence of this, the symmetric stretch vibration would become visible in infrared, while the asymmetric stretch would become Raman active, in agreement with experiment.

In Ref. [28] Wood *et al.* outlined a method for calculating the free energy of solvation for quantum mechanical solute–solvent interaction energies using mostly classical simulation. Firstly the classical free energy of solvation was calculated by growth of the solute from zero interaction ($\lambda = 0$) to full interaction ($\lambda = 1$), in stages, using thermodynamic integration. Next for a small set of statistically independent configurations sampled from this simulation, the classical solute model was replaced by a quantum mechanical model (in the form of an extracted cluster of solute and surrounding solvent molecules), and the free energy difference obtained from the change in configuration energy. Thus with relatively few quantum calculations the quantum free energy of solvation could be obtained. By extension the method showed the difference between good and bad solvent models by reference to the computed quantum corrections and the correspondence between normalised energy distribution histograms of $\Delta U/kT$ and $\exp(-\Delta U/kt)$. As an example the study showed that at a fluctuating charge TIP4P model of a solvated water molecule provided a superior description of the first solvation shell than the basic TIP4P model. However, the overall solvation energy was the same.

A subsequent paper by Sakane *et al.* [29] explored the sources of error in the classical/quantum free energy method of Wood *et al.*, these being: the *ab initio* quantum method; sampling the configurations; and the (classical) solvent model. The test system was the hydration energy of water, at two different state points. For the quantum calculation, the localised MP2 method gave good results, but gradient density functional theory (DFT) did not. The calculation cost was reduced by using a large cluster (60 molecules) to compute the solute–solvent pair interactions and smaller cluster (5–12 molecules) for the rapidly converging many-body interactions. Between 50 and 200 configurations were required to give an accuracy within $\pm 2\,\mathrm{kJ\,mol^{-1}}$. The TIP4P fluctuating charge model was found to be reliable, even under supercritical conditions. Excellent agreement was obtained between the best calculation and experimental data.

The effects of solute curvature on hydrophobic solvation has been investigated by Chau *et al.* in Ref. [30]. The NVT simulations consisted of SPC/E water with a single solute molecule, which interacted with the solvent via an adapted L–J potential of the form

$$V(r) = 4\epsilon\left[\left(\frac{\sigma}{r - r_0}\right)^{12} - \left(\frac{\sigma}{r - r_0}\right)^{6}\right],$$

in which the solute "hard sphere" radius r_0 was set to values of 0, 2 and 4 Å, and the parameters ϵ and σ set at the OPLS values for methane. At $\sim 310\,\mathrm{K}$, the solute-oxygen PRDF showed a declining first peak height and increasing width, with increasing solute radius. This was also seen in the solute-hydrogen PRDF, in which the peak also moved further out from the hard sphere radius. In the first solvation shell the water dipole was mostly aligned perpendicular to the solute-water vector, with some tendency to point at the solute for the $r_0 = 0$ case. An analysis of the hydrogen bonding in the solvation shell, which used four different H-bond criteria, revealed that the number of H-bonds per water molecule decreases with increasing solute size. However, when the volume available to a water molecule in contact with the solute sphere was taken into account, the number per unit volume is roughly constant and slightly more than in the bulk phase. This was evidence for the enhanced water structure due to a hydrophobic solute reported by others. The density of water in the solvation shell was slightly higher than in the bulk, and the number of water molecules with 3–4 neighbours increased at the expense of higher coordination numbers. The VAFs revealed the presence of H-bond network oscillations, but for different solute sizes the VAFs differed significantly. As the solute radius grew, the first minimum in the VAF gradually disappeared. Radial and tangential VAFs were similar, though the former had a broader frequency spectrum. The diffusion coefficient for water in

the solvation shell was approximately half that for the bulk, which in turn was similar to the experimental value ($\sim 2.9 \times 10^{-9}\,m^2\,s^{-1}$). Reorientational times were calculated from LOC functions, and in general were longer for the water molecules in the solvation shell. The O–H-bond relaxation time increased 18–38% over the bulk time, and the dipole axis relaxation time increased 33–40%. Overall, these results indicated the formation of a clathrate like structure of water around the solute, which became less prominent (i.e. less structured) as solute size increased. However, dynamical effects produced by the presence of the solute, were not sensitive to solute radius.

More recently Chau has examined the hydrophobic hydration of concave surfaces [31]. Three hemispherical surfaces were created from linked L–J sites (nominally carbon atoms) with radii 6.5, 9.3 and 12.3 Å and equilibrated in SPC/E water. Within the cavities the water was seen to form layers: one layer in the smallest cavity, three in the largest and two in the intermediate. The water dipole was found to lie preferentially orthogonal to the cavity radius (nearer to 70° in the smallest cavity). The enforced departure from quasi-tetrahedral structure of bulk water inevitably reduced the H-bonding in the cavity water molecules and the number of neighbouring molecules was also reduced. This new structure had little effect on the translational dynamics of water, but reorientational dynamics was accelerated, particularly in the case of the smallest cavity. Rough density calculations suggested de-wetting of the concave surface, as well as the external convex surface. These observations may help in understanding the (usually concave) reactive sites of enzymes.

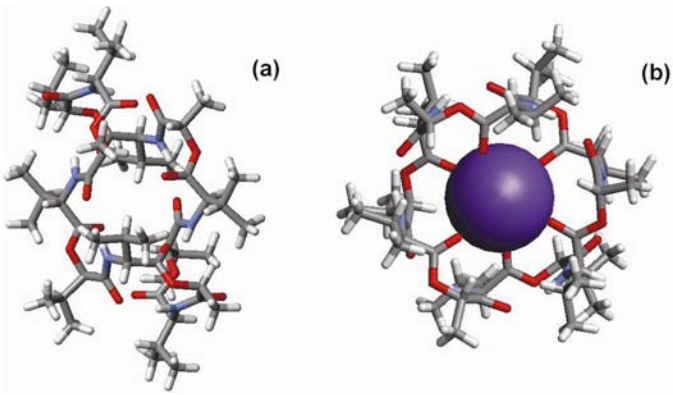

FIGURE 2 Valinomycin and potassium complex. Valinomycin in (a) the "twisted bracelet" form it adopts in nonpolar solvents and (b) the complex it forms with potassium ions [32]. Note the rôle of the (ester) carbonyl groups in chelating the potassium. In this form, the potassium may be transported though the living cell membrane. Figs. drawn by Weblab molecular graphics software from Molecular Simulation Inc.

The bio-molecule valinomycin (Fig. 2a) is of some importance in the transport of potassium in living tissue. This ionophore is a ring molecule, which encapsulates the potassium ion (Fig. 2b), effectively giving it a hydrophobic coat and thus facilitating transport of the ion through the cell membrane. (The ring resembles a peptide of 12 amino acids; nine valine and three alanine, except that the alanine amino groups are replaced by alcohol groups, giving rise to ester instead of amide linkages.) The properties of this molecule and its potassium complex in solution have been examined by Forester *et al.* [32] as part of a larger study into its biological activity. In this paper, the molecule and its complex were studied in a nonpolar L–J solvent and in water at 310 K. The force-field model was taken from a study of the crystal structures [53] with a SPC water model. A truncated octahedral periodic boundary condition was applied and an Ewald sum used to calculate electrostatic interactions. In a solution of 500 L–J molecules, valinomycin adopted a structure some way between two known crystal forms, known as the twisted bracelet (TB—Fig. 2a) and twisted propeller (TP) forms. The high conformational flexibility was demonstrated in a statistical analysis of the conformations of the 12 dihedral angles of the ring and it was postulated that many possible conformers of the molecule existed in such solutions. PRDFs and associated coordination numbers showed that the (hydrophobic) alkyl groups on the ring were the most solvated and the six ester carbonyl groups were less solvated than the amide carbonyls—a characteristic of all the simulations. The uncomplexed form in 1223 water molecules most resembled the TP crystalline form, but again, considerable conformational flexibility was apparent. The PRDFs and water oxygen coordination numbers revealed that coordination in general is lower in aqueous solution (due to quasi tetrahedral packing of water); but the (hydrophilic) carbonyl groups were now the most solvated, with ester carbonyls again being least solvated. The potassium–valinomycin complex (K^+–VM) in the L–J solvent closely resembled the crystal structure, with some additional flexibility. The ester carbonyl chelation of the potassium ion was augmented by a single amide carbonyl. Overall, solvent coordination of valinomycin resembles the uncomplexed form, allowing for the less open structure. The K^+–VM complex, as expected, proved to be instable in aqueous solution. Over a period of $\sim$100 ps, the complex structure opened to release the potassium ion. The procedure commenced with penetration by water molecules to the potassium ion at the centre, which gradually displaced the chelating ester carbonyls one after the other. The opening of the complex reflected the flexibility of the ring and the relative steric importance of the methyl and isopropyl substituents of the ring. This study thus revealed important insights into the biological function of the valinomycin molecule.

Spectroscopy

Spectroscopy is an important technique in the study of many systems of chemical interest. Though it is apparent that classical MD cannot handle the quantum mechanical aspects of spectroscopy, there are associated phenomena that can be treated quite adequately by classical means. The photon absorption and emission frequencies of molecules undergo a "solvent shift" when in solution which derives directly from the structure of the solvation shell. The "instantaneous" change in electronic structure resulting from a spectroscopic transition is dependant on the solvation energy and thus effectively probes the local structure at that instant. The distribution of solvation energies leads to broadening of the absorption (or emission) band. Brown *et al.* have applied DL_POLY to several investigations of this phenomenon [33–37].

In Ref. [33] the spectroscopy of coumarin 153 (C153) molecules (Fig. 3a) in a mixed solvent of 10 methanol and 216 hexane molecules were studied. It was found that, in the ground state, C153 was not strongly solvated (though with a slight preference for methanol solvation), while in the dipolar excited state, there was strong solvation by the methanol. In consequence, the solvent shift effect on absorption spectrum was minor, while the emission spectrum showed pronounced changes in the emission band, broadly in agreement with the observed spectrum.

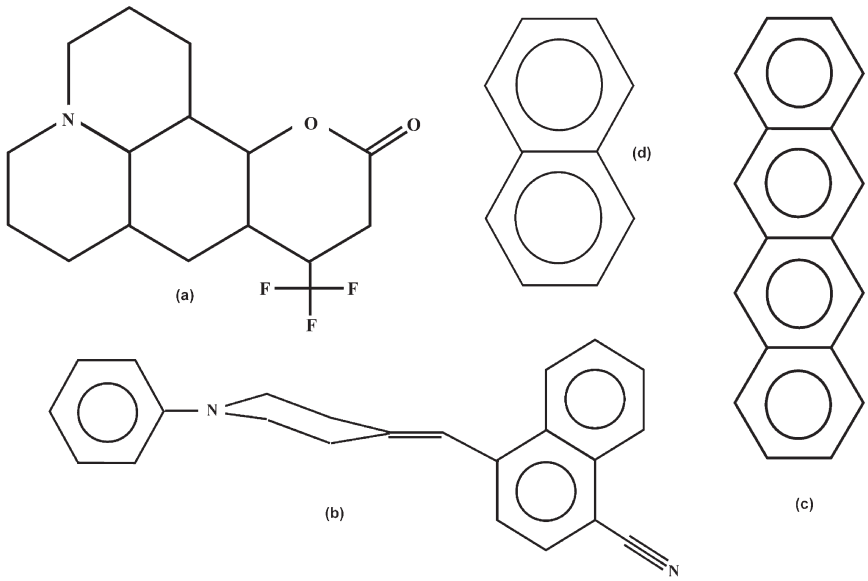

FIGURE 3 Spectroscopic species studied by molecular dynamics. Species studied by Brown *et al.* [33–37] in spectroscopic applications of DL_POLY: (a) coumarin 153 (C153); (b) fluoroprobe; (c) tetracene; and (d) naphthalene.

The main source of error in this approach was believed to be a poor representation of the C153 polarisability. The study also revealed that in the solvent mixture, translational motion of the methanol in the solvation shell was more significant than rotational motion in explaining the observed solvent shift. This differs from the pure methanol solvent.

In Ref. [34] the techniques were applied to the relaxation of a diethylether solvent around the fluoroprobe molecule (Fig. 3b). (This relaxation is apparent in spectroscopy as a time-dependent shift in the emission band—the so-called Stokes shift.) From an equilibrium simulation of the ground state fluoroprobe structure, 100 independent configurations were used as the starting point for the relaxation following an instantaneous conversion of the molecule to the excited state. From these the average solvent frequency shift was obtained as a function of time. Also calculated were the equilibrium fluctuations for both absorption and emission frequencies. The results showed that the time dependent spectral shift function (called the solvation function $C(t)$) closely followed the correlation functions of equilibrium absorption and emission frequency fluctuations, consistent with linear response theory. The dynamics of solvation shell formation were investigated using PRDFs calculated at fixed times during the relaxation, which clearly revealed the growth of new structure in response to changes in atomic charges, the effect of which was moderated by steric hindrance of the solvent. Close analysis of the solvation relaxation indicated that in this weakly polar solvent both translational and rotational motion of solvent molecules are important. It was also observed that the residence times for solvent molecules in the solvation shell exceeded the molecular reorientation time.

Solvation in clusters may be studied by molecular beam experiments and Wallenborn *et al.* have looked at the case of the tetracene molecule (Fig. 3c) in an alkane (heptane) solvent [35] and compared simulation with experiment. (The clusters were built from the "bare" tetracene, adding one heptane molecule at a time in a collision process with quencing. The clusters were designated $t - h_n$ with $n \leq 12$, corresponding to 12 solvent molecules.) Spectroscopic shifts were calculated from quantum perturbation theory with a distributed multipole expansion of the dispersion terms. Classical equilibrium simulations of the clusters were used to determine lineshapes. The cluster calculations revealed that heptane tended to lie along the length of tetracene, and six heptane molecules were sufficient to form a complete first solvation shell. The spectral shifts obtained were almost linearly dependent on solute–solvent interaction energy in the ground state, though a 10% systematic underestimate of the shift was noted. Armed with information about the structures of low order clusters it was possible, with a harmonic analysis, to associate peaks from the observed spectrum with specific clusters. With line broadening, the overall spectra of various clusters

were reasonably well reproduced, with the exception of the $t - h_6$ cluster, where it was thought that one of the solvent molecules possibly occupied the second solvent shell, leaving the inner shell incomplete.

The influence of solute polarisability on spectroscopic transitions has been investigated by Chichos *et al.* [36,37], using a combination of semi-empirical molecular orbital theory and MD. The former, with configuration interaction, was used to calculate the polarisability, which at each time step was fed into the MD forces calculations. In Ref. [36] (nonpolar) naphthalene (Fig. 3d) in acetonitrile was studied. Three relevant electronic states were identified S_0, S_1 and S_2, with $S_0 \rightarrow S_2$ being the main absorption and $S_1 \rightarrow S_0$ the main emission. The simulation consisted of one naphthalene in 256 acetonitrile molecules. All molecules were considered rigid. Equilibrium simulations were performed for all three states, using both polarisable and nonpolarisable solute molecules. PRDFs revealed that polarisability had little effect on the solvation structure, a result consistent with the energetics. Integrated PRDFs indicated that the negative end of the solvent dipole preferentially pointed towards the naphthalene, so that the average electric field on the solute was well defined and directed out of the solvent cavity, with no net dipole. In contrast, the instantaneous field was inhomogeneous and varied substantially over the length of the solute molecule. Also, since the solvent shell was not instantaneously symmetric, naphthalene possessed a nonzero instantaneous induced dipole, which differed between states S_0, S_1 and S_2, and a linear relationship was found between this induced dipole moment and the instantaneous mean electric field acting on the naphthalene. The effect of polarisability on the solvent induced shift distribution was to displace it towards red. It was also found that solvation response was faster for the polarised solute. Analysis of the multipolar contributions to the solvent shift showed that solute moments higher than dipole contributed $\sim 60\%$ of the total shift. Comparison of the dipole and quadrupole fluctuations revealed that the dipolar response was always the faster, though both were slowed by increased solute polarisability. The same correlation functions, which define the dipole and quadupole contributions to an electronic transition, also indicated their relative contributions to the solvation dynamics.

The second study was on coumarin 153 in methanol and acetonitrile [37]. Unlike naphthalene, C153 possesses a strong dipole moment (6.6 D) which increases markedly on excitation (~ 14 D). Methanol was chosen in addition to acetonitrile because of its H-bonding capability and lower dipole moment. Two electronic states of the solute were simulated, S_0 and S_1. In these cases, inclusion of polarisability had a significant effect on the observed PRDFs, which were rationalised in terms of the charge redistribution. The electrostatic energies were on a par with the van der Waals contributions. Results for the S_1 state with

polarisability suggested the effects were overestimated. Surprisingly, orientational ordering of both solvent molecules in the first solvation shell was weak. The ground state dipole is greatly enhanced in both solvents, but more so in methanol, despite its smaller intrinsic dipole. The structure of the respective solvation shells was thought to be the reason. The dipole enhancements agreed with homogeneous field calculations and were approximately linear with the electric field. The dipole of the S_1 state calculations did not agree with homogeneous field calculations. Solvation shell structure changes were invoked as the probable cause. The intrinsic dipole of C153 induced larger solvent shift effects than those seen in (nonpolar) napthalene and the polarisability enhanced the effects much further. The resulting shift spectral density distributions were considerably shifted and also broader. The emission shifts however were overestimated, a failure ascribed to the approximate semi-empirical method, with possibly inappropriate parameterisation.

DL_POLY has also been used in studies of luminescence in silicate glasses doped with rare-earth ions [73,74]. This is described in the section on glasses below.

Structure of Materials

One of the major areas of DL_POLY application is in the structure of ionic solids, either under ambient conditions or under extremes of temperature and/or pressure. Often this work is used to augment experimental work, but sometimes simulation is the only practical tool, particularly where minerals are involved. Also of interest are the effects of doping, particularly in inorganic systems, which lead naturally to questions concerning the diffusion and mobility of ions, usually with an eye to possible catalytic activity.

Ionic Solids

A good example of the application of DL_POLY to high pressure systems is Verma and Sharma's study of α-GeO_2 [38], which is a material isostructural with α-SiO_2. Experimental evidence suggested a phase transition in the region of 7–12 GPa, with a change in germanium coordination from 4 to 6 and the adoption of an amorphous structure. Simulations using a potential due to Oeffner and Elliot [39] were able to show a pressure induced phase transition at 8.5 GPa, signalled by a 12% drop in volume, with germanium coordination increasing to 5.16, rising with increasing pressure. A partially disordered phase, with some persisting periodic structure was observed up to 68 GPa. This group has also used MD to

subject α-SiO_2 cristobalite to various shock treatments (sudden changes of temperature and pressure) [40]. They observed the irreversible formation of a six coordinated, disordered stishovite-like phase at temperatures and pressures in excess of 1522 K and 18.1 GPa, respectively. The same phase, but not disordered, has also been observed at ambient temperature, by gradually increasing the pressure to 15 GPa.

The temperature dependent structural properties of cristobalite (SiO_2) in the β phase have been studied in detail by Bourova *et al.* [41], using both MD and static lattice methods. An initial lattice dynamics study of α-SiO_2 using both rigid ion and shell model potentials showed the rigid ion model to be the more reliable at high temperatures, due to a more realistic description of the Si–O–Si bond angle and the short-range O–O repulsion. Lattice calculations starting from the reference cubic β-SiO_2 structure were easily coaxed into three distinct stable structures differing in the disposition of the SiO_4 tetrahedra and consistent with the suggestion from experimental and theoretical evidence that β-SiO_2 is dynamically disordered. The NPT (constant temperature and pressure) MD simulations at increasing temperatures gave a system volume increase of ~10% up to 850 K and then flattened with the β phase formation. Very high temperatures produced a volume reduction. The thermal expansion showed strong hysteresis on cooling from 1400 to 700 K. Analysis of the PRDFs indicated that the α–β phase transition occured with a rotation about the tetrahedral centres. The oxygen atoms appeared to vibrate in a three well potential in the β-phase, which was consistent with the three isomorphic structures found in the lattice modelling. Disorder in the β structure was particularly evident in the Si–O–Si bond angle distribution which widened and shifted to larger angles with increasing temperature. Significantly the SiO_4 tetrahedrals retained their rigid integrity throughout the temperature range.

Garg and Sharma have used DL_POLY to take a detailed new look at the high pressure phases of berlinite (α-$AlPO_4$) [42]. Commencing from an α-quartz structure under ambient conditions, it becomes amorphous at high pressure (~30 GPa) and reverts back to the α-phase when pressure decreases. Raman scattering and X-ray diffraction experiments suggested previously unobserved phases at 6.6 and 12 GPa. Also, analogy with the iron and gallium α-isomorphs impled that a Cmcm space group structure might occur at very high pressures. NPT simulations of 2592 and 3456 atoms with a potential model due to van Beest *et al.* [43] were undertaken to explore these possibilities. The simulations gave an ambient structure consistent with experiment and previous simulation studies, and revealed a discontinuous 5% drop in the system volume as pressure was increased through 30 GPa. At the same pressure the Al–O coordination jumped from 4 to ~5.2, rising further to 5.8 at 65 GPa. Calculated powder X-ray

diffraction patterns exhibited decreasing structural order with rising pressure, which did not entirely vanish at the highest pressures. The atomic structure beyond 30 GPa was seen to be disordered, but retained some residual translational order. No evidence for a 6.5 GPa transition was observed, but some structural changes were perceptible at ~15 GPa and a change in the slope of the *c*/*a* ratio of the cell was also seen. A disordering of the oxygen atoms alone was determined to be the cause. An analysis of tetrahedral structure parameters for AlO_4 and PO_4 units showed the latter to retain their integrity over the pressure range studied, while the AlO_4 showed wide distortion, which may trigger the transformation to the disordered phase at 30 Gpa. Attempts were made to produce the putative Cmcm phase by annealing the disordered phase without success. Simulation commencing from the Cmcm phase also became disordered. However the phase was stabilised by shock loading at 20 GPa, which suggested that the Cmcm phase may be the preferred structure under nonhydrostatic stresses.

In Ref. [44] Jackson and Mort were concerned with the validity and transportability of potentials for molecular ions. Using alkali nitrates and ammonium halides, they demonstrated that parameters derived for these materials could not only describe their physical properties well, but could also be exchanged between related materials, even to combining them in different materials, as in ammonium nitrate, with a good measure of success.

DL_POLY is frequently applied in studies of the structure and properties of zeolites distinct from, but usually related to, their catalytic activity. Faux [45–47] provides examples of such applications, focusing on hydrated and dehydrated forms of Na^+-zeolite-4A. The zeolite-4A unit cell is derived from the chemical formula $(Na{\cdot}SiO_4{\cdot}AlO_4)_{96}$. The Si and Al atoms are at the centres of oxygen tetrahedra, and the whole structure is comprised of large cavities (α-cages) of 72 oxygen atoms and smaller cavities (β-cages) of 36 oxygen atoms. Within the structure 8-, 6- and 4-oxygen rings may be identified. The sodium atoms occupy the cavities and, in the presence of water, are solvated. In Ref. [45] a force-field for the (flexible) zeolite frame was obtained from literature sources and combined with an SPC/E water model to perform MD simulations of the dehydrated lattice (672 atoms) at 0 K (i.e. energy minimisation) and hydrated lattice (with 224 water molecules) at 298 K. The 0 K simulation yielded a structure in good agreement with X-ray diffraction data and with energy minimised structures obtained by others. The sodium ions were associated with the various oxygen rings: 64 were located at the centre of the 6-rings (site Na(1)), almost in the plane; all 24 8-rings (site Na(2)) had at least one sodium, and three had two, located in four possible sites within the rings; and lastly five sodiums were randomly arranged in sites above the 4-rings (site Na(3)). It was clear that the sodium atoms had moved

during the minimisation process. Addition of 224 water molecules produced a saturated structure. After equilibration the distribution of water molecules in the α- and β-cages were examined. In the α-cages, with a mean occupancy of 24.25 water molecules, no fewer that 44 sites were identified where water was preferentially adsorbed. This was significantly different from a dodecahedral arrangement postulated from X-ray data. The structural requirements implicit in these arrangements had a noticeable effect on the water–water PRDFs. In the β-cages, with an occupancy of 3.75 water molecules, six preferred sites were located. The PRDFs differed from experimental results, but this was rationalised in terms of the difference in water occupancy between the experimental and simulated systems. Each sodium ion was found to be hydrated by 2–3 water molecules.

In Ref. [46] Faux examined the diffusion of sodium in anhydrous and hydrated Na^+-zeolite-4A. Hydration of the 672-atom lattice ranged from 0 to 224 water molecules. The preferred sites for the sodium (Na(1), Na(2) and Na(3)) revealed in Ref. [45] (above) were retained in the hydrated lattice up to full saturation. Diffusion, as measured by the MSD, was almost entirely confined to ions occupying sites Na(2) and Na(3), consistent with the greater attachment energy of the Na(1) site. In general, the higher the hydration level, the higher was the diffusion. Diffusion rates varied between $7-100\times10^{-12}\,m^2\,s^{-1}$, but these corresponded to *intra*-cavity diffusion, and application to macroscopic measures of diffusion was thought uncertain. Nuclear Magnetic Resonance (NMR) estimates of the diffusion were smaller, but referred to much longer time scales and hopping rates between Na(2) and Na(3) sites were determined to be in the region $0.2-3.2\times10^{9}\,s^{-1}$. Conductivity experiments had suggested that Na(2) and Na(3) sites were solvated first, and as hydration increased solvation of Na(1) sites eventually occurred. There was some support of this from the simulations, but not for the increased mobility of the Na(1) site ions, which had also been proposed.

Using the same model system as above, Faux subsequently addressed the diffusion of water molecules in hydrated zeolite-4A, for different levels of hydration, up to full saturation [47]. The hydration energy ranged between $85\,kJ\,mol^{-}$ for low hydration and $57\,kJ\,mol^{-}$ for full hydration. It was found that the MSD of water increased with hydration up to about 75% saturation and diminished thereafter, an effect attributed to blocking of the water molecules at the higher water density. Diffusion involved the water molecules in the α-cages alone; water in the β-cages was non-mobile on the timescale studied. The calculated diffusion coefficents ranged over $2.7-6.8\times10^{-10}\,m^2\,s^{-1}$, for cell occupancies of 56–168 water molecules. The diffusion at full saturation was three times greater than that obtained from pulsed field gradient nuclear magnetic

resonance (PFG-NMR) experiments, however the simulated MSD plot was not considered to be of sufficient length to provide definitive comparison. Some evidence was obtained from MSD distribution plots for the hypothesis that water molecules closest to the cage walls diffused more slowly than those in the cage centre.

Islam *et al.* has applied DL_POLY to the study of ceramics, [48–51] particularly those possessing the perovskite stucture. The principal interest here is the mobility of the oxygen ion in these complex structures, which have potential application in fuel cells and oxygen separators. In Refs. [48,51] oxygen ion diffusion in the nonstoichiometric oxides $La_{1-x}Sr_xMO_3$, with M = Co or Mn, was investigated. Using Buckingham potentials to define the force-field, an examination of the PRDFs first showed that, while the cationic species resided in an ordered lattice, the oxygen ions in the nonstoichiometric materials were increasingly disordered with increasing temperature. The calculation of the corresponding MSDs revealed that the oxygen ions were indeed liable to diffusion, though this was not the case in the stochiometric materials (i.e. $x = 0$ in the above formula). The rates of diffusion were low (e.g. $1.5 \times 10^{-12}\,m^2\,s^{-1}$, for the cobaltate at 800 K with $x = 0.1$), but increased with both temperature and nonstoichiometry. Arrhenius plots of the diffusion coefficient gave activation energies for the oxygen diffusion close to the published experimental values. Analysis of the oxygen ion trajectories established a hopping diffusion process, with the diffusion path lying along the edge of the MO_6 (M = Co, Mn) octahedra.

Khan *et al.* extended the above study to zirconia (ZrO_2) and investigated the effects of doping the material with various divalent and trivalent cations (e.g. Ca^{2+}, Y^{3+}, Gd^{3+}, Sc^{3+}). The structure of the material and the oxygen ion diffusion were of interest. Once again, Buckingham potentials were used, and the study was supported by lattice calculations conducted with the GULP code [50]. Using GULP a wide range of cations were tested to determine those most able to stabilise the high temperature cubic polymorph of zirconia. Yttrium was found to be most effective, with calcium and gadolinium. The relative stabilities of different dopant-vacancy clusters were indicative of the bulk structure. Therefore, GULP calculations of dopant-vacancy binding energies were used to determine the favoured structures for different dopants. In general, smaller dopant ions preferred oxygen vacancies at the nearest neighbour sites, larger dopant ions favoured oxygen vacancies at next-nearest neighbour sites. These preferences also impacted on the displacement of oxygen atoms adjacent to vacancies. Doping zirconia with yttrium improves the solubility of the niobium cation (Nb^{5+}), which in turn improves the electrical conductivity of the material in reducing environments. GULP calculations of the niobium solution energy were able to establish the reason for the improved solubility. The diffusion of

oxygen in yttrium doped zirconia were calculated using DL_POLY. As with perovskite stuctures (above) the calculated PRDFs indicated a degree of disorder in the oxygen sublattice and the oxygen MSD showed the ion to possess a measurable temperature dependent diffusion above ~ 800 K. The calculated activation energy was 0.37 eV, in reasonable agreement with the experimental value (0.44 eV) obtained from tracer ion experiments.

Molecular Crystals

The central issue in molecular crystal studies is polymorphism: the possession of many crystal forms in close proximity on the phase diagram. It follows that many of the applications of DL_POLY in this area are concerned with elucidation of these forms and the precise computation of their structures. These activities constitute a severe test of any model force-field and proper identification of distinct structures is a difficult challenge. However, the results can be invaluable in resolving experimental uncertainties. The applicability of DL_POLY in this area results from its ability to handle many model molecular forms and intermolecular potentials. Its catalogue of electrostatic calculation techniques is particularly useful.

A typical application of DL_POLY in modelling molecular crystals is give by Sorescu *et al.* in their study of nitromethane [52]. The molecular properties of nitromethane (atomic charges, bond energies etc.), were computed from first principles and the potential energy surface fitted to standard analytical forms (Morse potential bonds, harmonic angles and cosine dihedrals). Special effort was given to accurate calculation of the normal mode frequencies. Intermolecular terms were taken from the authors' previous work on RDX crystals. This force-field was then applied to studies of the nitromethane crystal in static lattice (energy minimisation) calculations and MD, NPT simulations. The former calculations provided the ground state structure (in agreement with experiment) while the MD simulations provided the temperature (4.2–228 K) and pressure (0–7 GPa) dependence of the structure, measured in terms a wide range of properties, including cell parameters, atomic positions and bulk modulus. Of particular interest was the preferred orientation and rotational motion of the methyl group as a function of pressure. It was demonstrated that a high degree of accuracy in structure prediction was possible.

In a study of the properties of the biological transport molecule valinomycin, Forester *et al.* used a derived molecular force-field to investigate the structure of the valinomycin molecular crystal and that of the K^+-VM complex [53] (see Fig. 2). The force-field was based on an extended AMBER model, with atomic

charges derived from *ab initio* molecular orbital calculations. This was found to give a good account of the structures of both complexed and uncomplexed valinomycin in the solid state at ambient temperature, in terms of PRDFs, ADFs, H-bonding and molecular shape. A study of the isolated complexed form in a stochastic heat bath, over a range of temperatures) revealed that the complex remains stable, but there were significant changes in the chelation of the potassium ion (coordination number and chelating ligand, which included *both* ester and amide carbonyls, instead of ester carbonyls alone), and the valinomycin became considerably more flexible. The isolated uncomplexed form showed similar increased flexibility, with much reduced H-bond lifetimes, and the adoption of a more spherical structure. The simulation dipole moment agreed well with the experimental value (3.6 D versus 3.5 D).

Phase transitions in molecular crystals are sometimes particularly complicated, and MD simulation is well suited to unravelling the details. Bordat and Brown have applied DL_POLY to a study of the disorder–order transition in *p*-terphenyl [54] (Fig. 4a). The low temperature triclinic crystal structure undergoes a disorder–order transition at $\sim$190 K to a monoclinic structure, with two molecules in the unit cell. The disordering is associated with flipping of the aromatic rings, particularly the central ring between the two end rings. Several force-field models were investigated, taken either from the literature or constructed from empirical data and semiempirical calculation. Simulations using these were compared with experimental structual properties of the triclinic phase to select the best. Simulation of the triclinic system over a range of temperatures indicated that in the region of $\sim$190 K, the mean inter ring torsion angles diminished sharply from $\sim$17–25 to $\sim 5^\circ$ and down to zero at $\sim$350 K, consistent with a disorder transition. The torsion angle autocorrelation function (TAF) indicated increasing relaxation time (or residence time in the each branch of the double well potential) as temperature fell towards 190 K. At very low

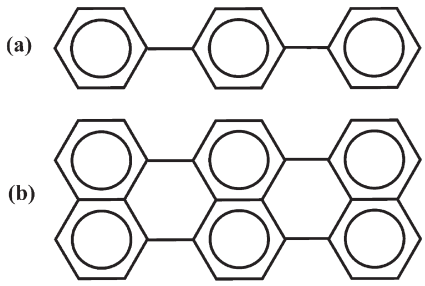

FIGURE 4 *p*-Terphenyl and terrylene. Molecular crystals studied by Bordat and Brown [54–56]; (a) *p*-terphenyl and (b) terrylene.

temperatures the TAF revealed "locking" of the rings in the minimum energy locations. Calculated residence times at 300 K however, were a factor of 10 too small, a result ascribed to an acute sensitivity to the intermolecular potential. Cross correlation of the torsion angles with neighbouring molecules was shown to persist over several monoclinic cell widths. The flipping rate (reciprocal of residence time) showed an Arrhenius temperature dependence when above 200 K, for which the activation energy (1.1 kcal mol^{-1}) agreed with experiment. However, this dropped dramatically as the critical temperature was approached. The slowing down corresponded to a growing intermolecular correlation as temperature fell.

Bordat and Brown have also applied DL_POLY to mixed crystals as model systems relevant to spectroscopic studies. In Ref. [55] the system examined was *p*-terphenyl with pentacene substitution. Below $\sim$190 K *p*-terphenyl crystallises in an ordered triclinic cell with four distinct molecular sites in the unit cell. Substitution at each of these sites by pentacene gives rise to four distinct origins for electronic absorption and emission spectra. However, the origin associated with each site is unclear and 24 permutations are possible, which earlier experimental studies had narrowed to eight. DL_POLY was used to perform simulated annealing experiments of the proposed structures, starting from the pure *p*-terphenyl crystal structure and substituting pentacene in the appropriate location. The force-field was derived from several literature sources, augmented by semi-empirical molecular orbital calculations. Spectroscopic experiments provided information on the orientation of the pentacene molecule relative to the crystal axes. Information was also available on intersystem crossing rates (from first singlet to first triplet state). From this information a unique assignment of the energy minimised structures with the electronic origins was possible.

In a study relevant to optical data processing Bordat and Brown have examined optical switching of terrylene (Fig. 4b) in a *p*-terphenyl crystal [56]. Following a similar procedure to [55] a model for the terrylene intra- and inter-molecular force-field was obtained and simulated annealing experiments conducted under constant pressure conditions to obtain the crystal structure of *p*-terphenyl with the guest molecule. As with pentacene (above) four insertion sites are possible below $\sim$200 K, corresponding to four electronic origins for the terrylene spectrum. One of the origins (labelled X1) undergoes a shift to red of 845 GHz under laser irradiation, which may be reversed under further irradiation. From evidence of the quadratic Stark effect it was deduced that each terrylene substitutes a single *p*-terphenyl molecule in the crystal. This conclusion was supported by simulation calculations of the free energy of substitution by a single terrylene molecule in the host crystal. Many annealing and quenching simulations commencing from each of the four substituted stuctures showed that two remain strongly fixed to

distinct points on the energy landscape. This allowed their immediate identification with the two most stable of the electronic origins. The precise assignment followed from consideration of the fluorescence intensity under polarised excitation. Simulations starting from the remaining two sites produced several local minima, and from their distibution and multiplicity assignment of the remaining electronic origins was possible. Detailed examination of the conformers in the minima revealed the role of *p*-terphenyl ring flipping in spectral transitions and the additive nature of the transition energies.

Amorphous Systems

Amorphous systems, which include both glasses and polymers in the category, are among the most difficult systems to study, whether by experiment, simulation or theory. DL_POLY is well adapted to modelling polymeric systems, since it supports a wide variety of intramolecular bonding descriptions, including atomic charges, and the ability to exploit parallel processing when the systems become excessively large.

Polymers

Abu-Sharkh and Hamad [57,58] and Abu-Sharkh [58] have addressed the issue of nonadditivity in polymer chains when determining the compressibility factor. In Ref. [57] a simple polymer model was adopted, consisting of L–J "beads" and rigid bonds. The interaction between beads was trunctated and shifted to zero at $2^{1/6}\sigma$. The beads were of two kinds and formed either diblock copolymers or alternating chains. Nonadditivity was introduced by scaling the usual cross term $\sigma_{ij} = (\sigma_i + \sigma_j)/2$ by a factor $(1 + \Delta)$ with $\Delta \geq 1$. (The same L–J energy parameter ϵ was used throughout.) Simulations were performed for chains of 2, 4, 8 and 16 beads in both diblock and alternating forms and at packing fractions of 0.37 and 0.45. The compressibility was obtained from equilibrated runs of 50,000 time steps. It was noted that for additive chains ($\Delta = 0$), the compressibility factor compared well with true hard-sphere results. The PRDF results showed that nonadditive diblock chains of length greater than 2, undergo microphase segregation for positive nonadditivity ($\Delta > 0$), which increases with density and chain length. This did not occur with alternating chains or chains with negative nonadditivity ($\Delta < 0$). A model for calculating the compressibility was derived from first order perturbating theory (after Wertheim), and shown to reproduce the simulated results for additive and negative non-additive chains, but over-estimated the compressibility for positively nonadditive chains. In the subsequent

paper [58], a second model incorporating the polymeric adaptation of the Percus–Yevick approximation for hard spheres, gave a better description of the positive nonadditivity data, but was slightly poorer for zero and negative nonadditivities.

Abu-Sharkh [59] has also applied DL_POLY to explore the validity of MD simulation in calculating the glass transition temperature (T_g) in the poly(vinylchloride) polymer. Also explored was the relative importance of "explicit atom" and "group atom" models (in which the CH_2 and CHCl groups were treated as dynamically rigid bodies). In both cases a single chain of 153 carbon atoms was used, in conjunction with a 12–6 interaction potential. In addition, fractional atomic charges were used with a distance dependent dielectric scheme to calculate the electrostatic interaction. The amorphous system was carefully prepared from a single chain relaxed from low density to 1.3 g cm^{-3} by gradual volume reduction at 600 K. Further annealing followed in which the full interaction potential was gradually "turned on" in several stages, each lasting 0.5 ns. Both systems were simulated at several temperatures above and below the expected T_g. A Nosé–Hoover NPT ensemble was applied to the flexible chain and a Berendsen NPT was applied to the chain with rigid units. A constant pressure of 500 atmospheres was necessary to maintain the required density. The results showed that the volume relaxation above and below T_g was qualitatively different, with rapid relaxation to equilibrium volume at high temperature, and slow relaxation at low temperature. A plot of the specific volume versus temperature allowed a discontinuity in the slope located slightly below the experimental T_g. The dispartity was thought due to the short length of the model chains, the very short simulated relaxation time and the high pressure required to maintain density. Results for both flexible and semi-rigid chains were similar, though the latter maintained a higher specific volume throughout. The simulated PRDFs were again similar, though more detail was apparent for the flexible chains, and the first peak for the semi-rigid chains was slightly displaced outwards.

An intriguing aspect of MD is that it offers the possibility of studying the dynamical effects in polymer systems. In response to growing experimental evidence that polymer dynamics results from the superposition of a spectrum of relaxation processes, Karatasos *et al.* [60,61] have conducted a detailed MD investigation of the relative dynamical importance of the many relaxational modes in linear polyethylene chains that are described by united atom representations of the methylene and methyl groups. The molecular description included rigid bonds, harmonic valence angles, and dihedral angles of the Ryckaert and Bellemans (RB) [62], and Steele [63] forms. Nonbonded forces were assumed to be of the L–J type. For each dihedral potential model, eight

simulations were undertaken at 400 K (above the glass transition): four were comprised of 50 chains of length 20 atoms; and four of 10 chains of length 100 atoms. In each case the system densities ranged over the values 0.29, 0.59, 0.7 ($g\,cm^{-3}$). The chains were prepared in the amorphous state using a Monte Carlo algorithm and equilibrated for 4 ns, following which the production runs were 18 ns in duration. A number of basic molecular properties (radius of gyration, end-to-end length etc) were calculated to check the validity of the model.

One of the experiments undertaken by Karatasos *et al.* in Ref. [61] was an examination of the conformation transition rates for different dihedral potentials, system densities and definitions of the conformational transition. It was found that transition rates were higher near the ends of chains, and overall rates were reduced at higher densities, though they were insensitive to the chain lengths. Clockwise and anticlockwise conformational "jumps" occurred in equal number. The transition rate was shown to be sensitive to the underlying dihedral potential, with RB potential rates ~ 1.5 times faster than for the Steele potential. Significant differences in transition rate were also found between similar definitions of what constitutes a transition. The possibility of coupling between conformational transitions was evaluated by calculating the average bond rotation angle occurring in indexed bonds either side of the transitional bond (indexed 0). It was found that bonds indexed 2 and 4 underwent significant rotations in response to the transition, with bond 2 the more affected. This coupling occurred at all densities studied, and for both dihedral potential models. There was some enhancement of the effect as density increased.

Analysis of the dynamical properties of the chains conducted by Karatasos *et al.* in Refs. [60,61] was based on P_2 second Legendre polynomial autocorrelation functions (ACFs) for several unit vectors: the bond vectors $\mathbf{b}_i$; chord vectors $\mathbf{c}_i$ (which is a vector sum of consecutive bond vectors); out of plane vectors $\mathbf{o}_i$ (based on the vector product of two consecutive bonds); and the in-plane vector $\mathbf{s}_i$ bisecting two consecutive bonds. Also calculated was the ACF of the dihedral angles. The time dependence of the ACFs was analysed in terms of a function: the normalised distribution of relaxation times (DRT), $F[\ln(\tau)]$, which is related to the ACF $C(t)$ via the formula

$$C(t) = \int_0^\infty F[\ln(\tau)]\mathrm{e}^{-t/\tau}\,\mathrm{d}\ln(\tau),$$

from which the DRT may be extracted by numerical procedures. The results show that the dihedral ACF for the RB potential decays more rapidly than the Steele potential, and has a wider range (dispersion) of timescales. The P_2 ACFs for the $\mathbf{b}_i$ vectors (which lie along the backbone) decay more slowly than the $\mathbf{o}_i$ and $\mathbf{s}_i$ vectors, which are similar. The relaxation could not be characterised by a single

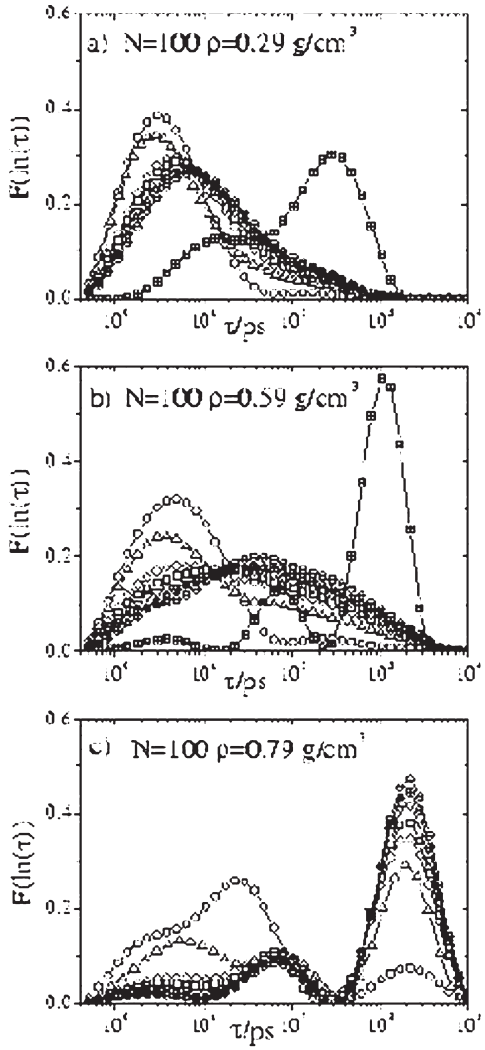

FIGURE 5 Polymer dynamics—DRTs. The DRTs of a 100 unit polymer at densities indicated [60,61]. On view are the DRTs for chord vectors c_i, with: $i = 1$ (circle); $i = 2$ (triangle); $i = 3$ (diamond); $i = 4$ (square); $i = 5$ (inverted triangle); $i = 6$ (circle plus); and $i = 7$ (circle minus). Also shown is the end-to-end vector DRT (square plus). Note the greater tendency towards multiple peaks for longer vectors as density increases, indicating timescale separation. Figure reprinted from Ref. [60] with the permission of the authors and the Journal of Chemical Physics.

exponential (or stretched exponential) decay, though good fits were possible once the DRT function had been obtained. Significantly the DRT function became more complex in structure as density increased and displayed more than one peak, which indicates a separation of timescales in the relaxation process.

The relaxation of slow modes was explored in detail by Karatasos *et al.* in Ref. [60], in which P_2 ACFs for all chord vectors in a chain (ranging from bond vectors, up to the end-to-end vector) were investigated. Plots of the DRT versus $\log \tau$ at low density for different chords of the shorter chains ($N = 20$) showed a one-peaked function for both small and long $\mathbf{c}_n$ vectors. However, as density increases the DRT for the intermediate and long vectors split into two peaks, with the long time peak dominating for the largest $\mathbf{c}_n$ vectors. This showed clearly the presence of two timescales in the dynamics of these chains, which were ascribed to (short time) bond reorientation and (long time) end-to-end reorientation. For the long chains ($N = 100$), the higher density plots revealed three peaks, the middle of which was thought to be related to the onset of the tangling regime (Fig. 5). Examination of the relative amplitudes of the slow modes of the short chains showed that these modes are relatively insensitive to increases in the system density.

Overall the work of Karatasos *et al.* represents a revealing example of what MD can provide in understanding molecular processes.

DL_POLY has also been used in the study of polymers at interfaces. Smith *et al.* has studied liquid alkanes at the vapour/liquid interface [64] and at a generic solid interface [65]. The study [64] was initiated by experimental evidence (surface tension, light scattering and X-ray scattering) of an ordered phase existing at the liquid surface at temperatures above the melting point. The hydrocarbon concerned was heptadecane ($C_{17}H_{36}$) in a united atom representation with rigid bonds and variable valence and dihedral angles. The system consisted of 384 molecules, arranged in a slab (i.e. with two surfaces) at a density of 0.738 g cm^{-3}. A lengthy procedure was required to prepare the system, including artificial surface forces to help with equilibration of the surface, though the free standing system was equilibrated for 300 ps before use. Simulations were performed at 244, 254 and 274 K, following 150 ps equilibration with each temperature change. The disordered liquid surface was also prepared after heating to 310 K and gradually cooling. Result of the simulation showed, in snapshot, the liquid surface was indeed ordered. The chains aligned perpendicular to both surfaces, with a disordered, liquid layer in between. The surface layers possessed a higher density than the liquid bulk and a zone of lower density formed between the distinct phases. The surface chains mostly adopted an all-trans configuration. The calculated P_2 order parameter reflected this structure on average, with a high degree of order in the surface regions, but averaging zero

in the middle region. The calculated grazing incidence X-ray reflection indicated hexagonal symmetry for the molecular arrangement in the surface zones and the q-dependent intensity compared well with experimental data. Dynamical studies showed the surface chains to possess measurable diffusion in the surface plane ($1.2 \times 10^{-9}\,m^2\,s^{-1}$), but motion in the bulk was significantly higher ($3.8 \times 10^{-9}\,m^2\,s^{-1}$). Motion perpendicular to the surface was bounded, but was quite large, with an amplitude ~ 3.5 Å. This behaviour was considered more representative of liquid crystals than true solid behaviour. The fully disordered system showed no comparable density variation, even close to the surface. A comparison of the system energies as a function of temperature revealed that the ordered system was energetically lower than the disordered, due primarily to intermolecular interactions. The estimated entropy was of the order $-3.3 - -5.3 \times 10^{-4}\,J\,m^{-2}\,K^{-1}$ (experimental $-7.7 \times 10^{-4}\,J\,m^{-2}\,K^{-1}$). In discussing why this phase existed, it was argued that the large motion of the chains perpendicular to the surface helped to stabilise the phase and the damping of these motions should a second layer form beneath the first explained why only a single layer arises.

The behaviour of alkanes near a solid surface was explored by Smith *et al.* in Ref. [65]. The solid surface was modelled as a featureless plane in the xy direction, exerting a force equivalent to a fixed layer of L–J atoms. The hydrocarbons studed were butane (480 molecules), octane (240 molecules) and a mixture of each (224/112 molecules respectively) and the temperatures were chosen to be a little above the freezing points of butane (135 K) and octane (216 K) and also well in the liquid regime. The mixture was simulated at 223 K. Both pure liquids showed density oscillations away from the solid surface to 4–5 layers above the substrate. Above this was a broad (30–40 Å) liquid layer. Adsorbed molecules at the substrate tended to lie flat on the surface. The mixture also showed density oscillations, but some segregation of the two hydrocarbons was also evident. The liquid/vapour interface was almost pure butane, and on the substrate, in immediate contact, butane dominated again, though overall in the first few layers, octane dominated. Molecular diffusion was measurable in all density layers, if lower than in the bulk, and it increased with rising temperature. This was evidence against these layers being in a solid phase. Butane diffusion was higher in the surface of the mixed system than in the bulk or pure butane liquids. Layering at an interface occurred, it was argued, because the packed molecules have larger free volumes and an associated entropy increase. The segregation of the butane and octane at the substrate was thought to be partly due to the greater ability of the smaller molecules to find vacancies on the substrate surface. The predominance of butane at the vapour/liquid surface was in keeping with its lower surface tension compared to octane, this in turn may have been due to greater free volume available to butane molecules near the surface.

Glasses

Glasses in general present a number of interesting challenges for applications of MD simulation. The first issue is the structure of the glass itself since, unlike crystalline materials, they do not provide a convenient starting structure, but must be generated in a way that plausibly resembles structures interpreted from experimental data, such as extended X-ray absorption fine structure (EXAFS), photoelectron spectroscopy (PES), magic angle spinning NMR (MASNMR) and NS. Secondly, there are interesting questions concerning transport phenomena in glasses, which give rise to anomalous diffusional behaviours. Matters are made considerably complicated by the slow relaxational times associated with glassy structures. To date, the majority of inorganic glasses modelled with DL_POLY have been silicate based, though borate glasses have also featured, and more abstract forms. The simulation of inorganic glasses by DL_POLY is facilitated by its ability to compute three-body forces.

Silica glass exhibits anomalous low temperature thermal properties, which have been attributed to the existence of low energy excitations, specifically involving tunnelling of (possibly many) SiO_4 units between the minima of double wells in the system. The basis of this attribution has been investigated by Trachenko *et al.* [66], who also studied the occurrence of "floppy modes"—low ω modes, that occur in both the glass and the parent crystal, β-cristobalite. The model glass was derived from defect-free models of amorphous silicon, with substitution by oxygen to make bridging oxygens (BOs). MD simulation was used to relax the structure to the working form, which was a continuous random network of linked tetrahedral units. Several structures were generated with 216, 512 and 4096 SiO_4 tetrahedral units. The PRDFs and structure factors obtained for these structures compared well with NS experiments. The putative tunnelling units were found by calculating the MSDs from the average atomic position. The trajectories of the units with largest displacements showed that these were indeed tunnelling events between two stable positions. The largest displacement observed was of the order 0.8 Å. Estimates of the number of SiO_4 units involved in a typical jump ranged from 30 to 100, consistent with the suggestion that floppy modes are present in these systems. The energy barrier was shown to be less than thermal fluctuation and was estimated to be ~ 0.01 eV by pinning the most displaced atom to prevent it entering either minimum. With regard to system size, it was noted that the frequency of tunnelling decreased markedly in the smaller systems. This was ascribed to correlation between active regions in the glass, which diminished when the system size increased and resulted in events that were more independent. The occurrence of floppy modes, which is associated with rigid unit modes (RUMs) (specifically, of the SiO_4 units), was evident in the

power spectrum of the weighted VAF and was shown to be a feature in common with β-cristobalite. The dynamic structure factor computed from the MD simulations also indicated the greater flexibility of silica glass in comparison with α-cristobalite. The authors evaluated the RUM model in detail using the "split atom" method, in which rigid tetrahedra are linked via harmonic springs, embodied in the program CRUSH. The results, compared with experimental NS data, strongly supported the occurrence of RUMs in silica.

Smith *et al.* [67] have used DL_POLY to investigate the "mixed alkali effect" in alkali disilicate glasses, a phenomenon which occurs as a catastrophic reduction in alkali ion diffusion when an equal mixture of unlike alkali ions is

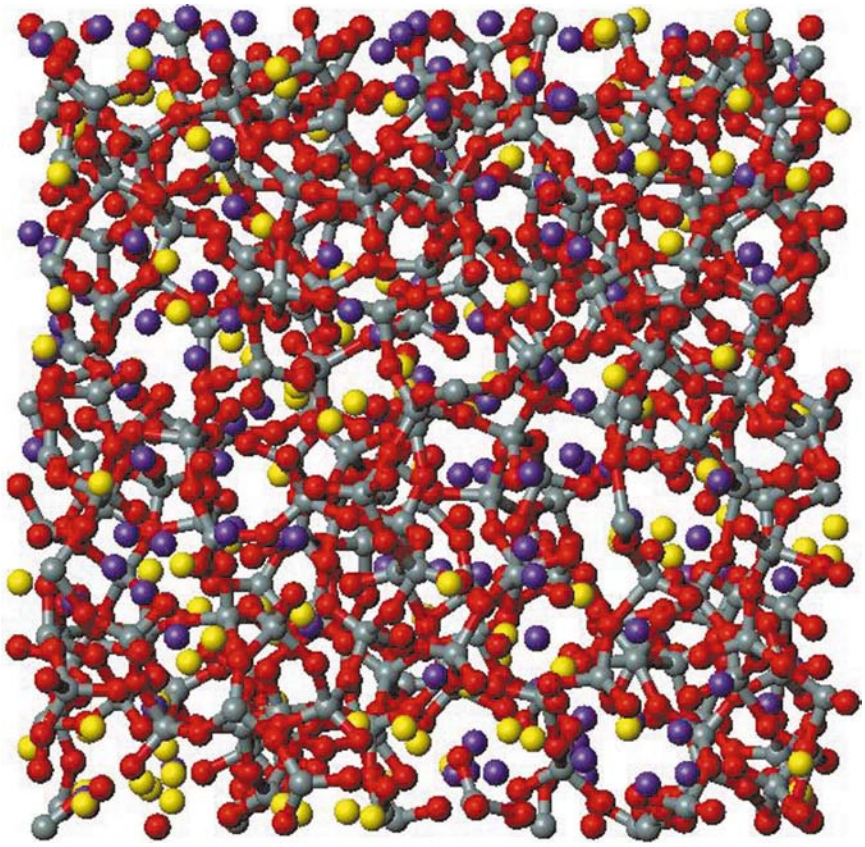

FIGURE 6 Alkali disilicate glass. The simulated structure of sodium potassium dislicate glass from Ref. [67]. Colour scheme: sodium yellow; potassium purple; oxygen red; and silicon gray. Note the tetrahedral SiO_4 units forming a continuous network through oxygen bridges and the presence of voids in the structure, in which the alkali ions reside and undergo diffusion. Fig. drawn by Weblab molecular graphics software from Molecular Simulation Inc.

present. The simulations used 1080 ions (240 M^+, 240 Si^{4+}, 600 O^2) and incorporated a silica glass potential devised by Vessal *et al.* [68], which contained three-body angular terms and carefully constructed two-body Si–O and O–O potentials. The model glass was generated in a procedure, which first swapped ions randomly on a lattice, which was then melted at high temperature before cooling in stages to the desired working temperature. The structure which spontaneously emerged from this procedure bore close resemblance to that determined from experiments on related silicate glasses (Fig. 6). It was found that the model glass possessed a mixed alkali effect under isobaric conditions, which was absent under fixed volume conditions. Calculated van Hove *self* and *distinct* space-time correlation functions revealed that alkali ion hopping (i.e. diffusion) was strongly influenced by the local environment of the alkali ion, which was comprised of mostly non-bridging oxygen (NBO) ions. Mobile ions paid an energy penalty when moving into locations vacated by dissimilar ions, thus giving rise to the mixed alkali effect. The MSD plots exhibited some curvature, which implied a non-Einsteinian diffusion, but was nevertheless within expected statistical error for a random walk process.

Another glass system displaying anomalous behaviour is the alkali alumino silicate glass $Na_2O{\cdot}xAl_2O_3{\cdot}(3-x)SiO_2$, which was examined by Montorsi *et al.* [69,70]. Such glasses show anomalies in physical properties, such as density, viscosity, conductivity, elastic modulus and refractive index, which occur at particular values of the ratio (R) of aluminium to alkali. It is believed that when $R \leq 1$, the Al atom subsitutes for Si in the SiO_4 units and thus behaves as a glass former. When $R > 1$ Al may either form AlO_6 units or give rise to three bridging oxygen (TBO) species (i.e. 3-coordinated oxygen). MD simulations using DL_POLY were carried out to investigate these possibilities. Starting from β-cristobalite a lengthy melting and quenching procedure was used to generate the model glasses, which possessed different R ratios ranging from 0 to 2. (Different starting conditions were also used to check the veracity of the results.) The structural properties of each glass were studied in detail, in order to explain the origin of the observed anomalies. The simulation results established that for BO species Na–BO and Si–BO, the concentration increased with increasing R, while the opposite occured for Al–BO, though Al accounted for 50% or more of all the BOs throughout the series. The concentration of NBO species decreased with increasing R, but few of these were bonded to Al. These changes were responsible for increased localisation of Na ions, which would therefore contribute to anomalous transport effects. Increasing R however, also led to increased TBO concentration, mainly associated with Al. The coordination number for Al remained at four across the R range studied, and it increased for Na continuously. For Si it fluctuated about four. Analysis of the Q_n species density (n is the number

of BOs bonded to a network forming atom) showed that Q_4 species dominated in all cases. However while no trends were observed in the Al Q_n densities with increasing R, noticeable compensatory changes were seen for Q_3 and Q_4 for Si. A trend towards smaller ring sizes with increased alumina content was noted, which was thought a probable consequence of reduced concentration of NBOs. These results clearly indicated that anomalous properties of these systems were related to the structural changes about the Si atoms. The consistency between the MD simulations and the glass structure according to experimental evidence has been summarised by Leonelli *et al.* in Ref. [71]. A clear consensus between the two is apparent.

Boron is another element capable of acting as a glass former. In Ref. [72] Gou *et al.* used DL_POLY to study the structure of the sodium borosilicate glass $(B_2O_3)_x(Na_2Si_2O_5)_{1-x}$. The interesting feature of borosilicate glasses is the possible existence of 3- and 4-coordinate boron: the trigonal BO_3 and tetrahedral BO_4 units, respectively. The modifying effects of added alkali represent an added complexity, as in the observed preference of Na^+ ions for the borate network observed in NMR experiments. The simulated systems were prepared from well established sodium disilicate glass systems, with random substitution of silicon by boron and the random removal of oxygen atoms to preserve stoichiometry. This provided systems with $x = 0.3$, $x = 0.5$ and $x = 0.7$. The new structures were relaxed under NPT conditions and annealed at 4000 K before quenching to the temperature 1000 K, where the MD simulations were performed. The potentials included both pair and three body terms. The structures obtained showed a tendency for the borate and silicate to gather into different regions as the fraction of borate increased. This was expected on geometrical grounds, from the respective sizes of the ions, however it has not been observed in X-ray diffraction. The PRDFs for B–O were asymmetric compared with Si–O and while the mean Si–O separation was constant with x, the B–O average increased with x. Furthermore the coordination number of silicon remained at four, while for boron it decreased from 3.7 to 3.4 as x increased from 0.3 to 0.7. The bond angle distribution O–B–O was broader than O–Si–O, and was taken as evidence of non-tetrahedral B–O geometries. These observations are consistent with an increasing proportion of BO_3 units. In parallel with an increasing B_2O_3 content a decreasing Na_2O content occurs. The PRDFs revealed an increase in the Na–B coordination and a fall in Na–Si, which supported the experimental observation. Associated with this was an increase in Na–O coordination, which corresponds to increasing number of NBOs with increasing borate concentration.

The doping of glasses by rare-earth ions provides a means for probing short range order through the phenomenon of luminescence. Bernard and collaborators [73–76] has applied DL_POLY in MD studies of such systems. From the

obtained short range order around the dopant ion a modified crystal field theory is used to predict the luminescence spectrum. Comparison with experiment thus provides evidence of the local structure.

In Ref. [73] Monteil *et al.* investigated the effect of pressure on europium (Eu^{3+}) doped sodium disilicate glass. The simulations showed that the average Si–O–Si bond angle decreased as the pressure rose to 10 GPa, with little effect thereafter up to 20 GPa. The number of NBOs reduced from 40 to 35% over this pressure range, while the Eu^{3+} ion coordination number rose from 7 to 8. (Practically all oxygen atoms coordinated to Eu^{3+} were NBOs.) Over the same region the mean Eu–O distance reduced only slightly. In consequence of these effects the crystal field strength only weakly depended on the pressure. However a red shift of the $^5D_0 \rightarrow ^7F_0$ transition indicates that covalency is important in reproducing the spectrum. Thus, a modification of the theory to allow for both Eu–O bondlength and Eu coordination number was required. This led to a calculated luminescence spectrum in closer agreement with experiment.

Silica–titania glasses are technologically important as waveguides, with a refractive index determined by the TiO_2/SiO_2 molar ratio. Doping by rare-earth ions also introduces the property of luminescence. Chaussedent *et al.* [74] investigated the properties of erbium doped silica–titania glass by MD and compared results with experimental interpretations. The model glass had a Ti/Si atomic ratio of 8.5% with 0.7% erbium (Er^{3+}) in the bulk. A total of 5000 atoms with Buckingham pair potentials and three-body silica potentials due to Feuston and Garofalini [75]. Three-body titania potentials were not included. The glass was formed by a lengthy melting and staged cooling procedure, reducing from 8000 to 300 K. Four glass systems were produced to permit an improved statistical analysis of the structural properties. It was found that the vitreous silica network was structurally indistinguishable from pure silica in most aspects, with Si retaining four-fold coordination, and preserving Si–O and O–O correlations. However a ring size distribution analysis indicated a depletion in 3- and 4-membered rings, which had an observable effect on the Raman D_1 and D_2 bands. Based on EXAFS experiments the Ti/Si ratio of 8.5% was expected to permit both tetrahedral (TiO_4) and octahedral (TiO_6) units. The simulation gave 68% and 32% four- and five-coordinated titanium ions, respectively. Titanium ions were found to be fairly uniformly distributed through the bulk and a cluster analysis, based on the Ti–O–Ti linkage, established that most (70%) were isolated (i.e. not clustered), a result consistent with Raman spectroscopy and waveguide experiments. Some clustering was observed however, and larger clusters were associated with higher coordination of the titanium. A shoulder to the first peak of the Ti–Ti PRDF, was thought due to Ti–Ti linking via

two common oxygen atoms. Despite the low erbium concentration, the local structure of the erbium ions was clear. An average of 4.92 oxygen atoms surrounded each at a separation of 2.2 Å. Sixty-two percent of erbium ions had 5 oxygens, 23% had 4 and 15% had 6. The Er–Er PRDF possessed two clear, sharp peaks at 2.94 and 3.35 Å, which were ascribed to erbium clustering (via Er–O–Er links). The first peak arose from erbium atoms sharing three oxygens and the second from sharing two. The size of the clusters was seen to correlate with the coordination number of the erbium ions. An analysis of the oxygen coordination showed that the doped glass possessed a small fraction of free oxygens i.e. not associated with any network former. These proved to be coordinated to erbium ions and increased in frequency with increasing erbium coordination number. The consequences of all these structural observations for rare-earth luminescence were predicted to be an increased quenching rate with increasing dopant concentration, and a decreasing crystal field strength with increasing dopant coordination number.

Recently Bernard *et al.* [76] directed this methodology towards germano-silicate glasses, doped with europium (Eu^{3+}) ions. The glass composition had the ratio $Ge/Si = 1$ and 1.17 mol% EU^{3+}. Three body forces were included for both SiO_4 and GeO_4 units in the glass, the latter parameterised to fit the total correlation function ($T(r)$) obtained from NS. The PRDFs obtained revealed that both silicon and germanium had a coordination number of four. Europium had an average coordination of 6.4, arising from a mixture of 6- and 7-coordinated atoms. The Ge–Si and Ge–Ge PRDFs showed each germanium had ~ 3 silicon and 1 germanium as neighbours and a cluster analysis of europium, based on the Eu–O–Eu linkage, indicated that 60% of germanium ions are isolated. This homogeneous dispersion of the silicon and germanium were consistent with the structure inferred from Raman spectroscopy. Sixty-seven percent of BOs were shared between a silicon and a germanium atom and the small number of NBOs were mainly associated with germanium, which implied a more flexible network structure for this element. This was consistent with the observation that the europium medium range environment was richer in germanium than silicon, since the former favours higher coordinated sites. Three and four-fold ring structures were more numerous in the binary system than in the single component glasses, which supported observations concerning Raman D_1 and D_2 bands. From details of the europium environment, the luminescence spectrum was calculated. The result compared favourably with experiment and revealed a reduction in crystal field strength with increasing Eu^{3+} coordination. The splitting of the $^7F_1$ level was larger for the six-fold coordination than for seven-fold. It is clear from the work of Bernard *et al.* that a consistent description of these mixed glasses is emerging, which that ties in well with experimental luminescence spectroscopy.

Biological Systems

The versatility of DL_POLY has made it a useful tool for biological simulations, and it has found application in several fundamental areas, some of which have required large simulations, fully exploiting the parallel capabilities of the code. Also essential is the ability to handle many different molecular topologies and models simultaneously, and many different force-field terms, including Coulombic interactions. The examples below highlight the versatility of DL_POLY in the areas of membranes and proteins, though it is not confined to these.

Membranes

One of the earliest applications of DL_POLY to biological systems was a study of valinomycin at the water/membrane interface by Forester *et al.* [77]. This large simulation (18,866 atoms in all) consisted of eight valinomycin molecules (four in the K^+-VM complexed form), a model membrane consisting of 196 41-bead-spring chains, 3144 SPC water molecules and 27 KCl molecules to preserve ionic strength. The model system was built in stages, commencing from the membrane construction and adding the valinomycin (close to the membrane surface) and water later. The final stage was an equilibration of the system for 200 ps at 310 K (during which the K^+-VM complex was stabilised by additional intramolecular restraints, which were released when the proper simulation began). The production simulation of the system was 100 ps in duration. The results showed that the uncomplexed valinomycin moved to the water/membrane interface where it underwent a pronounced "flattening out"; the hydrophobic (alkyl) parts of the molecule preferring the membrane side and the hydrophilic parts (CO and O groups) preferring the water side. The thickness of the molecule at the interface compared well with small angle X-ray diffraction measurements. The molecular dipole was aligned perpendicular to the interface, and was larger than the experimental dipole in homogeneous solution (and is a plausible factor in attracting wandering potassium ions). Detailed study of the molecular dihedral angles showed clearly that the structure of the molecule at the interface and in solution was quite different. For the K^+-VM complex, there was less tendency to move to the interface, possibly because the hydrophilic interactions were saturated by the potassium ion. However, two of the complex molecules dissociated in the course of the simulation, a reaction triggered by penetration of water molecules into the complex centre. Perhaps significantly, the success of the decomplexation reactions seemed to hinge on the orientation of the complex relative to the surface. Overall the study suggested that the interface has profound

effects on the structure and chemistry of valinomycin and its K^+ complex, and that experimental studies in homogeneous solution should be interpreted with caution.

Smondyrev and Berkowitz, have exploited DL_POLY in a number of impressive studies of phosphatidylcholine membranes in various solvents, often in conjunction with cholesterol (CH) [78–85]. The first priority was to construct a model force-field for these systems, and in Ref. [78] a united atom model was developed and tested on the dipalmitoylphosphatidylcholine (DPPC)/water system (Fig. 7). The derived force-field was based on the AMBER force-field and followed a procedure due to Schlenkrich *et al.* [86]. Atom charges were taken from related work by Chui *et al.* [87]. Special efforts were made to obtain an accurate description of the dihedral potentials. To achieve this the DPPC molecule was sectioned into five distinct parts, each of which were parameterised by reference to "template" molecules sharing the same structural features. The Gaussian code was used to calculate the *ab initio* energy profiles to which the model potentials were fitted. The templates used were ethyltrimethylammonium,

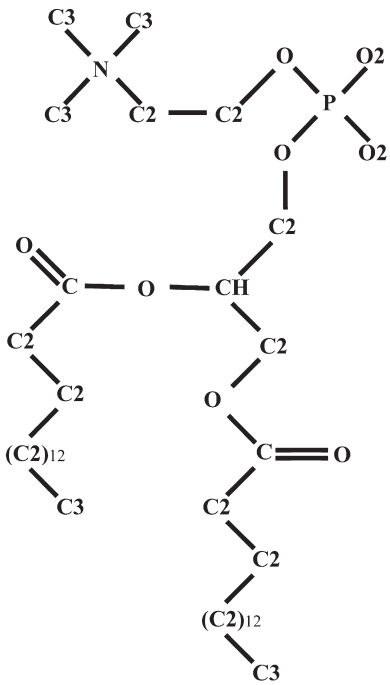

FIGURE 7 Dipalmitoylphosphatidylcholine (DPPC). DPPC is an amphiphile which forms stable bilayers in aqueous systems and which may host additional biological species such as cholesterol. The vector $P \rightarrow N$ in the head group is important in defining the chain orientiation in the bilayer [78–85].

choline, dimethyl phosphate, methyl acetate, ethyl acetate, methyl proprionate. The Ryckaert–Bellemans potential was used to describe the hydrocarbon chains. To test the model, a 1 ns simulation of a 64 molecule DPPC bilayer with 1312 TIP3P water molecules was performed at 323 K and zero pressure, following a lengthy initialisation and equilibration procedure. It was found that the bilayer remained stable over this time, with an equilibrium head area of 61.6 Å^2 and lamellar spacing 59 Å, in good agreement with experiment. It was observed that the head group $P-N$ vector lay almost parallel to the surface. The computed density profiles differed slightly from experimental, but were generally acceptable and the electrostatic bilayer potential was satisfactory. A detailed inspection was made of the dihedral angle distributions throughout the DPPC molecule. This served to show the departure of several important dihedrals from the crystalline structure, and the broad range of the angular variation that arises.

A detailed description of the conformational properties of the two hydrocarbon chains (S_{n-1} and S_{n-2}) in the DPPC/water system was provided in Ref. [79]. The order in the chains was characterised by the S_n^{CD} parameter, as obtained by NMR experiments using isotopic substitution. The S_n^{CD} parameter was related to the simulation data via the equation

$$S_n^{CD} = \frac{2}{3} S_n^{xx} + \frac{1}{3} S_n^{yy},$$

in which

$$S_n^{\alpha\beta} = \frac{1}{2} \langle 3 \cos \theta_\alpha \cos \theta_\beta - \delta_{\alpha\beta} \rangle$$

and $\theta_\gamma (\gamma = x, y, z)$ is the angle made to the bilayer surface normal by the local molecular axis of the nth carbon atom. It was found that the results for the S_{n-2} chain agreed with experimental results and previous simulations. The S_{n-2} and S_{n-1} chains were similar, though for low indices n, the S_{n-1} was the more ordered, while for larger n, it was the less ordered (Fig. 8, top). Also calculated was the order parameter S_n^{CC} :

$$S_n^{CC} = \frac{1}{2} \langle 3 \cos^2 \theta_z - 1 \rangle$$

which showed a marked "even–odd" effect for both chains, particularly the S_{n-1} chain, thus the difference between the chains was more evident for this parameter (Fig. 8, bottom). Experiment suggested that the "even–odd" sequence of the two chains was out of phase with each other, but this was not strongly evident in the simulation. The recurrence relationship

$$-2S_k^{CD} = S_k^{CC} + S_{k+1}^{CC}$$

was tested and found true within a $\sim 5\%$ error. The calculated probability of gauche defects in the chains compared well with infrared (IR) data. Expressions describing the end-to-end length of the chains in terms of the S_n^{CD} and S_k^{CC} order parameters were also investigated and found to be correct within statistical error.

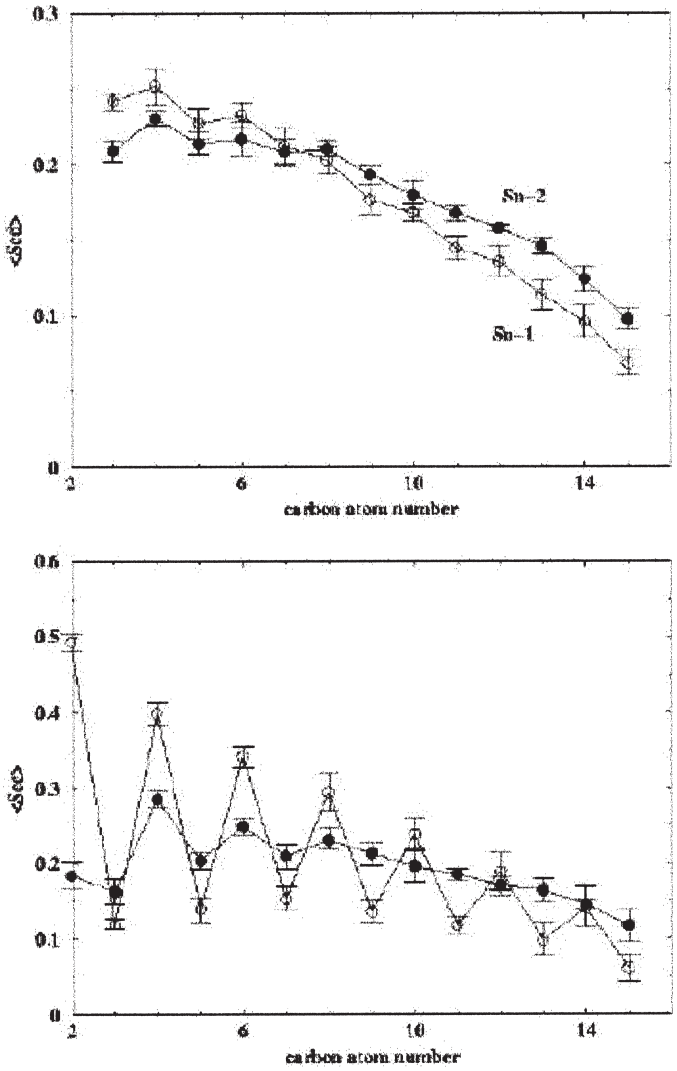

FIGURE 8 DPPC chain order parameters. Variation of the S_n^{CD} (top) and S^{CC} (bottom) order parameters for DPPC in a membrane. The first shows the gradual decay in order with sequence number in the chains and the second shows the strong even–odd behavior. (Key: open-circles S_{n-1} chains; filled circles—S_{n-2} chains.) Fig. reprinted from Ref. [79] with the permission of the authors and the Journal of Chemical Physics.

In Ref. [80] Smondyrev and Berkowitz performed a study of DPPC in dimethylsulfoxide (DMSO), a pharmacologically active solvent, which is thought to modify the structure of bio-membranes. In constant pressure simulations at 323 K it was found that both the headgroup area and the lamella spacing of the DPPC were only slightly diminished, compared to the DPPC/water system (61.6 versus 60.4 $Å^2$ and 58.7 versus 59.0 Å, respectively) and the S_n^{CD} order parameters were little affected. Significantly however, the $P–N$ vector, which made an angle 9° to the lamellar plane in water, was angled $-4°$ in DMSO. The PRDFs showed that repulsion between choline groups was greatly reduced and it was believed that phosphorous atoms had been displaced up and down in the z-direction. Calculations of the electrostatic potential across the bilayer revealed that the overall sign reversed when the solvent was changed (350 mV in DMSO and -600 mV in water). The head group orientation was shown to be a significant factor in this. An analysis of solvent penetration into the bilayer indicated that DMSO was not obviously different from water, though the latter possessed a higher mobility. It was concluded that the repulsive forces between the membranes in DMSO are reduced when compared to water, and that this encourages a closer approach of the membranes.

Cholesterol (CH-Fig. 9) is known to be essential to the functioning of biological membranes. Thus in Ref. [81] Smondyrev and Berkowitz examined the effects of adding CH to the DPPC membrane in both high (1:1) and low (1:8) molar ratios. Simulations of two high cholesterol systems were undertaken: one with alternating DPPC and CH molecules (system A); and one with the CH and DPPC molecules arranged in strips (system B). Also performed was a low

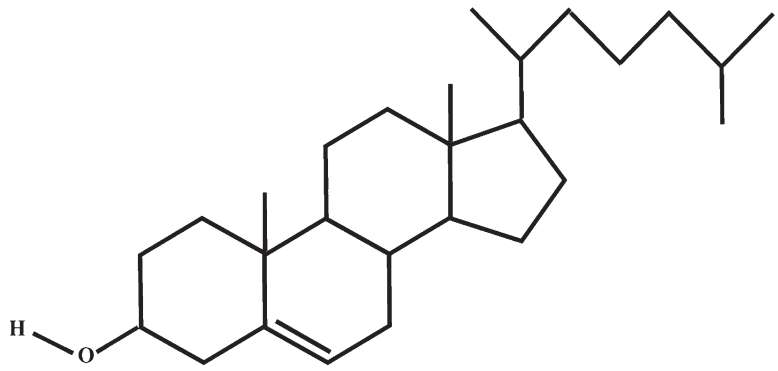

FIGURE 9 Cholesterol. The steroid cholesterol has important biological functions and is known to modify the structure of lipid bilayers. (Note the presence of the hydrophilic OH group and the hydrophobic chain.) Its role in bilayer structure has been investigated by Smondyrev and Berkowitz [81–85].

cholesterol simulation in which the CH molecules were fully solvated by the DPPC chains. All simulations were 2 ns in duration and were at zero pressure and 323 K.

From the initial configurations systems *A* and *B* relaxed to give areas for the DPPC:CH heterodimers of 78.5 and 76.7 $Å^2$, respectively. The CH area alone was estimated as 32 $Å^2$, yielding DPPC areas of 46.5 and 44.7 $Å^2$ for systems *A* and *B*. The low CH system relaxed to a DPPC area of 58.3 $Å^2$. However, it was noted that the membrane surface was rough and contained voids filled with water, making these estimates unreliable. In general the head area per DPPC molecule decreased with increasing CH content.

The important *P*–*N* vector showed an increasing average angle out of the membrane plane towards the water layer as CH concentration increased, though interestingly, the 1:8 system indicated two distinct *P*–*N* populations, reflecting those DPPC molecules close to CH and those more distant.

There were also significant differences in the electron density profile across the membrane compared to the pure DPPC system. With increasing CH content the separation between density maxima (the "hydrophobic thickness") increased and a flat regions appeared between the peaks. These results were analysed in terms of the *z*-densities of individual atoms in DPPC and CH (the *z*-axis being the membrane normal), which revealed, among other things, that the CH hydroxyl group oxygen and the DPPC carbonyl groups have significantly similar *z*-density locations.

The chain ordering was once again characterised by the S_n^{CD} parameters, which revealed little change for the 1:8 system, but increased by a factor of ~ 2 for the 1:1 systems, in agreement with the experimental trend. Also the order factor was more affected in the middle of the chains than the ends. The S_n^{CC} order parameters for the S_{n-1} chains again showed the even–odd effect, and on addition of the CH the effect in the S_{n-2} chain alternates out of phase with the S_{n-1} chain. Interestingly the even–odd effect was almost absent from S_{n-2} chains in system *A*. Closer analysis suggested that the even–odd effect is sensitive to the chain bend near the chain start and the arrangement of the CH in the membranes. It was also apparent that increasing concentrations of the CH reduced the number of chain gauche defects.

CH also increased the magnitude of the membrane dipole potential from ~ 600 mV to ~ 900–1000 mV as concentration rose to the 1:1 ratio. The CH tilt angle, measured against the membrane normal diminished from $\sim 20°$ at low concentration to ~ 11–$12°$ at 1:1, a trend for which there is some experimental evidence. The authors also found evidence of a correlation between the tilt angle and the location of the CH hydroxyl group normal to the membrane plane.

DPPC–water H-bonding was independent of CH concentration and was a factor of three times greater for the S_{n-2} carbonyl oxygen than for the S_{n-1}, as also found in IR experiments. Apart from forming H-bonds with water, CH formed H-bonds with the *P*-oxygen or the S_{n-1} and S_{n-2} carbonyl groups at low concentrations. At high concentrations in system *B*, the CH H-bonding preferred the S_{n-2} chain carbonyl, while in system *A* H-bonding was shared between the S_{n-2} carbonyl and the *P*-oxygen. It was also found that H-bonding with water was reduced when the CH was deeper in the membrane.

DPPC and the related molecule DLPC (dilauroylphosphatidylcholine) both form monolayers at the air/water and carbon tetrachloride/water interfaces. Experimental evidence suggests that DPPC (with 15 CH_n groups in the chains) forms a more ordered chain structure than DLPC (11 CH_n groups) at the air/water interface, with the reverse being true at the CCl_4/water interface. In Ref. [82] Dominguez *et al.* investigated this by simulation. The *z*-densities of the water, head groups and chains for the four systems studied were closely similar, though, as expected, the profile for the chains was wider for DPPC. The *z*-densities for the CCl_4 liquid revealed that relatively few solvent molecules had penetrated the hydrocarbon chains to reach the interface, where the head groups resided. This was confirmed by simulations commencing from different starting conditions. The average angle of the *P*–*N* vectors for DPPC and DLPC were slightly increased in the CCl_4/water interfaces, with the DLPC *P*–*N* vector angle having the larger value. However, for DLPC in the CCl_4/water system, this was clearly the average of two populations pointing above and below the plane of the membrane. By analysing the dependence of chain length on the order parameter S_n^{CC} it was concluded that the chains were tilted, with S_{n-2} chains possessing the larger tilt angles. The results were in reasonable agreement with X-ray and IR experiments, but were subject to large uncertainties. The tilt of the $C_1 - C_n$ connecting vectors indicated a stronger alignment with the interface normal in the CCl_4/water systems. The S_n^{CD} order parameters for DPPC showed that the chains were more ordered in the CCl_4/water system for small and medium values of *n*, but there was a crossover at the 12th carbon, and the order of the chains was thereafter significantly less. The DLPC showed similar behaviour, but in this case the shorter chains did not reach a crossover length. Overall the simulations were not able to confirm the experimental deduction about the relative order of the DPPC and DLPC chains at the different interfaces, though the observed behaviour of the chain ends was in accord with experiment.

The sulfate derivative of cholesterol (CS), also a pharmacologically active compound, was examined by Smondyrev and Berkowtz in a DPPC membrane [83] to determine its difference from the parent steroid [81]. The (1.4 ns) simulation of the 1:1 DPPC/CS system was conducted at zero pressure and 323 K.

Their first observation was that the DPPC/CS system relaxed to a larger area (90 $Å^3$) than DPPC/CH (78.5 $Å^2$). The relaxation was much faster in the CS case. The thickness of the layers in the DPPC/CS system and the electron density profile was intermediate between DPPC/CH and the pure DPPC system and the underlying atomic positions reflected this. The decreased hydrophobic thickness of the DPPC chains in DPPC/CS was reflected in the steroid angle against the membrane normal, which was $\sim 19°$ and larger that found in DPPC/CH. The sulfur of the CS molecules occured at a similar height in the membrane as the DPPC phosphorus and carbonyl atoms. Meanwhile the sodium counter ions remained close to the sulfate groups and formed bridging interactions with the DPPC phosphate. A H-bond analysis showed that membrane hydration in the DPPC/CS system differed from DPPC/CH because the CS molecule was itself more solvated, but also that its presence modified the solvation of the DPPC headgroups. The *P–N* vector in DPPC/CS was close (82°) to the pure DPPC value (81°) and lay closer to the membrane than in the DPPC/CH system (72°), an effect thought due to choline headgroup-sulphate group attraction. Experiment suggested that chain ordering in DPPC/CH was greater than in DPPC/CS. This agreed with calculated S_n^{CD} parameters which indicated that DPPC/CH was more ordered than DPPC/CS, which in turn was more ordered than DPPC alone. Similarly gauche effects and chain lengths were intermediate in the DPPC/CS system. The calculated dipole potential across the bilayer of DPPC/CS was smaller in magnitude (-200 mV) and opposite in sign from the DPPC/CH system (1000 mV). These differences were explained in terms of the different average *P–N* vector angles adopted by these systems and the relative location of the sulfate groups and sodium counter ions in the DPPC/CS system.

Overall the work of Smondyrev and Berkowitz on membrane systems [85] exemplifies the remarkable wealth of detail that may be extracted from MD simulations of these highly complex systems and their relevance to understanding experimental results. It is difficult to imagine how these insights could have been gained by any other approach.

Proteins

The thermodynamics of ligand–receptor interaction in an enzyme/water system has been studied by Chau [88], using a novel modification of the DL_POLY code. In this, pseudo-charges were allocated to the atoms of the ligand and receptor, which interacted via a Coulomb-like force dependent on the distance between the ligand and receptor centres of mass. The pseudo-charges were slowly increased with time, causing the unbinding of the ligand from the receptor. The increase

was slow enough to ensure equilibration throughout the process. This method permitted calculation of the Helmholtz free energy of the ligand-receptor binding, via the difference in energy between the bound and unbound states in the Nosé–Hoover NVT ensemble. The method was successfully applied to the complex of retinol and bovine serum retinol-binding protein, where a 850 ps simulation separated the retinol and the protein in a manner consistent with experiment and at the same time yielded a binding free energy of $\sim 180\,\mathrm{kJ\,mol^{-1}}$, which is almost entirely accounted for by the entropy change. The simulation also showed the increase in hydrophobic hydration of retinol as it withdrew from the complex and the change in the water structure that accompanied this.

The structure and stability of proteins *in vacuo* and in solution is a major issue in bio-chemistry and one rich with experimental data. Melchionna *et al.* [89] have examined the stability of the homodimeric enzyme Cu, Zn superoxide dismutase (SOD) (Fig. 10) over a range of temperatures from 80 to 300 K, using the MD package DLPROTEIN [90], which is a development of DL_POLY with an enhanced ability to build and simulate protein systems. On cooling SOD undergoes a "glass-like" transition at $\sim 200\,\mathrm{K}$, from anharmonic to harmonic dynamics, which is observable in quasi-elastic neutron scattering (QENS) experiments. However, the experimental Debye–Waller (DW) factors, which characterise the thermal motions of the nonexchangable H atoms in the enzyme, do not reveal the processes underlying this transition. SOD is a globular protein consisting of two subunits of 16 kD mass, each held stable by eight β strands into a "flattened barrel" structure, which also includes a number of flexible loops and the Cu and Zn ions. The Cu ion is catalytically active, while Zn helps to maintain structural integrity. To explore the stability of SOD, Nosé–Hoover NPT

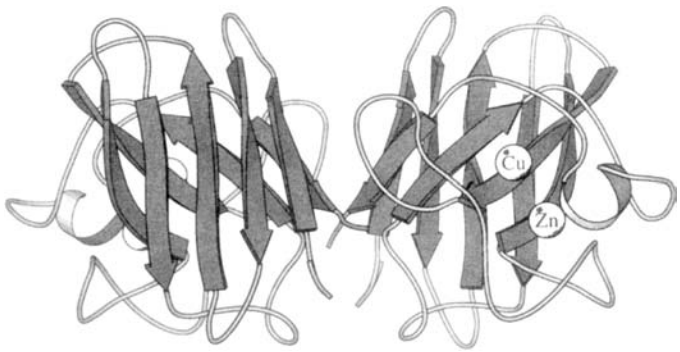

FIGURE 10 Cu, Zn superoxide dismutase. Schematic view of bovine Cu, Zn superoxide dismutase from Refs. [89,92]. The arrows indicate β-strands and the three major loops and four turns are represented by thin wires. Figure reprinted from Ref. [92] with the permission of the authors and Elsevier Science.

simulations were performed, firstly in a solution of 1847 water molecules ($1.06\,\mathrm{g\,H_2O\,g^{-1}}$ protein), and secondly *in vacuo*. In both cases temperatures of 80, 130, 200, 225, 250 and 300 K were investigated. The initial structure was taken from the Brookhaven Protein Data Bank, and the GROMOS 37c and 37d force-fields [91] provided the potential parameters. The system electrostatics were calculated with the Ewald sum and bonds were maintained by the SHAKE algorithm. Several parameters were used to characterise the protein structure. First of these was the "square configurational distance" (SCD) defined as

$$\mathrm{d}^2(t) = \frac{\min}{T,R}\frac{1}{N}\sum_{i=3D_1}^{N} |r_i(t) - r_i(t_0)|^2,$$

where the distances of the atoms from their original positions at time t_0 are minimised (compensated) with respect to the translational (T) and rotational (R) displacement. Also of interest were the second to fourth moments of the distributions of atomic displacements from the mean position ($\sigma^2_{i\alpha}$, $\sigma^3_{i\alpha}$, $\sigma^4_{i\alpha}$; $i = 1, N$; $\alpha = x, y, z$), in which $\sigma^2_{i\alpha}$ is the DW factor. The higher terms provided the anisotropic factors, A_1, A_2 (ellipticity of the displacement distributions) and anharmonicity factors, α_3, α_4 (skewness and kurtosis of the distributions). The 300 K simulations showed that the enzyme structure was stable in water and *in vacuo*, though the latter was more contracted (possessing more internal H-bonds), suggesting the importance of a proper treatment of the solvent. The SCD calculations showed that, at all temperatures studied, the dry SOD had greater structural fluctuation than the solvated form, though both showed increasing fluctuation with increasing temperature. The DW factors, as a function of temperature, agreed well with QENS results up to 250 K, for the solvated SOD, but not the dry form, which were consistently too large. Significantly, there were signs of a transition at about 200 K in the solvated system, where the glass-like transition was expected. The anisotropic and anharmonic factors also showed the dry SOD to be structurally less well defined, while the solvated system again showed signs of a transition near 200 K. Analysis of the contributions to the DW factors from various parts of the enzyme established that the flexible chains contributed most variability to the solvated SOD, while the Cu and Zn ions maintained the most rigid local structures. Analysis of the DW factors of the two monomers separately showed that, above the suspected transition temperature, the two units had different vibrational amplitudes. Finally, a study of the DW factors at different depths within the enzyme ellipsoidal globule, revealed that most of the variability in the structure occurred in the outer reaches, where interaction with the solvent was most significant.

The asymmetry of SOD as a function of temperature was examined in further detail by Falconi *et al.* in Ref. [92]. Once again using the DLPROTEIN variant of

DL_POLY, aqueous SOD was studied in the isothermal–isobaric (NPT) ensemble, at temperatures of 200, 225, 250 and 300 K. Analysis of the secondary structure was made in terms of the peristence of H-bonds in the enzyme backbone and the displacement cross correlation map (DCCM), defined by the correlation coefficient

$$c_{ij} = \frac{\langle \Delta \mathbf{r}_i \cdot \Delta \mathbf{r}_j \rangle}{\sqrt{\langle \Delta \mathbf{r}_i^2 \rangle \langle \Delta \mathbf{r}_i^2 \rangle}}.$$

In addition the time evolution of the dimer was followed through the time dependence of the Voronoi volume of each subunit. The H-bond analysis showed that H-bonds were conserved over 200–25 K, but decreased significantly in the 300 K simulation, where the two subunits were also markedly differentiated (i.e. asymmetric). Plots of the DCCM revealed increasingy different *intra*-subunit correlation between each subunit and also the growth of *inter*-subunit correlation as temperature increased. The Voronoi volume was approximately constant at 40,000 Å^3 over the range 200–250 K but increased to 41,400 Å^3 at 300 K. The static cross correlation of Voronoi volumes from different subunits showed that correlation was strongest at 300 K, in agreement with the DCCM data. However the time dependent cross correlation functions revealed a rapid loss of correlation at 300 K, while long lived oscillation occurred at 200 K. The simulations thus present a picture of this system in which the two subunits are asymmetric and in rapid communication at 300 K, but are symmetric with slow communication at lower temperatures.

Luise *et al.* has applied DLPROTEIN in a study of the solvation of the globular protein azurin [93]. The simulation details were similar to the above examples (i.e. Nosé–Hoover NPT, GROMOS force-field etc.), with the azurin in a cell of 3658 water molecules (or 5 g H_2O g^{-1} protein) and a carefully equilibrated system at 300 K. The stability of the model system was established by examining the RMS deviation for the starting structure and the RMS fluctuations, both of which were satisfactory. The solvent accessible surface (SAS), defined as the surface traced by a solvent-sized sphere "rolling" on the globular surface, was calculated for each protein atom, and the mean residence time of solvation (MRTS) calculated as the "survival probability function" $P_\alpha(t)$ which measures the average number of water molecules that reside within a solvation shell α for a time interval not less than t. (For fitting purposes $P_\alpha(t)$ was assumed to be a single exponential decay.) The first solvation issue examined was the MRTS in relation to protein secondary structure. Most sites had residence times less that 20 ps, though a small number were 100 ps or longer. Those with extreme residence times were trapped in surface holes or crevices. Residence times for the protein

backbone and side chains for different secondary structural elements were similar and it was possible to account for differences by examining the local structure more closely. However, no definitive relationship between structural elements and solvation could be discerned. The next issue studied was the influence of specific atom types, considering such factors as atomic charge and coordination number. Average residence times (τ) for azurin were found to follow the order

$$\tau_{OH} > \tau_{O^-} > \tau_{N^-} = \tau_{NH} > \tau_{CH_2/CH_3} > \tau_{CO} > \tau_{NH_2}$$

which resembled the crystallographic hydrophobicity scale for crystallographic water in proteins. The basis for this resemblance was not fully established, though there was evidence for some water molecules possessing low B-factors in the crystal also having long residence times. Coordination number did not show any clear effect on MRTS. With regard to atomic electrostatic, properties, the order

$$\tau_{\text{charged}} > \tau_{\text{polar}} > \tau_{\text{non-polar}}$$

was found, though it was also noted that this observed order did not apply to all proteins. To assess the influence on MRTS of solvent accessibility to the atomic site an attempt was made to correlate the MRTS with the average SAS of the different atom types. It was found that sites with SAS areas $\geq 16\,\text{Å}^2$ had residence times < 20 ps, irrespective of the properties of the atomic site. SAS areas $< 16\,\text{Å}^2$ for certain atoms, such as charged nitrogen and charged and polar oxygen on lateral chains, were associated with long residence times. However, this observation did not apply to the protein backbone. Residence times for carbon atoms were usually short, irrespective of SAS area. Finally, a detailed study of particular cases, where very long residence times had been found, revealed that the degree of H-bonding in the vicinity of the site concerned was a key factor. If the opportunity for intra-protein H-bonding was low or absent, full H-bonding with the water led to long residence times. Overall the results of this research showed that solvent residence times in proteins are strongly influenced by the SAS, and that the individual characteristics of the atomic sites have only a subordinate influence.

Surfaces and Interfaces

The study of interfaces is an important and very active subject of research. The surface is where a great many chemical processes take place. Most of the simulation studies of inorganic solids using DL_POLY are based on Born model [94] of solids which assumes that the ions interact via short-range forces which can be described by simple analytical functions, such as the Buckingham potential, and long-range electrostatic Coulombic interaction. In DL_POLY the

latter interactions are treated with the Ewald summation method for three-dimensional periodic systems. The surface materials are usually modelled as periodic slabs, infinite in two-dimensions and separated by sufficiently large periodic gaps in the third dimension to minimise interactions between slabs. Ewald based molecular simulations with DL_POLY provide atomistic descriptions, and hence clues to a variety of interfacial processes in many real systems. In most cases, with proper selection of potential parameters, good qualitative, and in some cases quantitative, agreements have been obtained between simulations and experimental results.

Solid Interfaces

In environmental sciences it is widely known that mineral surfaces play important roles in geochemical processes such as mineral dissolutions and element cycles at the Earth's surface. However, studies of mineral interfaces are complicated by the fact that most of the geochemical processes occur in aqueous medium and marked differences in behaviour exist between vacuum and aqueous medium interfaces. The complex properties of water makes studies of aqueous interfaces particularly challenging.

In order to understand the water molecule structure at solid interfaces, de Leeuw and Parker [95] have considered a simple ceramic oxide: MgO. Using DL_POLY, they have derived a new water potential model compatible with existing potential models for inorganic solids with an aim of simulating aqueous surfaces. The model was empirically fitted to reproduce the experimentally determined water structures and dipole moment. In addition, the model also included a dynamic variant of the shell model of Dick and Overhauser [96,97] to incorporate the effects of polarisability of the oxygen ion. Two MgO surfaces have been considered: the most stable (001) surface consisted of a MgO $4 \times 4 \times 4$ supercell containing 256 MgO units with 30 Å gaps between repeating surface slabs; and the (310) surface consisted of 384 MgO units and repeating gaps of 25 Å. The structure of the latter surface consisted of a series of tilted (001) planes terminated with steps to represent the experimental model of the (001) surface. The gaps were filled with NPT equilibrated bulk water with a density of $\sim 1\,\mathrm{g\,cm^{-3}}$ and the system simulated under NPT (Nosé–Hoover) conditions. The *in vacuo* conditions were simulated as an NVT system. The structure of water at the surfaces was analysed in terms of RDFs and MSD diffusion coefficients. Both surfaces showed a marked decrease of densities and an increase of diffusion coefficients when compared with the simulated bulk water. In the case of the (001) surface the RDF and density profile showed there was a preferred

orientation of the first layer of water molecules towards the surface. However, this ordering was quickly disrupted due to the energetically unfavourable interactions between adsorbed molecules and bulk water molecules. As a result, there was an absence of layer ordering beyond the first layer. In the case of the (310) surface there was a preferential adsorption of the oxygen atoms from the water in the interstitial lattice oxygen sites between a step edge and a plane below. However, there was no similar pattern of adsorption on the remainder of the (001) planes making up the stepped (310) surface.

The same water model was also applied to study dissolution processes of calcite mineral ($CaCO_3$) [98]. In this paper, the most stable calcite surface was considered. The surface is more complicated than that of MgO whereby the plane is terminated by two different monatomic steps: an acute monatomic step with the carbonate groups on the edge overhanging the plane below; and an obtuse step with the carbonate groups on the step edge leaning back with respect to the plane below. The dissolution process was determined by calculating surface energy and dissolution energy. The results showed that the dissolution trends both *in vacuo* and in aqueous conditions were rather similar, with dissolution processes occurring preferentially at the obtuse steps. However, in aqueous conditions the surfaces were stabilised by the adsorption of water molecules and this produced a larger difference in dissolution energies between the two different steps. Furthermore, the adsorption patterns of water molecules were different for the two different steps, even though both steps contained a similar plane. A schematic representation of step-by-step removal of calcium carbonate units with associated dissolution energies was presented. This illustrated possible dissolution pathways and the formation of the kink sites on the dissolving edge of the obtuse step was identified as the rate-determining step. These findings, both *in vacuo* and in aqueous conditions were found to be in good agreement with the experimental observations.

Warne *et al.* [99] used DL_POLY to study the behaviour of water molecules at the complicated surfaces of kaolin ($Si_2Al_2O_5(OH)_4$) and silica (SiO_2). The (001) surfaces considered in this work have a net dipole moment. At the (001) surface the kaolin clay can be terminated by either Al or Si atoms. In order to eliminate the dipole moment, two kaolinite slabs consisting of 425 atoms were inverted with respect to each other in the simulation cells. 820 TIP3P water molecules were added to the interlayer separation. Similarly, two silica slabs were also constructed with 800 water molecules in order to simulate the aqueous conditions. The MD simulations were carried out using the NVT ensemble and a Berendsen thermostat was used to maintain the temperature at 298 K. Density profiles of the water molecules showed that there was significant ordering of water molecules at the clay surfaces. At the Si surface one or both water

hydrogens could be involved in H-bonding to the surface, whereas at the Al surface all the atoms in the water molecules could form H-bonding to the surface. Conversely, the ordering at the silica surfaces was much less apparent when compared with the kaolinite, may have been due to the amorphous nature of the silica surfaces. Unlike the water interactions on MgO surfaces mentioned above [95] the calculated diffusion coefficients decreased relative to bulk water, signifying a marked increase in the ordering of water molecules. These observations were also supported by the determination of rotational correlation time of the water molecules, τ_c, derived from the P_2 ACF of the angle subtended by the intramolecular H–H-bond vector. Intuitively the kaolinite system was expected to give a smaller diffusion coefficient and a larger value of τ_c, due to a higher degree of ordering of water molecules when compared with the silica system. However, this was not observed in the simulations and the authors attributed these findings to the trapping of water molecules in the cage-like amorphous silica surface and hence the effective surface area was larger than expected. Using the calculated values of diffusion coefficent and τ_c the NMR relaxation time for water has also been estimated.[‡] The ratio of the NMR relaxation times in water and at the silica surface were found to be in good agreement with those obtained from (PFG-NMR) spectroscopy. In addition, Na^+ and Cl^- ions were included in order to study the effect of ionic strength on water adsorption. The results showed that significant ordering was still observed as the ionic strength was increased. However, the ordering at kaolinite surfaces was found to be more sensitive to ionic strength than the silica.

The DL_POLY code has also been used to perform simulations of solid oxide surfaces relevant to industrial applications. For example, Sayle and Watson [100] have carried out large-scale simulations to study thin film support, an important technique in industrial and engineering applications. In this study, they constructed an ultra-thin film of MgO supported on a (001) BaO substrate. The support slab, which defined the size of the simulation cell, was 154.4×154.4 Å^2 corresponding to 28 BaO repeat units. This gave an area of *ca.* 24,000 Å^2, which approaches the meso-scale. The model was divided into two regions: Region I, which contained the MgO thin films and the first few layers of the support where dynamical simulations were carried out; and Region II, which contained fixed atoms representing the rest of the support crystal bulk. All atoms were considered as rigid ions in order to reduce computation costs. An initial coherent structure of MgO was constructed so as to accommodate a +27% lattice misfit with the

[‡]Estimation of NMR relaxation time is beyond the scope of this review article. Readers are advised to refer to Ref. [99] for their brief description and the references therein.

support. In order to simulate thin film rearrangement into a lower energy configuration it was induced to undergo amorphous transition prior to recrystallisation. An initial high temperature of 1000 K was used to induce amorphisation and was then progressively reduced until a final simulation at 0 K was performed, effectively as an energy minimisation, until the energy of the system converged. The MgO thin film did not melt throughout these simulations, as was confirmed by MSD and RDF calculations. The final optimised system showed that the MgO film retains the usual rocksalt structure and the interfacial region is strained compared to the MgO structure further from the interface, an observation which accords with the experimental data. In addition, both MgO and BaO structures were highly defective at the interface. Cation migrations were observed in which some barium ions were found to occupy the magnesium lattice sites within the thin film and vice versa. The large simulation cells also revealed a variety of structural features observed in the real system, such as dislocations, defects, pseudo-hexagonal MgO and even grain boundaries.

Sayle and Watson extended their studies to larger thin films of alkaline-earth metal oxides (CaO, SrO and BaO) supported on MgO (001) [101]. These gave rise, respectively, to lattice misfits of +13, +20 and +27%. The area of the surface substrate studied consisted of 42 MgO repeat units for each side of simulation cell giving an area of *ca.* 31,100 $Å^2$, large enough to reveal the interplay between neighbouring surface defects in one single model. This was in contrast with most previous simulations in which a particular surface structure (e.g. defect or dislocation) was investigated in isolation, so that realistic surface features arising from a lattice misfit could not be adequately shown. The methodology was similar to their previous work [100]. Deconvolution techniques were used to identify the various modified interfacial features, which were then displayed graphically to aid interpretation. Numerous complex interfacial structures were identified. For example, in the CaO/MgO (001) system, regions coherent with the underlying MgO support and of area *ca.* 300 $Å^2$ in size, adjoined with incoherent regions of similar sizes. These were separated from one another by both screw and edge dislocations. In the coherent regions the ions shared favourable coulombic interaction and as a result the CaO plane lay close to the MgO support with a normal interfacial distance of about 2.4 Å. Conversely, unfavourable coulombic interaction between the CaO film and the MgO support resulted in the incoherent regions being lifted up, so the interfacial distance increased to about 4 Å. Such lifting effects were made possible by the formation of screw dislocations. In the case of SrO/MgO (001) and BaO/MgO (001) systems, due to higher lattice misfits, no coherent region could be observed. In the former case a range of domains commensurate between the thin film and support were observed, each with varying degree of reduction in lattice misfits. For example, a

domain was identified where eight SrO lattice units were matched with 10 lattice units of the underlying MgO support. The SrO had expanded slightly to match with the MgO lattice and the lattice misfit was reduced to about 2.3%. Similarly, for the BaO/MgO (001) system, domains rotated relative to the surrounding BaO lattice were observed. Other features were identified, such as defects and lattice slips. This work further highlights the fact that a variety of structural modifications can be observed in a single large simulation model. In this way, a particular feature can be more realistically investigated and the cause identified.

The same researchers [102] have also studied more complicated support materials, such as the perovskite $SrTiO_3$, which are used as substrates for the epitaxial growth of superconducting films. In this work, the MgO and BaO are used as thin films. A surface of the perovskite (001) with an area of *ca.* 24,400 $Å^2$ was constructed corresponding to 40×40 $SrTiO_3$ repeat units. The vacuum gaps between the periodic support slabs were 80 Å for the $MgO/SrTiO_3$ system and 65 $Å^2$ for the $BaO/SrTiO_3$ system. Once again, rigid ion model was used and the Coulombic interactions treated with the three-dimensional Ewald summation method. The perovskite (001) can have two different surfaces: SrO or TiO_2 terminated surfaces and hence two sets of results were reported for each support system. The results showed that both systems show different structural characteristics depending on the lattice misfit occurring in each system. For example, the MgO film was oriented at $\mathring{0}$ with respect to the underlying $SrTiO_3$ while the larger BaO film underwent rotation about an axis normal to the support surface so as to reduce the lattice misfits.

San-Miguel and Rodger [103] have carried out MD simulations of wax deposition, an important industrial phenomenon that affects the efficiency of transport processes in oil and gas pipelines. The model consisted of hematite (Fe_2O_3) (0001) surface and C28 alkane chains (*n*-octacosane) were used to represent wax. The hematite surface was used since pipelines are usually made of mild steel that forms an oxide film. In addition, the authors have performed simulations for the adsorption of oleic imidazoline, which is a corrosion inhibitor. The aim was to investigate how the inhibitor affects wax deposition. A non-polar Fe-terminated hematite slab of 1920 particles was constructed with a vacuum of 60 Å between its periodic images. Both the wax and the C12 alkane tail of the corrosion inhibitor were described by a united-atom model. The head of the inhibitor consists of an imidazoline ring with an aminoethyl group, which was represented by an all-atom model using the CHARMM force-field. Charges, derived from Hartree-Fock calculations, were also assigned to the head group. The simulations were carried out in the NVT ensemble using the Ewald summation method to evaluate the electrostatic interactions. To relax the system, the temperature was maintained at 2 K rather than the 0 K for the usual

minimisation method in order to reduce symmetry restrictions while at the same time encouraging structure optimisation. Using different starting configurations, the wax was found to adsorb favourably in a straight line between two rows of surface cations. To simulate wax deposition, monolayers of the alkane chains were added in stages and the 2 K minimisation procedure was carried out for each stage. The RDF for the deposited wax was shown to be quite similar to that of C28 crystal, which implies that the hematite surface provides a suitable platform for the crystal growth of wax. In the case of inhibitor deposition the head group was strongly bound to, and hence blocked, the active surface cations. At high coverages the hydrocarbon tails adopted an angle of 10–30° to the surface, forming a hydrophobic film that was resistant to water in a pipe. The initial study also indicated that the wax crystal could be deposited, in a physisorbed manner, onto the inhibitor films. The energies of adsorption varied according to the tilt angle of the hydrocarbon tails and this indicated the possibility of reducing wax deposition by changing the tail ordering.

In a real system, the wax may also self-crystallise in oil and this poses a problem in oil production and transportation. A simulation study [104] was carried out to investigate how the addition of a growth inhibitor may affect the paraffin wax crystal growth. The simulation system consisted of the periodic crystal slabs of the C28 wax and represented by a united atom model. The inhibitor chosen was poly(octadecyl acrylate) (PA-18), a comb-like polymer which is known to be effective in inhibiting wax formation. The model inhibitor consisted of two hydrocarbon side-chains represented by a united atom model and a short segment of backbone. Atoms close to the backbone were assigned with charges derived from *ab initio* calculations. A direct Coulomb interaction, with a cut-off of 15 Å, was used to describe the electrostatic contributions. This ensured that electrostatic contributions from periodic self-images were not included. The NVT simulations were carried out at 2 K to obtain relaxed structures (see above) and at 293 K to determine the properties of the surfaces. In addition, NPT simulations were carried out to determine relaxed crystal structures. In both ensembles Nosé–Hoover methods were used to control the temperature and pressure. The simulation showed good alignment of the inhibitor on all the low index surfaces (100, 010 and 110) with the side-chains aligned with the wax surface molecules, while the backbone segment of the inhibitor lay over or close to the crystal lamellae gap. This was consistent with the notion that inhibitors need to be compatible with surface structure of the host crystal. Two simulation procedures were used to study the effect of the inhibitor. The first involved step-wise additions of two layers of "perfect wax crystal" to the surface, with the intention of assessing the structural influence of the inhibitor with minimum disruption to the crystals. It was found that structures and energies of

the wax alkane molecules near to the inhibitor changed markedly according to the conformations of the latter. In the second procedure, crystal growth was simulated by adding an alkane chain in stages. While the growth introduced surface steps which masked the effect of the inhibitor, it was evident that the PA-18 dimer, adsorbed with side chains pointing in the opposite direction, introduced long-range disorder into the growing crystal.

DL_POLY is not confined to equilibrium simulations. Some workers have adapted the code to study non-equilibrium process at interfaces. For example, Tepper and Briels [105] have applied the code to the growth and melting processes of the atomic fcc (100) interface. The aim was to investigate the kinetics of the solid–liquid phase transition i.e. to address crystallisation and melting processes at the solid/liquid interface and show whether or not the interface response is symmetric around the equilibrium temperature. A simple system was constructed without long-range interactions and corrections. Spheres were used as the atomic model, interacting via the short range modified 12–6 L–J potentials introduced by Clarke *et al.* [106]. This potential form has been modified so that it is exactly zero beyond the cut off distance without changing the location of the potential minimum. The Nosé–Hoover thermostat and barostat were used in the NPT simulations. The relaxation times were chosen such that both liquid and solid fcc phase gave correct pressure and temperature distributions and the fluctuations of both properties did not interact. Initially, a solid phase and a liquid phase were independently equilibrated by NVT simulation. After that the two boxes were combined at the $x-y$ plane to produce a solid/liquid interface. To resolve particle overlaps at the interface NVT simulations were carried out with strict temperature scaling at every time step. After which, NPT simulations were performed to study growth and melting processes. To distinguish particles in the solid phase from the liquid phase, an octahedral order parameter was calculated, which probed the formation of octahedral symmetry of the nearest neighbours around a particle in an fcc crystal. In this way the crystal growth rate (obtained from the slope of a plot of the number of solid particles versus time) for a given temperature was determined. A plot of growth rate versus temperature revealed a discontinuity near to the equilibrium point (zero growth rate). In other words, the growth and melting rate near to the equilibrium temperature were asymmetric in nature. The particle configurations revealed that the asymmetric feature might arise due to the formation of lattice imperfections during crystal growth. However, if a simulation was repeated from a final configuration with a given undercooled temperature and superheated by the same amount referenced at the equilibrium point the asymmetry between growth and melt rates completely disappears. This highlights the subtlety in the preparation of initial configurations.

High-energy particle beam implantations and depositions are important techniques often used to modify chemical and physical aspects of materials. Kholmurodov *et al.* [107] have applied DL_POLY to a study of cluster-surface impact processes. Prior to the study, the original DL_POLY code was modified to perform efficiently on the Fujitsu VPP700 vector computer, a platform for which the original code was not designed. The modifications enabled particularly large simulations, in this case consisting of a large surface substrate of 36,000 aluminium atoms and a cubic Al cluster projectile of 864 atoms. The Sutton-Chen potential [108] was used to describe the metallic forces and a Berendsen thermostat was applied to maintain temperature control during the simulations. To model an impact the projectile was thermalised to 5 K and "fired" at the surface with various incident energies: (i) $E_{\text{inc}} < 0.15\,\text{eV atom}^{-1}$ (soft landing regime); (ii) $E_{\text{inc}} = 0.56\,\text{eV atom}^{-1}$ (spreading droplet regime); and (iii) $E_{\text{inc}} = 3.5\,\text{eV atom}^{-1}$ (implantation regime). In case (i) the impact layers of the projectile rose in temperature to ~ 400 K and the projectile density increased by 50%, but there was no melting and penetration of the surface was slight (~ 2 Å). The bulk below the surface was only slightly perturbed by the impact and the system returned to a normal thermal condition in ~ 3.0 ps. In case (ii), on initial impact the cluster density was little affected and the temperature was surprisingly higher (1500 K) in the centre than at the leading or back faces, though after ~ 5 ps the centre was cooler than the faces. Penetration of the surface was again slight (~ 3 Å), but the projectile spread out thinly on the surface, a process said to resemble the spreading of a molten droplet on a cold solid substrate. In the highest energy impact (iii), the temperature profile of the projectile initially followed the same pattern as case (ii), though the local temperatures were much larger (> 3000 K in the projectile centre). After a lapse of ~ 5 ps the projectile temperature was highest at the leading face, but was already much reduced (200 K). Penetration of the surface was deep (~ 7 Å) and a liquid like phase occurred where projectile and surface atoms mixed easily. Evidence for this new phase was provided in the MSD plots, which were markedly different from the solid state. Spreading of the projectile during the impact was considerable and throughout the impact process there was substantial inhomogeneity in the temperature and particle distributions. There was no significant reflection of shock waves from the system boundaries, an effect that was attributed to the thermostat used.

Liquid Interfaces

Among the most common simulations involving liquid surfaces are those of water, due to its natural importance in biological, environmental and industrial

processes. The gas–liquid interface may be modelled as a liquid slab, while for a liquid/liquid interface both liquid components may be equilibrated in separate simulation boxes before they are combined into one large system. Somasundaram *et al.* [109] have used DL_POLY to study the passage of a single gas solute molecule across a water/vapour interface. The simulation systems consisted of periodically repeated slabs of liquid water, 15 Å thick, using the SPC/E water model. A range of solutes was simulated with differing polar properties: CO_2 and N_2 (molecules with quadrupole moments); acetonitrile CH_3CN (a dipolar organic molecule); and argon (a neutral molecule). Combining rules were used to obtain the L–J parameters for the solute–water oxygen interactions. The adequacy of the selected potential parameters for CO_2 and N_2 had been established in previous work [110], which also used DL_POLY, and which found various bulk solution properties in good agreement with experiment. The free energy profiles, $A(z)$, were used to quantify the passage of the solutes across the interface. The coordinate pathway in this work was the perpendicular axis, z, to the water surface.

$$A(z) = U(z) - TS(z)$$

To obtain the free energy profile, the centre of mass of the water molecules was constrained at $z = 0$ throughout the simulation, meanwhile the solute was held at a fixed position; $z = z_s$, at which the z-component of the mean force was calculated. Integration of this force over a range of fixed positions provided the free energy profile [109]. The result was that for all solutes a free energy minimum near to the interface was obtained which corresponded to an adsorbed state, where the solutes lay on the water surface. The free energies gradually increased until steady bulk values were obtained at around 5 Å beneath the water surface. To compliment the local structure analysis, the authors determined the passage of solutes at the water/vapour interface to be a two-stage process: passage from vapour to the adsorbed state and subsequently incorporation of the solute into bulk. To determine the rate-determining step DL_POLY was used to obtain the kinetic information of the CO_2 and N_2 passage through the interface [111]. The results indicated that the solutes were less likely to penetrate into the bulk solution than escape back to the gas phase and hence the rate-determining step was the second stage or the surface-liquid step. In addition, a similar model has also been used to investigate the velocity distribution of the desorbing molecules [112]. The results were found to agree with the Maxwell thermal flux distribution and there was no peak in the free energy profile for the desorption.

Properties of the interfacial region between two immiscible liquids have also been studied by Fernandes *et al.* [113] who has simulated the water/1,2-dichoroethane (DCE) interface. The water/DCE system was constructed from

two separate triclinic simulation boxes, one containing 363 water molecules and the other 100 DCE molecules, both at their correct bulk densities. The two systems were equilibrated separately in the canonical ensemble under three-dimensional periodic boundary conditions for 250 ps. After which, the z-periodic boundary conditions were removed and both systems re-equilibrated for a further 250 ps. Each open box produced two liquid/vapour interfaces in the $x-y$ plane and a bulk liquid region. Finally, the two boxes were combined to give one unified box with open ends in the z-direction. The resulting simulation box, containing both liquids, was equilibrated for 500 ps. Results were obtained from a further run of 250 ps with the thermostat removed. Measurements such as density and positional profiles showed a sharp interface with no mixed region and small interpenetrations. Furthermore, the interface was found to be non-planar due to the thermal motion of the interfacial molecules of both liquids.

In order to study ion transfers between liquid/liquid interface, a process that is still poorly understood, Fernandes *et al.* [114–117] carried out a series of MD simulations of water and 2-heptanone (HPT2) interfaces. The organic solvent has been widely used in industrial ion extraction processes due to its low toxicity. Because of the complexity of the subject the investigation was carried out in stages. Suitable potential sets were first tested in the simulations of bulk liquid HPT2, both in pure form and saturated with water [114]. The water was described by the SPC/E model, while for the organic solvent the carbonyl group was explicitly treated and a united atom model used to represent the hydrocarbon groups. The CHARMM force-field provided the intramolecular interactions in the HPT2 molecules. Rigid water molecules were chosen for computational efficiency; coupling of internal motions such as vibration and bond bendings between water and the system being regarded as unimportant. In the simulations of pure HPT2 the OPLS and CHARMM force-fields were used with combinations of charges derived from different methods. In the case of the saturated form the potential parameters for H_2O–HPT2 interactions were obtained by the usual combination rules:

$$\sigma_{ij} = \frac{\sigma_i + \sigma_j}{2} \quad \varepsilon_{ij} = \sqrt{\varepsilon_i \varepsilon_j}$$

The results indicated that the different potential models did not affect the simulation results to any significant extent. For example, densities and thermodynamic data of pure HPT2 liquid, such as heat of vapourisation, were rather similar between potential models and in reasonable agreement with experiment, suggesting transferability of the potential sets without further reoptimisation. This may be the case in systems such as HPT2, where coulombic interactions are not a major contribution to the interaction.

Using the potential models from their previous work [114], this research group [115] has carried out calculations on the water/HPT2 interface. As in the case of [113] the system initially consisted of two separate simulation boxes: one containing 794 water molecules and the other with 168 HPT2 molecules saturated with 15 water molecules. Independent equilibrations were carried out in the NPT ensemble to avoid any anomalous influences on the formation of the interface due to volume constraints. The boxes were then joined in one single box of same cross sectional area. A scaling factor was used for H_2O/HPT2 intermolecular interactions. This scaling factor was initially set at a very small value and gradually increased during equilibration runs until the interaction potentials reached their full values. This was to stabilise the system at the interfacial region when the simulation boxes were combined. Afterwards, equilibration of the interface system was carried out for 150 ps. Data collections were performed for the subsequent 300 ps run. The temperature and pressure were maintained at 300 K and 1 bar respectively using the Nosé–Hoover methods.

The density profile perpendicular to the interfacial plane, revealed two stable interfaces with the correct bulk density and the percentage of water in HPT2 at an average value of 1.57% (w/w), close to the experimental value. The profile also revealed interpenetration of the liquid molecules at the interfacial region. However, the density profile only indicated the global structure as it was obtained over the whole area for a given distance profile. In order to probe local interfacial structure, the interfacial plane was divided into $N \times N$ squares and within each square local surface structure and width of interface were determined for each saved equilibrium configuration. The distribution of surface widths as a function of N revealed a shift toward smaller values of width with increasing peak sharpness as N increased. This signified that at the water/HPT2 interface underwent shape deformation rather than interpenetration. In other words, the structure of the interface was very corrugated by short wavelength capillary waves. It is noteworthy that if there was a gradual change of liquid composition over the interface, as the density profile suggested, the distribution curves would be expected to centre at the same position.

In addition, the RDFs of various atomic pairs have been determined to probe the atomic structure at the interface. Coupled with the orientational information such as the angle between the molecular or dipole moment vector with surface normal, a detailed description of the molecular structure of the liquids could be obtained. For example, at the interfacial region, the hydrophilic carbonyl group tended to point towards the aqueous phase and the hydrophobic hydrocarbon chain towards the organic phase. The second HPT2 layer reversed this orientation to form a bilayer structure. Such ordering gradually vanished when moving into

the organic bulk. On the other hand, the water structure was only slightly affected by the presence of the organic phase. Hydrogen bonds formed between water hydrogen and the carbonyl oxygen. The arrangement of the water molecules was such that their dipole vectors were parallel to the interfacial plane. Such ordering extended for 2–3 molecular layers into the aqueous phase. The dynamical properties, such as diffusion coefficients, showed that the diffusion of both liquids occured quicker in directions parallel to the interface plane, and slower perpendicular to it.

Fernandes *et al.* [116] also performed MD simulations of the water/iso-octane (ISOC) interface to compare with the water/HPT2 interface. The structure of ISOC is essentially a hydrophobic analogue of HPT2 whereby the oxygen atom of the HPT2 is replaced by a methyl group. This work presented a new way to calculate the density profile. Instead of a fixed reference origin to define the static volume of slabs in the density calculations, the slabs were redefined by reference to the instantaneous interface position at a given simulation time. The interfacial planes were sub-divided into 4×4 equal square areas and in each the molecules with the largest coordinate displacement (largest protrusion into the other phase) was determined so as to define the local interface positions. The new method, refered to as the non planar dynamics slabs (NPDS), showed the packing of liquids against each other at the interfacial region (Fig. 11). For water/ISOC the results clearly showed that the organic solvent had a more pronounced packing effect which propagated strongly into the bulk. Similar packing behaviour was observed in the case of water/HPT2 interface. The local interfacial structure, obtained by similar methods to those outlined above [115], showed once again, that the interfacial structures were highly corrugated by capillary waves, similar to the water/HPT2 interface. The liquid phases protruded into each other, without actual solvation taking place. The average width of the interfacial region between water/ISOC and water/HPT2 were rather similar and this indicated that changing the nature of solvent had little effect on the interpenetration of the solvents.

The detailed understanding of the interfacial behaviour of the above-mentioned interfaces has also paved a way for the study of ion transfer. The iodide ion was chosen for an investigation of the ion passage across the liquid interfaces [116], for which the free energy profile was determined. The reaction coordinate in this case was the distance of the ion from the interface, starting from the bulk liquid phase. At each fixed ion position, following equilibration for 0.5 ps, the forces acting on the ion were collected over 2 ps. The ion was then moved along the reaction coordinate by 0.05 Å and the calculation repeated. The procedure was repeated until the iodide ion reached the other bulk phase. The potential of mean force (PMF) profiles showed a gradual increase, with no peak, of the Gibbs free energy as the ion left the aqueous phase and moved towards the

organic phase. This showed that the iodide ion was more stable in the aqueous phase, as expected. The Gibbs free energy for the iodide transfer across the water/HPT2 interface was calculated as $-24.7 \pm 3.4\,\mathrm{kJ\,mol^{-1}}$ which agreed well with the experimental result ($-21.9\,\mathrm{kJ\,mol^{-1}}$). From the PMF profiles it was shown that the I^- in the water/ISOC system had a much higher Gibbs free energy than in the water/HPT2 system. This is reasonable since the ion was expected to be less soluble in ISOC than in HPT2. The RDFs and animated trajectories

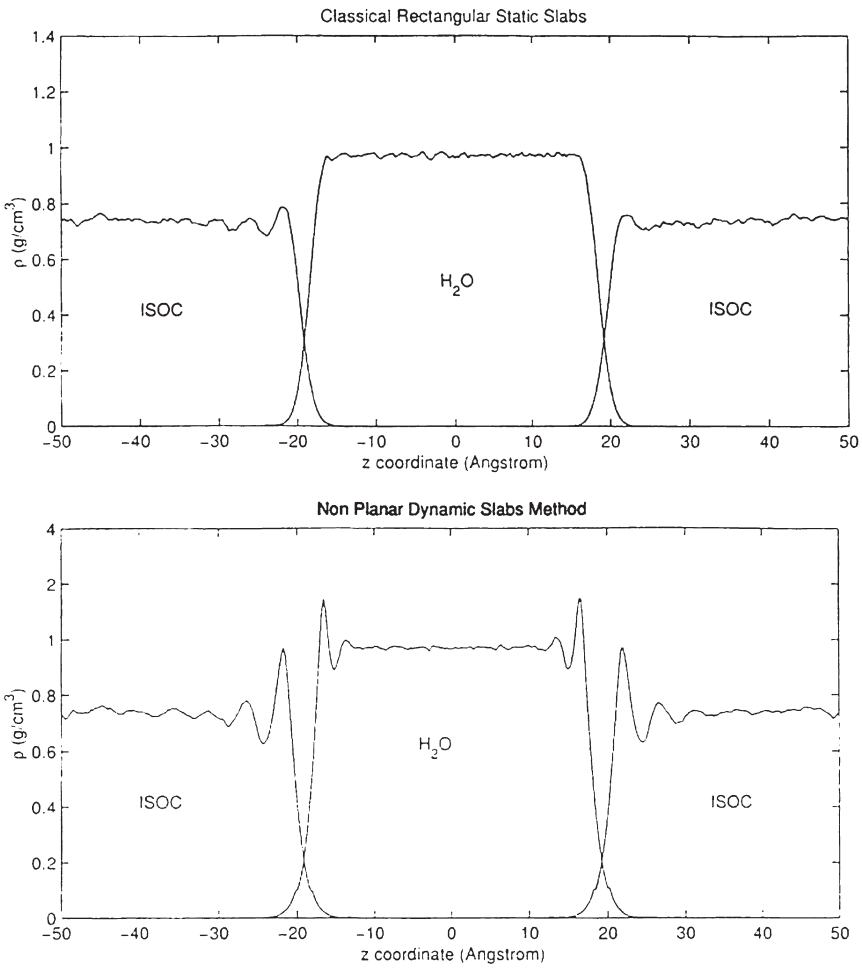

FIGURE 11 Density profiles for the H_2O/ISOC system. The density profile of the water/iso-octane interface by the traditional method (top) and the nonplanar dynamical slabs method (bottom). The greater structural detail available is apparent in the second method. Reprinted from Ref. [116] with the permission of the authors and the Journal of Physical Chemistry.

showed clearly that in both types of interface "water cones" were formed for both forward and reverse passages of the ion. As the ions moved towards the organic liquid phases, they remained connected to the water phase through water chains. The chains could be lengthened for about 9 Å before they disrupted and retracted. Conversely, as the ions moved from the organic phase toward the aqueous phase, a nearby capillary wave was attracted towards the ion to form a similar "water cone" structure. The wave protruded more deeply into the organic phase to reach the ion at $\sim 9-10$ Å from the interface.

A further study [117] of ion transfer using a range of different ion types has shown that the transfer behaviour of all ions is basically similar. More recently, Fernandes *et al.* [117] have considered transfers of: alkali ions Na^+, K^+ and Rb^+; Sr^{2+}, an alkaline-earth ion; and $N(CH_3)^{4+}$, an organic ion; across the water/HPT2 interface. The PMF profiles for all ions showed similar qualitative behaviour to the iodide ion: there was a gradual increase of free energies, with no peak, as the ions moved into the organic liquid. However, the free energy increased with ionic charge and decreased with the ionic size. These trends were expected since the change in free energy links closely to the exchange of the solvation shell of ions. The more tightly bound the hydration shells (especially the first layer) to the ions, the higher the change of free energy that would occur. The change was observed to involve mainly partial replacements of the first hydration shell of water by HPT2 molecules. Similarly, as for the iodide ion, the formation of water chains was observed. For the organic and the alkaline ions the protrusions could be up to 10 Å long, while for the Sr^{2+} ion, up to 14 Å. The latter ion, with a larger charge, had a capacity to attract more distant water molecules.

Catalysis

As with spectroscopy, classical MD cannot properly handle the electronic aspects of catalysis, nevertheless it can treat many of the associated phenomena, which are often rate determining. A good example of this is diffusion, which controls the rate of many catalysed reactions, and in many instances is within the scope of classical simulation. Not surprisingly, in view of their catalytic importance, zeolites provide the most frequent examples of DL_POLY in catalytic studies. Catlow *et al.* has pioneered much computational modelling in this area [118–121,124–127] (exploiting many other software packages and techniques, besides those available in DL_POLY—see [118]). In all of these examples, the diffusion in the zeolite of a sorbate (usually an alkane or aromatic), is the issue of prime interest, since this process underlies the shape selectivity inherent in zeolite catalysis. Simulation studies can be used in conjunction with direct diffusion

experiments or with QENS or PFG-NMR, generally yielding diffusion coefficients in good agreement with experiment. It should be remarked that these studies are computationally intensive, and require typically several thousand processor-hours of a Cray T3E for a full study.

The diffusion of two ortho- and para-xylene in the siliceous zeolite CIT-1 has been addressed by Sastre *et al.* in [118–121]. This zeolite is characterised by channels constructed from 12- to 10-membered rings (MR) which introduce the possibility of shape selectivity operating to different degrees in the different channels. Using an established force-field for the (flexible) zeolite framework and a standard, flexible model for the aromatics, simulations of equal mixtures of the xylene isomers and of pure isomers were conducted at 500 K. The simulated system was most often comprised of 8 xylene molecules and 2688 zeolite atoms (or a $4 \times 2 \times 4$ macrocell), and sometimes 32 xylene molecules were used. These simulations were supplemented by computer experiments (not using DL_POLY) in which the xylene was drawn through each channel and the interaction energy with the zeolite calculated at intervals to determine the reaction path. These latter experiments revealed a low activation energy (6.21 and 7.03 kcal mol^{-1}) for *p*-xylene and *o*-xylene respectively, in the 12 MR channels, but much higher (20.93

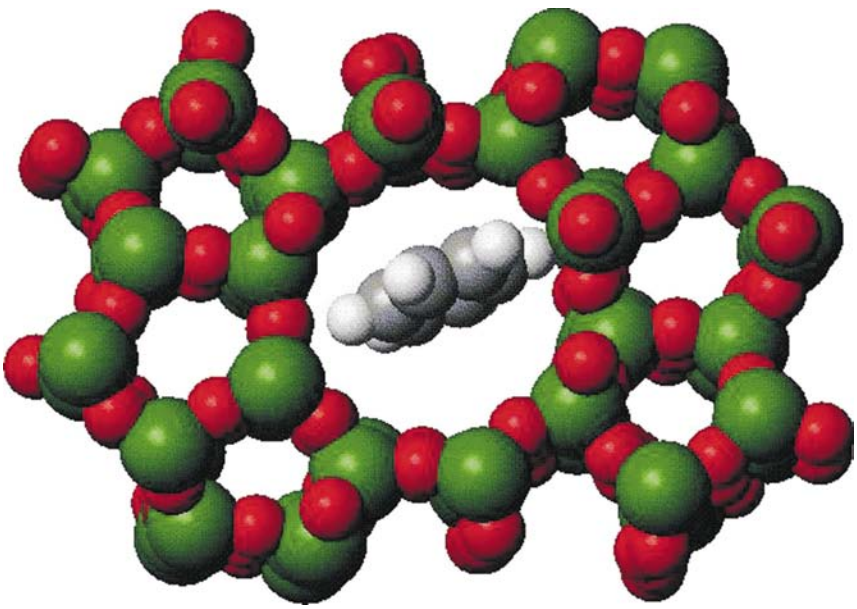

FIGURE 12 Benzene in silicalite-1. Benzene in the straight channel of silicalite-1, used to represent the zeolite ZSM-5 in the simulations [122]. The limited space available to the benzene is apparent, but diffusion in the channel can effectively be modelled using the "Bluemoon" technique. From Ref. [123]. Figure drawn by Weblab molecular graphics software from Molecular Simulation Inc.

and 110.31 kcal mol^{-1} respectively) in the 10 MR channel, with clear consequences for selective diffusion of the isomers. So it proved in the MD simulations: while both xylene isomers possessed demonstrable diffusion, the *p*-xylene generally diffused much faster, though with increased loading of the sorbate, the diffusion was much reduced—a common feature of diffusion in zeolites. Close inspection of the diffusion paths clearly indicated that diffusion in the 12 MR channels was much preferred, though some diffusion by *p*-xylene was present in the 10 MR channels. The *o*-xylene showed only restricted incursions into the 10 MR channels, and this was considered to be the cause of nonlinearity if the *o*-xylene MSD. There was also some evidence for *p*-xylene inhibiting the diffusion of *o*-xylene in the mixtures.

The diffusion of an aromatic molecule in a zeolite was handled differently by Forester and Smith [122], who exploited the "Bluemoon" method of Carter *et al.* [123] to investigate benzene in silicalite-1, a structural analogue of the zeolite ZSM-5. ZSM-5 possesses two types of 10 MR channel: straight and sinusoidal; in directions perpendicular to each other. The benzene is capable of diffusing along both (Fig. 12), though the mean diffusion coefficient is very low (2.2×10^{-14} m^2 s^{-1}). Using a force-field derived principally from literature sources, a series of equilibrium simulations was performed with the benzene centre of mass constrained to a fixed coordinate along a diffusion channel. The mean benzene position in each simulation provided the reaction path, and integration of the constraint force along the reaction path provided the free energy profile (i.e. adsorption sites and activation energies for escape). Further simulations, commencing with the benzene located at the free energy maximum, were used to calculate the transmission coefficient. The rate constants for the hopping of the benzene between adsorption sites were calculated from transition state theory and used in a lattice Monte Carlo simulation to model the diffusion. The MSDs were computed on a *microsecond* timescale and yielded a mean diffusion constant (3.4×10^{-14} m^2 s^{-1}), which was close to the experimental value. In the simulations, both rigid and flexible silicalite-1 frameworks were considered. The effect of the rigid framework was to raise the activation energies markedly. Activation energies were of the order 10–35 kJ mol^{-1} for the flexible system and 30–110 kJ mol^{-1} for the rigid system.

In Ref. [124] Sastre *et al.* report DL_POLY simulations of benzene and propylene in MCM-22 zeolite (Fig. 13), a mixture of species relevant to the production of cumene in a proton catalysed reaction. MCM-22 provides a framework of interconnected sinusoidal 10 MR channels, with perpendicular channels of interconnected 12 MR cavities linked via 10 MR windows. Important factors in the catalysed reaction are the preferred locations of the reactants and their diffusion rates in the framework. Initially two simulations were undertaken

of a $2 \times 2 \times 2$ macro-cell of a structurally optimised siliceous form of MCM-22 (ITQ-1) with 16 guest molecules (8 benzene, 8 propylene) at 650 K. The first located the molecules in the sinusoidal channels and the second in the large (super-)cavities. Both flexible and rigid zeolite frameworks were tested. Trajectory plots of the molecular motion revealed that benzene did not diffuse in either channel system over a 200 ps simulation. In the sinusoidal system, the benzene was strongly located at the minimum energy position. The lack of diffusion in this case was ascribed to the particular narrowness of the 10 MR channels and their "tortuosity", which inhibited motion. In the large cage channels, benzene motion explored the supercavites, showing a preference for locations near the 10 MR windows, but diffusion between cavities was not observed. Propylene, on the other hand, diffused relatively freely in both channels, though it did not linger near the 10 MR windows, where the configuration energy was higher. The effect of using a rigid framework was to slow down the propylene diffusion significantly, while benzene diffusion increased slightly. Calculated PRDFs suggested that any alkylation of benzene in the 10 MR channels would rapidly block the channels, which would therefore have little effect on the overall reaction. Meanwhile possible occupancy of the supercavities by both benzene and propylene, suggests these cavities are important to the catalytic process. Computation of the energy profile for benzene "dragged" through the 10 MR windows, suggested that increased temperature or

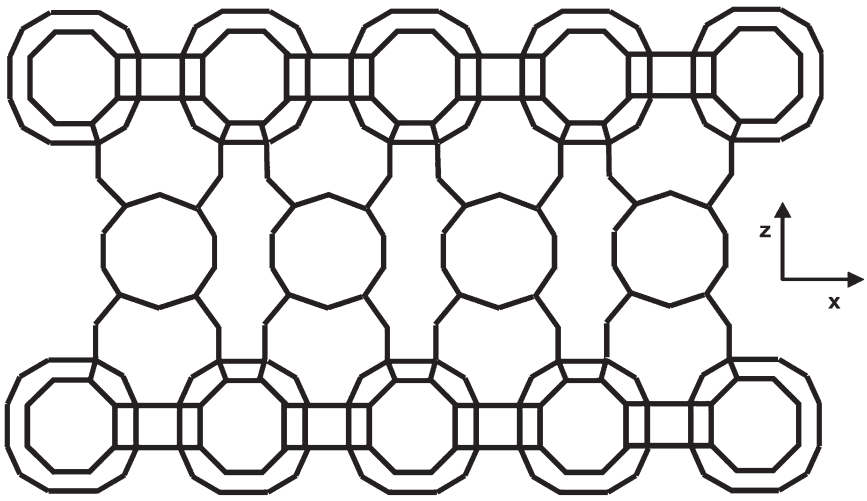

FIGURE 13 The zeolite MCM-22. MCM-22 has a framework of interconnecting sinusoidal 10 MR channels (in $x-y$ plane of figure) and 12 MR cavities in the z-direction linked through 10 MR windows. The diffusion of hydrocarbons through this framework has been simulated in Ref. [124].

longer simulations would permit the observation of benzene hopping between supercavities. A 1 ns simulation at 850 K, using a rigid lattice, provided confirmation of this. It was proposed that the catalytic reaction mostly occurs at or near the zeolite surface.

Corma *et al.* [125] has examined *n*-heptane and its isomer 2-methylhexane in the siliceous ITQ-1 structure. Once again a $2 \times 2 \times 2$ macrocell was used, with 12 heptane molecules, described with explict hydrogen atoms. Two computer experiments were conducted—one for each isomer at a temperature of 450 K. Six alkane molecules were initially placed in the 10 MR sinusoidal channels and six in the supercages. No diffusion of the 2-methylhexane was seen in the 10 MR channels over 200 ps. Also the molecular motion in the supercavities was highly localised in one of two places in most cases, though one molecule was seen to migrate across the cavity. No intercavity motion through the 10 MR window was seen. *n*-heptane however, was seen to diffuse quite markedly in the 10 MR channels, though a nonlinear MSD was obtained. In the supercavities however, the molecular motion was again strongly localised, which suggests that it is potential energy, rather than steric hindrance that inhibits diffusion, as it affects both isomers. It was argued that intercage diffusion should be possible in this system, and most likely for the *n*-heptane.

Alkane molecules in the sinusoidal and linear channels of the zeolite ZSM5 exhibit different diffusabilities, with differering temperature dependencies. Thus Raj *et al.* has studied the diffusion of octane in silicalite with DL_POLY, to account for these observations [126]. The simulations were of a $3 \times 3 \times 3$ macrocell of silicalite (7776 atoms) and 8 octane molecules with explicit hydrogen atoms. The initial zeolite framework was energy minimised using GULP at the start, and the octane molecules inserted into the straight channels. Insertion caused a phase transition in the framework from orthorhomic to monoclinic, which is in accord with experiment. The energy minimised form of the transformed structure formed the basis for the subsequent MD simulations at 300 and 450 K. At the lower temperature trajectory plots showed that octane diffused mostly via the sinusoidal channels, in which they preferentially located. The MSD plots were approximately linear and the calculated total diffusion coefficient was $4.67 \times 10^{-10}\,\mathrm{m^2\,s^{-1}}$. At 450 K the diffusion was $13.87 \times 10^{-10}\,\mathrm{m^2\,s^{-1}}$ and the diffusion now involved both straight and sinusoidal channels, indicating that diffusion in the former was more affected by the temperature change. It was proposed that diffusion in the sinusoidal channels requires rapid conformational changes in the hydrocarbon chain to "adapt" to the channel shape, while such changes are not necessary for the straight channels, which are therefore able to show increased diffusion rate at higher temperatures. This factor was expected to increase with chain length. (In shorter chained

hydrocarbons diffusion in the linear channels was preferred at 300 K and occupancy of the sinusoidal channels was less.) It is significant that MD simulations were able to exhibit these differences.

The study [125] of diffusion of heptane in ITQ-1 has been extended by Sastre *et al.* to higher temperatures of 550 and 650 K [127]. The higher temperatures failed to promote diffusion of 2-methyhexane in either the 10 MR sinusoidal channels or between the supercavities, though intracage motion between stable sites in the supercavities did occur. The higher temperatures enhanced the diffusion of *n*-heptane in the 10 MR channels as expected and the motion between the sites in the supercavities was increased. Significantly however, intracage motion commenced at a lower temperature for *n*-heptane. This study also included an examination of the diffusion of 2-methyhexane in the zeolitic structure ITQ-2, which resembles ITQ-1 in having sinusoidal 10 MR channels, but in place of a supercavity, is an "open cup" cavity. The material is a layered structure, with the open cups forming the surface of the layers. Simulations at temperatures 450, 650 and 850 K, showed that the 2-methylhexane, preferred to reside within the cups rather than in the interlayer space, though with increasing temperature excursions into the interlayer space became more frequent and led to migration of the sorbate to other cups. It was argued that the freedom of the sorbate to escape the cups implied a higher selectivity for isomerisation reactions and that trapping of the sorbate in the supercavities of the ITQ-1 structure implied a greater selectivity to cracking reactions.

In Ref. [128] Sastre *et al.* examined the diffusion of five different isomers of heptane in the zeolitic structures ZSM-48 and Theta-1. These zeolites resemble the 10 MR straight channel structure of ZSM-5, but possess no sinusoidal channels, and differ from each other in that Theta-1 possesses narrower channels. Both zeolites were structurally relaxed prior to the simulations. The isomers of heptane chosen were: *n*-heptane; 2-methyl-hexane (2MeHex); 1-isopropyl-2-methylcyclopropane (liPr2MeCp); 1-propyl-2-methylcyclopropane (1Pr2MeCp); and 2,3-dimethylpentane (2,3diMePen). These isomers were selected to represent the reactant, products and possible intermediate species in the zeolite catalysed isomerisation reaction. Simulations were performed at 450 K, with the sorbate molecules isolated in separate channels. The calculated MSDs revealed that *n*-hexane and 1Pr2MeCp diffused most rapidly in both zeolites, indicating that the cyclopropane ring alone had little effect on the diffusion of heptane in these zeolites. (The diffusion coefficient for both sorbates in ZSM-48 was $\sim 31 \times 10^{-10}\,m^2\,s^{-1}$ and about half this in Theta-1). Diffusion of the remaining isomers (2MeHex, 1iPr2MeCp, 2,3diMePen) were similar in ZSM-48 (~ 8, ~ 9, $10 \times 10^{-10}\,m^2\,s^{-1}$, respectively) all of which offered at least one methyl branch to hinder diffusion. The corresponding diffusion coefficients in Theta-1 (~ 5,

~ 2, $\sim 1 \times 10^{-10}\,\mathrm{m^2\,s^{-1}}$, respectively), were significantly lower, and by their relative magnitudes indicated an increasing steric hindrance in the order: $2\mathrm{MeHex} < 1\mathrm{iPr2MeCp} < 2,3\mathrm{diMePen}$, in line with reasonable expectation. Some practical conclusions were drawn from these simulations. For example, the ability of the ZSM-48 channels better to accommodate the proposed intermediate and product structures than Theta-1 implied the latter will provide higher yields of monomethyl over dimethyl product. Also, the larger channel diameters of these zeolites in comparison with the 10 MR channels of MCM-22 (see above), implied they will yield more branched (isodewaxing) products.

Complex Materials

The category "complex materials" is introduced here to exemplify materials which possess complicated, or perhaps unexpected, phase behaviours derived from unusual molecular structures (as in liquid crystal studies) of from the competing properties of dissimilar molecules in a mixture (as in clathrate hydrates). DL_POLY is useful for investigating such systems because if its ability to deal with complicated molecular stuctures and mixtures of disparate types of structure. Often such simulations need to be large to address the range of order that emerges, and in this regard too, DL_POLY is well suited to the task.

Liquid Crystals

Cook and Wilson have used DL_POLY extensively in modelling a series of liquid crystals with atomistic potential models. Their initial simulations used a non-polar mesogen (4,4-di-*n*-pentyl-bibicyclo [2.2.2] octane, or 5,5-BBCO) in relatively small systems (64 or 125 molecules—about 3000 interaction sites) with long simulation times (*ca.* 10 ns) to examine the nature of the isotropic-nematic phase transition [129]. The system was studied at a series of temperatures in the range 200–500 K, in each case starting from two different initial configurations, one with nematic-like and one with isotropic molecular orientations. They found that it was possible to observe the spontaneous formation of a nematic phase from the isotropic phase. This had been seen before in model systems (such as Gay–Berne ellipsoids), but not with an atomistic potential. The simulated phase change was found to occur on a similar timescale to that observed with Gay–Berne potentials, but involved considerably more computational effort as much shorter time steps were required to incorporate the intramolecular motions in the atomistic model. The phase behaviour predicted from the simulations was found to be in qualitative agreement with the experimental data for 5,5-BBCO, but both

the melting and the clearing point occurred at much lower temperatures than for the real system. This was thought largely to be due to the use of a united atom potential, in which non-polar hydrogens were merged into the heavy atom to which they were bonded, but some effects of finite system size were also noted.

In subsequent work [130], Cook and Wilson simulated the behaviour of an intriguing pair of mesogens: 4-(trans-4-*n*-pentylcyclohexyl)benzonitrile (PCH5) and 4-(*trans*-4-*n*-pentylcyclohexyl)chlorobenzene (PCH5-Cl). These two molecules differ only in the polar substituent on the phenyl ring, yet show substantially different orientational correlations in the isotropic liquid phase. In particular, PCH5 exhibits a nematic phase with clearing point at 328 K, whereas PCH5-Cl melts to the isotropic liquid at 305 K. In this case, the mesogens were modelled using all-atom OPLS potentials [17][¶] in MD simulations with 125 molecules (about 5000 atoms) and simulation times of about 1 ns. Comparison of these simulations with experimental data gave very encouraging results, with calculated densities at ambient pressure being within 1% of the experimental values, and semi-quantitative agreement with experimental Kirkwood correlation factors

$$g_1 + 1 + \frac{1}{N}\langle \sum_{i}^{N} \sum_{j \neq i}^{N} \cos \theta_{ij} \rangle$$

where (θ_{ij} is the angle between the long axes of molecules i and j. In particular, the simulations correctly predicted that $g_1 < 1$ in PCH5, indicating a preference for anti-parallel alignment, but $g_1 > 1$ in PCH5-Cl, implying a preference for parallel alignment. The simulations were analysed to give a detailed understanding of the molecular structure present in the isotropic liquid. The analysis included a Legendre polynomial projection of the centre of mass RDF, $g_l(r)$, and a novel two-dimensional distribution function based on distance and displacement along the molecular long axes, $g(r, |z|)$. From this it was possible to show that the Kirkwood correlation factors actually arose as a complex superposition of a number of different favoured dimer geometries, with both parallel and anti-parallel dimers being present in both systems. While the stronger dipole in PCH5 was found to favour anti-parallel dimer configurations, quadrupolar interactions between the aromatic groups and packing effects due to van der Waals interactions were also found to be important in determining the orientational correlations. They concluded that all atom potentials can give an accurate representation of real mesogens, but that some finite system effects were

[¶] and references therein.

still evident, and so larger simulations would be needed to give quantitative agreement with experiments at temperatures just above the isotropic/nematic phase transition.

One important conclusion from [130] was that the quadrupolar interactions arising from aromatic moieties were important, and required something like an all-atom force-field to reproduce accurately. Cook and Wilson therefore undertook a very careful force-field development programme [131], in which they took the existing amber force-field for molecules with similar moieties, and extended this to account for the extra functional groups found within the liquid crystals. They were also concerned with five dihedral potentials that were not included in the AMBER force-field, but which were crucial for describing the shape and flexibility of the liquid crystal molecules. An ideal torsion potential was tabulated by constraining the torsion angle and then performing a full geometry optimisation on the remaining degrees of freedom using restricted Hartree-Fock calculations with the 6-31G* basis set. Analogous constrained optimisation calculations were then performed with the proposed force-field and DL_POLY, and the energy differences between the two calculations used to fit a Fourier representation of the dihedral potential. The resulting potential was checked in MD simulations of liquid state properties for various fragment molecules and found to give good agreement with experimental data.

This all-atom potential was then used to simulate two different mesogens (me5NF—Fig. 14a and GGP5Cl—Fig. 14b) [132], and examine the orientational correlations that persist in their isotropic phase. Both systems were simulated at a temperature 6 K above the respective nematic/isotropic phase transitions. The analysis involved calculating a Legendre polynomial projection of the radial distribution function (RDF, $g_l(r)$), which was then used to determine the Kirkwood correlation factors, g_l. The $g_l(r)$ all vanished within about 15 Å, which was considerably smaller than the size of the simulation box used (46 Å for the smaller mesogen). For me5NF, the calculated g_1 was in excellent agreement with the experimental value. Some discrepancy was found for GGP5Cl, however; this was thought to be due to the neglect of polarisability in the force-field model: GGP5Cl contains both strongly polar groups and highly polarizable aromatic moieties. Based on an extensive analysis in terms two-dimensional distribution functions defined in a molecule-fixed axis system, Cook and Wilson were also able to show that there was significant dimer and trimer formation within the isotropic phase, with both parallel and anti-parallel arrangements of the molecular dipoles being common. The driving force for dimerisation was identified as favourable quadrupolar interactions between the phenyl and halogenated phenyl groups, which in turn highlighted the need for a very careful treatment of the electrostatic interactions in such mesogens.

Most recently, Cook and Wilson have used very large scale atomistic MD simulations of the mesogen PCH5 (4-(*trans*-4-*n*-pentylcyclohexyl)benzonitrile) at a temperature of 343–15 K above the nematic/isotropic phase transition [133]. This is a system in which large, transient oriented clusters are believed to form, and so there was considerable interest in determining whether the spontaneous formation of such clusters could be observed in MD simulations. Simulations were performed on a system of 1000 PCH5 molecules (*ca.* 40,000 atoms) with total trajectory times of about 1 ns to calculate the equilibrium properties. This was the first time that atomistic simulations of mesogens had been performed on this scale. In general the simulations gave a very good reproduction of available experimental data: the computed density at ambient pressure ($929 \pm 2\,\mathrm{kg\,m^{-3}}$ compared with $926\,\mathrm{kg\,m^{-3}}$ from experiment), the diffusion coefficients ($D = 1.1 \pm 0.1\,\mathrm{m^2\,s^{-1}}$ at 343 K, cf 1.0 at 333 K from experiment); and the Kirkwood correlation factor, g_1, (0.886 ± 0.015 calculated, 0.88 expt) were all in essentially exact agreement with experimental values. One of the major purposes of this study was to identify the scale of simulation required to reproduce the orientational order in mesogens near a liquid crystal phase transition. To achieve this, Cook and Wilson again calculated the Legendre polynomial projections of the RDF, $g_l(r)$. While $g_1(r)$ was found to be truly short-ranged, decaying to zero within 10–15 Å, the same was not true for $g_2(r)$. Indeed, $g_2(r)$ remained non-zero for separations beyond 35 Å. It was concluded that, while many of the properties were reproduced with excellent, quantitative accuracy, some finite size effects

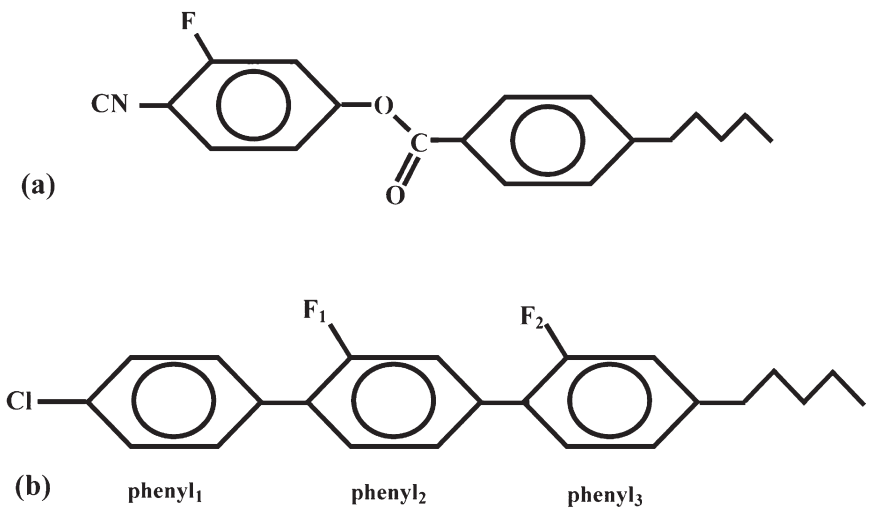

FIGURE 14 Mesogens me5NF and GGP5Cl. The molecular structure of (a) me5NF and (b) GGP5Cl from Ref. [132].

were still evident in the 1000 molecule mesogen simulation—particularly relating to the onset of long range orientational order as the isotropic/nematic phase transition is approached.

Chiral Aluminium Phosphates

In a series of papers, Ramirez-Cuesta *et al.* have combined DL_POLY with DFT calculations and inelastic neutron scattering (INS) experiments to characterize and understand the stability of some novel layered inorganic compounds [134–136]. The compounds of interest were based on aluminium phosphate (AlPO) layers into which propeller-shaped compounds of the form $[CoL_3]^{3+}$ had been intercalated, where L was either $NH_2CH_2CH_2NH_2$ (en) or $NH_2CH_2CH_2CH_2CH_2NH_2$ (tn); the overall stoichiometry of the materials is $[CoL_3]$ $A1_3(PO_4)_4$. These compounds were of particular interest because the aluminium layers contain chiral features and, in the case of the $[Co(tn)_3]^{3+}$ intercalate, spontaneously form as enantiomerically pure crystals even when a racemic mixture of the transition metal complex is used.

The first paper in this series was designed to identify the nature of the interactions that stabilised the chiral structures [134]. A series of model potentials was adopted for the $[Co(tn)_3]^{3+}$: a simple charged sphere; a united atom model that described the shape of the complex but did not allow for features such as hydrogen bonding; and a fully atomistic model that did include hydrogen bond interactions. Initially, the fully atomistic model of the cobalt complex was used with two published aluminium phosphates potentials in constant stress/constant temperature MD calculations. The results were compared with experimental properties such as the crystal structure and IR spectrum and it was shown that quantitative agreement could be obtained using a two-body potential for the AlPO and the all-atom potential for the intercalate. Subsequent calculations showed that the AlPO structure was completely unstable with a charged sphere intercalate, but, showed mechanical stability with the shape-dependent model. It was concluded that the stability of the material resulted from a combination of packing forces around the propeller-shaped intercalate and hydrogen bonding between the NH_2 group on the intercalate and dangling P=O groups in the AlPO layers; water of crystallisation was found to play an important role in mediating these hydrogen bonds.

The two subsequent papers probed the structural role of water in stabilising the two materials. In Ref. [135], the INS spectrum of $[Co(en)_3]$ $Al_3(PO_4)_4$ was determined both from MD simulations and from experiment. The MD and experimental spectra were found to be in excellent agreement, particularly in the

range usually associated with water librations: $400-700\,cm^{-1}$, and thereby allowed both the location and orientation of the water molecules to be determined and the water peaks assigned unambiguously; such assignments had not been possible from the experimental crystal structure and INS spectra alone. The third paper in the series, [136] involved a very detailed comparison of calculated and experimental INS spectra for $[Co(tn)_3]$ $Al_3(PO_4)_4$. In this Case the whole spectrum in the range $0-1000\,cm^{-1}$ was measured and calculated. In general, the agreement between theory and experiment was good (Fig. 15), and in particular, the water librational region of the experimental spectrum ($400-800\,cm^{-1}$) was in excellent agreement with the spectrum that had already been published in Ref. [134] using classical MD simulations with DL_POLY. On the basis of their calculations, Ramirez-Cuesta *et al.* were able to assign regions of the spectrum to different characterisitic modes of motion. These included the water librational modes ($400-800\,cm^{-1}$), intramolecular skeletal vibrations of the $[Co(tn)_3]^{3+}$ ($200-600\,cm^{-1}$), constrained rotations and translations of the $[Co(tn)_3]^{3+}$ ($250-350\,cm^{-1}$) and phonon modes of the AlPO layers ($0-150\,cm^{-1}$). The latter were particularly interesting as intensities in the INS spectrum are completely dominated by scattering from the H atoms, yet the AlPO layers contain no H atoms. Nevertheless, the experimental spectrum was very well described using the classical density of states calculated just from atoms in the AlPO layers. This

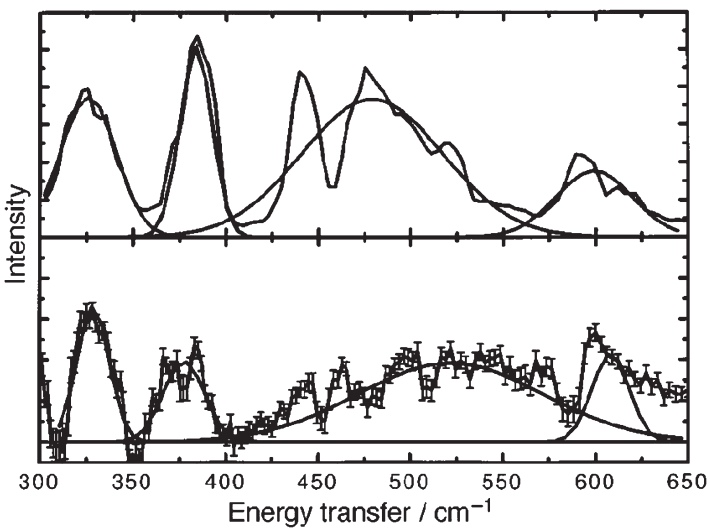

FIGURE 15 Dynamics of aluminophosphate templated water molecules. Comparison between the calculated vibrational denisty of states for water (top) with the experimental difference spectrum from Ref. [136]. Also shown are the underlying Gaussian profiles of the four principal peaks.

was taken to imply that the motion of the AlPO layers and the molecules in the interlayer space were synchronised through the hydrogen bonding interactions. In consequence, INS was shown to be a much more powerful probe of inorganic materials than had previously been thought, as such correlated motion can allow it to be used together with classical simulation methods to study the non-hydrogenated regions of inorganic materials.

Clathrate Hydrates

As a final example of the use of DL_POLY to study complex materials, we cite some work by Rodger and co-workers in simulating clathrate hydrate interfaces [137,138]. Clathrate hydrates are crystalline solids formed from mixtures of water with small, typically hydrophobic, molecules like methane. At present, there is considerable interest in understanding the nucleation and growth of clathrate hydrates. Given the hydrophobic nature of the "guest" molecules involved (such as methane), this nucleation and growth is known to be dominated by interfacial effects. In a couple of papers, Rodger and co-workers have simulated the interface between methane hydrate and methane gas. The simulations were performed using two-dimensional periodic boundary conditions. The limits of the third-dimension were defined using a frozen layer of hydrate molecules to terminate a region of mobile hydrate, and either reflective boundary conditions or a soft repulsive wall to confine the gas. In the first paper [137], Rodger *et al.* used relatively small simulations (typically 2000 atoms) to map out the conditions over which the interface was stable. Using SPC water and a one-site L–J model of water, they found a surprisingly good match between the calculated and experimental phase diagram. For example, at 270 K the hydrate was found to be unstable at 1 MPa, but stable at 100 MPa: experimentally the hydrate is found to melt below 3 MPa at this temperature. Given that that phase diagram of pure SPC water is shifted relative to experiment by some 70°C, this concurrence with experiment for clathrate hydrates suggested an important role for the methane excluded volume in stabilising the hydrate phase. The simulated interfaces were analysed using both standard distribution and time correlation functions and novel order parameters designed to characterise local order in ice-like systems. These showed that the interfacial region, defined by average structural considerations, spanned about 15–20 Å. There was also some evidence of longer-ranged dynamical correlations, with anisotropics in the MSD of water molecules correlating with topological features of the surface of the frozen hydrate boundary layer over separations as great as 20 Å.

The phase diagram identified in Ref. [137] was then used to target a study of the so-called memory effect in hydrate nucleation experiments. This is an effect whereby in successive melt/thaw cycles, hydrate nucleation times for the first cycle are long with large variances (typically 6–24 h, depending on sub-cooling) but are much shorter and more reproducible on subsequent cycles, and is generally interpreted in terms of long-lived clathrate-like clusters remaining in the melt. The effect can persist even when the system is heated to 10–15°C above the melting point for about 1 day. Rodger looked for evidence of residual structure in the melt by performing MD simulations of a hydrate interface just above the melting temperature [138]. Based on [137], simulations were performed at 290 K and 1.5 MPa so as to provide relatively gentle superheating and thereby maximise the chance that any residual structure would be found in the melt. Larger simulations than in Ref. [137] were used: typically 14,000 atoms, with initially a 100 Å thick hydrate layer above the frozen hydrate boundary, and a similar thickness of methane gas. Simulations were performed for ca 1 ns, by which time about 35 Å of the hydrate surface had melted. For this study the order-parameter analysis was extended to allow an assignment of individual water molecules to hydrate-like, ice-like or liquid-like local structures. The results (Fig. 16) showed that there was a small increase in water molecules with hydrate-like local order in the melt compared with pure, bulk liquid water under the same conditions. However, much more residual structure was found in the form of enhanced ice-like water molecules. Given the short timescales and small thermodynamic driving force used in the simulations, it was considered unlikely that residual water structure in the melt could be responsible for the observed

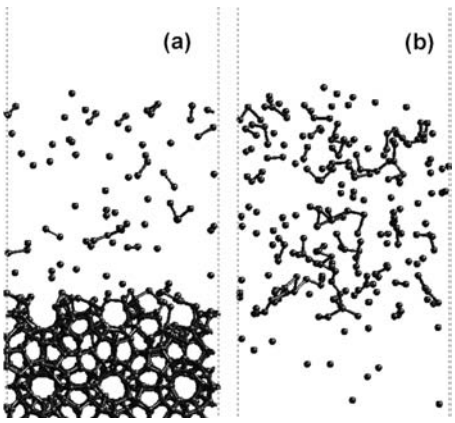

FIGURE 16 Memory effect in methane hydrates. Snapshots of (a) residual clathrate and (b) ice structures in the hydrate melt after 600 ps simulation, from Ref. [138].

memory effect, but that persistence of a supersaturated methane solution might be a more likely explanation.

Novel Simulations

This section presents examples of unusual uses of DL_POLY.

In MD it is sometimes of interest to enhance or diminish the contribution of particular frequencies to the motion of the atoms. In Ref. [139] Phillips and Essex described a form of digitally filtered molecular dynamics (DFMD), in which the velocity of each atom is sampled for an interval then a sequence of digital filters is applied, which selectively adjusts the frequency distribution. The simulation then recommences from the filtered velocities and the corresponding atomic positions, with the required frequency adjustment in place. In Ref. [139] DFMD was applied to selection of molecular systems, and used to promote or remove particular frequencies. It was particularly effective at projecting out modes of vibration in complex molecules.

A good example of how DL_POLY can readily be extended is found in the simulations of Elliott and Windle [140]. They were interested in identifying how particle shape affected the maximum packing fraction that could be occupied by the filler particles used in polymer composites and so performed a study of packing efficiency in mixtures of spherical and cubic particles. Cubic particles were modelled as rigid bodies composed of an array of fused spheres, and all spheres interacted with a repulsive r^{-n} potential. Since hydrodynamic interactions are implicated in the equilibrium microstructure of polymer composites [141], they chose to use dissipative particle dynamics (DPD) rather than Monte Carlo or MD methods to simulate a range of cube/sphere mixtures (Fig. 17). Thus, they extended DL_POLY to incorporate the frictional and random forces in DPD; DL_POLY was chosen for this purpose because it already incorporated algorithms for solving rigid body equations of motion. The extended program was tested against analytical equations for the packing density of both monodisperse and polydisperse collections of spheres, before then simulating systems of cubes, followed by mixtures of cubes and spheres. The simulation of cubic particles of length l showed the existence of a cubatic phase—i.e. a phase which shows short-range orientational order but no long-range translational order—at a reduced pressure $p^*(= pl^3/kT) = 12$. They then performed a series of simulations with equimolar mixtures of cubes (length l) and spheres (diameter d) at a fixed reduced pressure of 20. The maximum packing fraction was about 0.78, and occurred with very small spheres: $d/l < 0.1$. The simulations also identified a minimum packing fraction of about 0.67 when $d/l \approx 1.2$. For

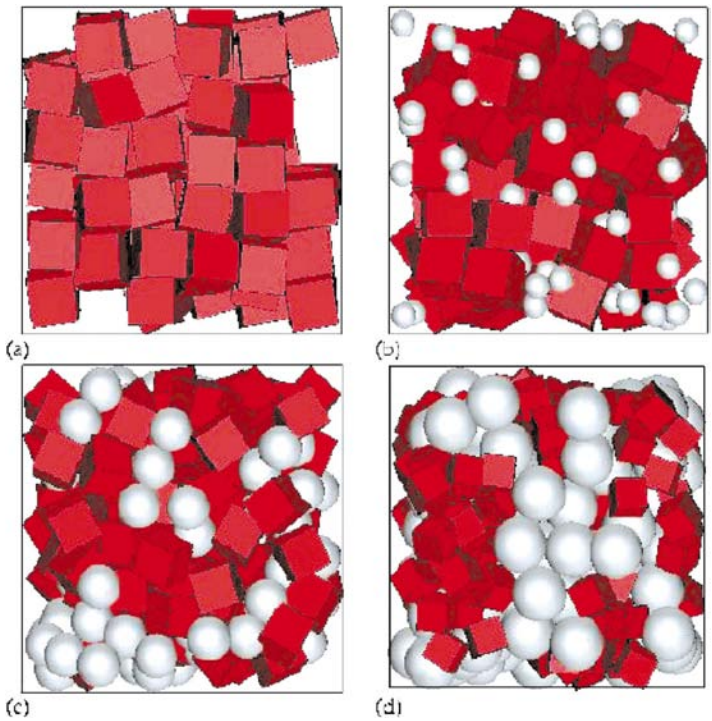

FIGURE 17 Simulations of cubes and cube/sphere mixtures. Visualisation of a mixture of fused soft spheres (cubes, side length l) with soft spheres (diameter d) at fixed reduced pressure $p^* = 20.0$ as a function of d/l: (a) no spheres, (b) $d/l = 0.549$, (c) $d/l = 1.020$, and (d) $d/l = 1.804$. The packing fractions were $\xi = 0.730$, 0.716, 0.680 and 0.705 respectively. Figure reprinted from Ref. [140] with the permission of the permission of the authors and the Journal of Chemical Physics.

comparison, in single component systems of spheres or cubes the maximum packing fractions were found to be 0.64 and 0.73, respectively. Orientational order between the cubes persisted to $d/l \approx 1.6$, this being the size ratio at which the cubes started to occupy the interstices created by packing the large spheres. An interesting complicating factor in these simulations was the observation of entropy-driven de-mixing. This was not universally observed, but did occur in at least one simulation with $d/l = 1.255$. Segregation of the mixture into separate sphere and cube domains were found to be accompanied by a small decrease in packing fraction. Although there is also an enthalpic driving force to adopting larger volumes for these repulsive particles, the major driving force for demixing was concluded to be entropic, arising from greater translational entropy at the lower density of the segregated system.

An unusual crystalline structure that has relevance for amorphous systems has been investigated by Simdyankin *et al.* [142]. This is the one-component σ-phase.

The structure occurs naturally in binary alloys, but the one-component analogue is considered to be a crystalline counterpart for glasses with icosahedral local order (so-called IC glasses). This work sought to derive the vibrational characteristics of the σ-phase crystal, for comparison with the vibrational spectrum of IC glass. Simulations of the σ-phase structure, using over 20,000 particles interacting via a specially constructed pair potential were undertaken, and the structural stability and dynamical properties determined over a range of temperatures and pressures. Of interest were the vibrational density of states (VDOS) and phonon dispersion curves. The properties calculated included the VAF, dynamic structure factor and current density correlation functions. It was found that over a wide range of temperatures and pressures the model potential gave a stable σ-phase. Comparison of the VDOS with that of an IC glass showed a similar frequency spread, quite distinguishable from an example BCC structure. The high temperature σ-phase and the low temperature IC glass were particularly alike, indicating the close similarity between the high temperature crystal and a structurally amorphous solid. Harmonic analysis provided the phonon dispersion curves, which revealed mode softening for the lowest frequency optic mode with increasing and deceasing pressure. The MD results provided information on the vibrational anharmonicity, and showed that the σ-phase is harmonic over a wide temperature range ($T^* < 0.2$).

Very recently, DL_POLY has been used to investigate commensurate contact interactions between two MgO (001) surfaces [143]. How two bodies make contact at the atomistic level is clearly fundamentally important in the understanding of frictional phenomena. It is believed that in reality surfaces are rarely atomically flat and contacts between surfaces inevitably occur in a number of discrete areas. For this reason, the model adopted in this study consisted of a slab of the periodic MgO (001) surface and an isolated MgO block (the probe) of finite cross-sectional area, which represents a raised projection of the other body. The MgO slab was represented as 16×16 rows of MgO lattice cross section six layers thick with a vacuum gap of 39 Å replicated in the z-direction. Various MgO probes of $n \times n$ atoms (where $n = 2$, 4, 6, 8 and 10) and six layer thick were considered. The probe was arranged to enable commensurate contact between the surface slab and probe surfaces at close contact. All atoms were classified into three different regions: (a) atoms from the first three innermost layers where contacts would occur were allowed to move freely; (b) atoms from the subsequent two layers were coupled to the Berendsen beat bath maintained at 300 K; and (c) atoms from the last planes were held rigid. All atoms were treated as rigid ions interacting via Buckingham potentials and the Ewald method was used to evaluate the long range electrostatic forces. Contact behaviour of the MgO probe was monitored by measuring the normal forces, F_z, experienced by

the rigid plane of the probe as it made contact with the MgO slab surface. In addition, graphical representations of atomic configurations were obtained to depict a mechanistic view of the processes. In order to obtain the form of the F_z as a function of distance the probe was brought towards the slab at a rate of $5\,\mathrm{m\,s^{-1}}$. This was achieved by advancing the probe's rigid plane in steps of 0.5 Å and equilibrating the whole system for 0.5 ps after each step. The equilibration was followed by data sampling and averaging over subsequent 0.5 ps. After which the whole procedure was repeated. It was found that probes of all sizes gave rise to a characteristic "jump" in the value of F_z, when the probe was abruptly more strongly attracted towards the surface slab. A typical profile is shown here (Fig. 18) for the 4×4 MgO probe. The magnitude of this jump varied according to the area of the probe and can be characterised by a logarithmic exponent of $q = 0.12$. Interestingly, equivalent calculations were also carried out for NaCl systems that yielded a similar value. In addition, the complementary calculations involving the withdrawal of the probes at the same rate as that incoming have been performed. In all cases hysteresis was observed and was followed by a similar jump, albeit at larger values of F_z than for the incoming case. The resulting F_z plots showed a complex saw tooth pattern. From the atomic configurations, it was found that probes underwent necking processes, with progressive reduction of cross sectional area. This involved plastic flow with systematic atomic dislocation as the probes were drawn away from the surface. An example of F_z profile for probe withdrawal is also shown here (Fig. 18) for the 4×4 MgO

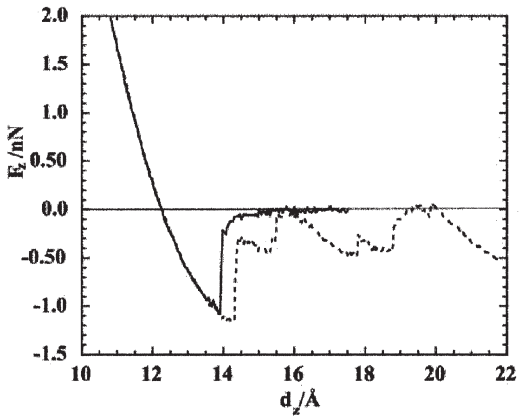

FIGURE 18 Contact forces in MgO. The z-component of the force on a 4×4 MgO probe near to a MgO surface. The bold line shows the force on approach, the broken line the force on withdrawal. The approach is characterised by a marked jump in the attractive force at ~ 14 Å (measured from base of probe). Withdrawal shows a similar discontinuity, with some hysteresis, and a saw-tooth profile at larger separations. From Ref. [143].

probe. Through such simulations it is hoped that the complex atomic processes underlying friction will be brought to light.

SUMMARY

Retrospective

It is clear from the many examples given above that DL_POLY is a successful software package that is making a useful contribution to scientific research. The reasons for this success are many and for the most part obvious. However there some aspects that are worth highlighting.

The first remark we should make concerns the adoption of RD parallelisation strategy, which is at the core of DL_POLY. Choosing this strategy was undoubtedly the reason that DL_POLY was written so quickly and to such a high level of functionality, and this helped ensure its early adoption on the UKs national supercomputers. However, the strategy has its limitations, particularly in performance scaling with the number of processors, from which it is difficult to recover. This has been partially offset by the pace of hardware developement, which has provided a boost to its expected range of applicability. It should also be said that the adoption of the code by a large number of single-processor workstation users indicates the value of platform independence, which is implicit in the RD approach. However, it remains true that DL_POLY is unlikely in its present form to be a 1000 processor or a 1,000,000 particle application code, for which there is currently a real demand. Domain decomposition methods are the correct strategy for such large systems, but it is much more difficult then to introduce the same degree of functionality that DL_POLY currently encapsulates.

The second point is that DL_POLY has, without question, benefited from a policy of openness. It was part of our initial brief to promote adoption of good programming practice, and for this reason we made the code available in source form. Users have benefited from being able to adapt the code to new applications, and we have benefited in return from feedback on software bugs and inconsistencies. We are honest (sometimes painfully) about the errors that are discovered, but this is surely better than burying them. Sometimes the users cure the bugs for us. In furtherance of our aims here we have found it to be a great advantage to manage the software, rather than release it under a "freeware" scheme. We ask users to sign a licence not merely to protect our own intellectual property rights, but to establish a proper working relationship between user and supplier. The main advantage of this is the communication procedures we necessarily have in place, to advises users of new developments and software

fixes. We would argue that this is essential for software packages undergoing continual development.

Finally we consider functionality. DL_POLY is as general-purpose as we could make it. This was (and is) a big factor in users adopting the code. However, it has meant that we do not support a standard or universal force-field, such as is provided by AMBER, CHARMM or GROMOS. This leaves our users without the support tools these packages readily offer. This in itself is a huge issue and one we are now having to address seriously. One aspect of force-fields we believe we were correct about however, was our adoption from the start of what we believed were the best methods for handling long ranged forces. By this we mean Ewald's method. Unfortunately, this choice meant that in the early days the simulators of biological systems, whom we regarded as important potential users, would not use the code, citing complexity and slowness of the code as the principal reasons. These points were debatable even then, but now that methods like SPME are standard in biological simulation packages, we feel the main point has been proven. The lesson for all software developers is that there is sometimes a suprising amount of resistance to best practice to be overcome when a new code is introduced.

Trends and Developments

We conclude our review with some of the current and likely future developments of DL_POLY.

One of the earliest spin-offs of DL_POLY was the DLPROTEIN code [90] developed by Melchionna and Cozzini at the University of Rome. This is a serious attempt to address DL_POLY's shortcomings in its application to the biological area, principally proteins and nucleic acids. For this purpose, it provides software for building DL_POLY FIELD and CONFIG files directly from protein databank structure data. The MD code is also stripped-down to provide faster execution and supports fast algorithms such as SPME [13] and RESPA multiple timestep [144,145]. The code is recommended for users with special interests in these biological areas.

DL_POLY_3 is a domain decomposition version of DL_POLY, which is being written for large scale simulations (of order 10^6 atoms) on large scale distributed parallel machines. The program does not support all the features of DL_POLY, particularly those pertaining to rigid body motion, but its does support macromolecular systems, long ranged forces (by SPME) and rigid (contraint) bonds. As with DL_POLY, development of this code will continue under CCP5's auspices.

DLMULTI is an adaptation of DL_POLY, written by Leslie at Daresbury Laboratory, to incorporate distributed multipole methods for accurate modelling of molecular crystals. This code incorporates a full Ewald sum scheme for spherical harmonic multipoles up to arbitrary order.

DL_POLY has been adopted by the Institute of Chemical and Physical Research (RIKEN) in Japan and in collaboration with Daresbury Laboratory has undergone major adaptations to optimise it for vector parallel machines such as the Fujitsu VPP700E/128 [146]. A version of the code has also been adapted for the unique molecular dynamics machine (MDM) [147] developed at RIKEN. These developments are already taking DL_POLY into many new areas of science.

DL_POLY is also implemented in the software package **ChemShell** [148] which is a computational chemistry environment based on the Tcl interpreter. ChemShell provides interfaces to a number of quantum chemistry and molecular simulation codes including G AMESS-UK, MNDO, TURBOMOLE, CHARMM, GULP, GROMOS and DL_POLY. It also provides geometry optimisers, interfaces to quantum mechanics/molecular mechanics coupling schemes and useful utilities such as molecular and data visualisers, file converters and potential energy surface mapping.

Finally, in recognition of the fact that DL_POLY, in common with many complex software packages, presents an intimidating challenge to novice users, a graphical user interface (GUI) for DL_POLY is currently being developed. This GUI is being written in the Java language, from SUN Microsystems, which has many advantages for graphical software developers, not least its portability and free availability. In keeping with the aims of the DL_POLY project, the source code for this GUI will be accessible to the user.

Such developments, we anticipate, will continue the growth in the DL_POLY user base for some time to come.

Acknowledgements

The authors of DL_POLY are pleased to acknowledge the support given to the development of the code. The motivation for developing the code was provided by Professor Dominic Tildesley, who was CCP5 Chairman at the critical time. The EPSRC provided support via grants from the Computational Science Initiative and the Science and Materials Computing Committee, which ensured that the process of writing the software had sufficient manpower in the early days. In this context, Tim Forester is thanked for his major contribution to the development of the original package. The package continues to enjoy support

from EPSRC through the Daresbury/EPSRC SLA. Since the earliest days, DL_POLY has been strongly supported by successive CCP5 Chairman: M.J. Gillan, M.P. Allen, D. Heyes and J. Harding, who have helped to promote and direct the development of the code. The authors also wish to thank the many users of DL_POLY for adopting the code and putting it to good use. This also applies to the Materials Consortium under C.R.A. Catlow and the Liquid Crystals Consortium under M.P. Allen who were swift to adopt the package and thus contribute to its widespread use. Those users who have contributed queries, suggestions, bug fixes and occasional pieces of software, are too numerous to mention, but their contributions have always been greatly appreciated.

Finally the authors of this review express their thanks to the many people who directed us to their work and provided copies of papers and figures. We sincerely hope their work is properly presented here.

References

[1] For more details on CCP5, please see the CCP5 website: http://wservl.dl.ac.uk/CCP/CCP5/.
[2] Allen, M.P. and Tildesley, D.J. (1989) Computer Simulation of Liquids (Clarendon Press, Oxford).
[3] Smith, W. and Forester, T.R. (1994) "Parallel macromolecular simulations and the replicated data strategy I. The computation of atomic forces", *Comput. Phys. Commun.* **79**, 52.
[4] Smith, W. and Forester, T.R. (1994) "Parallel macromolecular simulations and the replicated data strategy II. The RD-SHAKE algorithm", *Comput. Phys. Commun.* **79**, 79.
[5] Smith, W. (1992) "A replicated data molecular dynamics strategy for the parallel Ewald sum", *Comput. Phys. Commun.* **67**, 392.
[6] Forester, T.R. and Smith, W. (1998) "SHAKE RATTLE and roll: efficient constraint algorithms for linked rigid bodies", *J. Comp. Chem.* **19**, 102.
[7] The DL_POLY website is http://www.dl.ac.uk/TCS/Software/DL_POLY/.
[8] Smith, W. (1991) "Molecular dynamics on hypercube parallel computers", *Comput. Phys. Commun.* **62**, 229.
[9] Ryckaert, J.-P., Ciccotti, G. and Berendsen, H.J.C. (1977) "Numerical integration of the Cartesian equations of motion of a system with constraints: molecular dynamics of *n*-alkanes", *J. Comput. Phys.* **23**, 327.
[10] See for example http://www.dl.ac.uk/TCS/Software/DL_POLY/dl_poly.t3e.htm.
[11] Smith, W. and Forester, T.R. (1996) "DL_POLY_2.0: a general purpose parallel molecular dynamics simulation package", *J. Mol. Graph.* **14**, 136.
[12] See http://www.dl.ac.uk/TCSC/disco/Benchmarks/dl_poly.html. The data at this site are maintained by the Distibuted Computing Support group at Daresbury Laboratory and updated annually.
[13] Essmann, U., Perera, L., Berkowitz, M.L., Darden, T., Lee, H. and Pedersen, L.G. (1995) "A smooth particle mesh Ewald method", *J. Chem. Phys.* **103**, 8577.
[14] Hautman, J. and Klein, M.L. (1992) "An Ewald summation method for planar surfaces and interfaces", *Mol. Phys.* **75**, 379.
[15] Neumann, M. (1985) "The dielectric constant of water. Computer simulations with the MCY potential", *J. Chem. Phys.* **82**, 5663.
[16] Benmore, C.J. and Loh, Y.L. (2000) "The structure of liquid ethanol: a neutron diffraction and molecular dynamics study", *J. Chem. Phys.* **112**, 5877.
[17] Jorgensen, W.L. (1986) "Optimized intermolecular potential functions for liquid alcohols", *J. Phys. Chem.* **90**, 1276.

[18] Bianchi, L., Kalugin, O.N., Adya, A.K. and Wormald, C.J. (2000) "The structure of liquid methanol: a molecular dynamics study using three-site models", *Mol. Simul.* **25**, 321.
[19] Jorgensen, W.L., Chandraskar, J., Madura, J.D., Impey, R.W. and Klein, M.L. (1983) "Comparison of simple potential functions for simulating water", *J. Chem. Phys.* **79**, 926.
[20] Fidler, J. and Rodger, P.M. (1999) "Solvation structure around aqueous alchohols", *J. Phys. Chem. B* **103**, 7695.
[21] Astley, T., Birch, G.M., Drew, M.G.B. and Rodger, P.M. (1999) "Lifetime of a hydrogen bond in aqueous solutions of carbohydrates", *J. Phys. Chem. A* **103**, 5080.
[22] Berendsen, H.J.C., Postma, J.P.M., van Gunsteren, W.F. and Hermans, J. (1981) In: Pullman, B., ed, Intermolecular Forces (Dordecht, Reidel).
[23] Carver, T.J., Drew, M.G.B. and Rodger, M.P. (1999) "Molecular dynamics calculations of *N*-methylpyrrolidone in liquid water", *Phys. Chem. Chem. Phys.* **1**, 1807.
[24] Brooks, B.R., Bruccoleri, R.E., Olafson, B.D., Stats, D.J., Swaminathan, S. and Karplus, M. (1983), *J. Comput. Chem.* **4**, 187.
[25] Lynden-Bell, R.M. and Rasaiah, J.C. (1997) "From hyrdophobic to hydrophilic behaviour: a simulation study of solvation entropy and free energy of simple solutes", *J. Chem. Phys.* **107**, 1981.
[26] Berendsen, H.J.C., Grigera, J.R. and Straatsma, T.P. (1987) "The missing term in effective pair potentials", *J. Phys. Chem.* **91**, 6269.
[27] Lynden-Bell, R.M., Kosloff, R., Ruhman, S., Danovich, J. and Vala, J. (1998) "Does solvation cause symmetry breaking in the I_3^- ion in aqueous solution", *J. Chem. Phys.* **109**, 9928.
[28] Wood, R.H., Yezdimer, E.M., Sakane, S., Bariocanal, J.A. and Doren, D.J. (1999) "Free energies of solvation with quantum mechanical interaction energies from classical mechanical simulations", *J. Chem. Phys.* **110**, 1329.
[29] Sakane, S., Yezdimer, E.M., Liu, W., Bariocanal, J.A., Doren, D.J. and Wood, R.H. (2000) "Exploring the *ab initio*/classical free energy perturbation method: the hydration free energy of water", *J. Chem. Phys.* **113**, 2583.
[30] Chau, P.-L., Forester, T.R. and Smith, W. (1996) "Curvature effects on hydrophobic solvation", *Mol. Phys.* **89**, 1033.
[31] Chau, P.-L. (2001) "Computer simulation of the hydrophobic hydration of concave surfaces", *Mol. Phys.* **99**, 1289.
[32] Forester, T.R., Smith, W. and Clarke, J.H.R. (1996) "Molecular dynamics simulations of valinomycin and its potassium complex in homogeneous solvents", *Biophys. J.* **71**, 544.
[33] Cichos, F., Brown, R., Rempel, U. and von Borczyskowski, C. (1999) "Molecular dynamics simulations of the solvation of coumarin 153 in a mixture of an alkane and an alcohol", *J. Phys. Chem. A* **103**, 2506.
[34] Brown, R., Middelhoek, R. and Glasbeek, M. (1999) "Solvation dynamics of fluoroprobe in diethylether", *J. Chem. Phys.* **111**, 3616.
[35] Wallenborn, E.-U., Wild, U.P. and Brown, R. (1997) "Analysis of the optical spectra of aromatic-alkan clusters", *J. Chem. Phys.* **107**, 8338.
[36] Chichos, F., Brown, R. and Bopp, P.A. (2001) "Coupled molecular dynamics/semiempirical simulation of organic solutes in polar liquids: I. Naphthalene in acetonitrile", *J. Chem Phys.* **114**, 6824.
[37] Chichos, F., Brown, R. and Bopp, P.A. (2001) "Coupled molecular dynamics/semiempirical simulation of organic solutes in polar liquids: II. Coumarin 153 in methanol and acetonitrile", *J. Chem Phys.* **114**, 6834.
[38] Verma, T. and Sharma, S.M. (1999) "Investigation of high pressure phase transitions in α-GeO_2 through molecular dynamics calculations", *Proc. Solid State Phys. Symp.* **42**, 176, Also "Study of pressure induced phase transitions in α-GeO_2 using molecular dynamics simulations", Proceedings of the Fifth National Conference on High Pressure Science and Technology, 148.
[39] Oeffner, R.D. and Elliot, S.R. (1998) "Interatomic potential germanium oxide empirically fitted to an *ab initio* energy surface", *Phys. Rev. B* **58**, 14791.
[40] Karmakar, S., Garg, N. and Sharma, S.M. (1999) "Molecular dynamics simulations of α-cristobalite SiO_2 under shock an static conditions", *Proc. Solid State Phys. Symp.* **42**, 174.
[41] Bourova, E., Parker, S.C. and Richet, P. (2000) "Atomistic simulation of cristobalite at high temperature", *Phys. Rev. B* **62**, 12052.

[42] Garg, N. and Sharma, S.M. (2000) "A molecular dynamical investigation of high pressure phase transfromations in berlinite (α-$AlPO_4$)", *J. Phys. Condens. Matter* **12**, 357.
[43] van Beest, B.W.H., Kramer, G.J. and van Santen, R.A. (1990) "Force fields for silica and aluminophosphate based on *ab initio* calculations", *Phys. Rev. Lett.* **64**, 1955.
[44] Jackson, R.A. and Mort, K.A. (2000) "Computer modelling of complex molecular ionic materials", *Comput. Sci. Mater.* **17**, 230.
[45] Faux, D.A., Smith, W. and Forester, T.R. (1997) "Molecular dynamics studies of hydrated and dehydrated Na^+-zeolite-4A", *J. Phys. Chem.* **101**, 1762.
[46] Faux, D.A. (1998) "Molecular dynamics studies of sodium diffusion in hydrated Na_+-zeolite-4A", *J. Phys. Chem.* **102**, 10658.
[47] Faux, D.A. (1999) "Molecular dynamics studies of hydrated zeolite-4A", *J. Phys. Chem.* **103**, 7803.
[48] Islam, M.S., Cherry, M. and Catlow, C.R.A. (1996) "Oxygen diffusion in $LaMnO_3$ and $LaCoO_3$ perovskite-type oxides: a molecular dynamics study", *J. Solid State Chem.* **124**, 230.
[49] Khan, M.S., Islam, M.S. and Bates, D.R. (1998) "Cation doping and oxygen diffusion in zirconia: a combined atomistic simulation and molecular dynamics study", *J. Mater. Chem.* **8**, 2299.
[50] Gale, J.D. (1997) "GULP—a computer program for symmetry adapted simulation of solids", *J. Chem. Soc. Faraday Trans.* **93**, 629.
[51] Islam, M.S. (2000) "Ionic transport in ABO_3 perovskite oxides: a computer modelling tour", *J. Mater. Chem.* **10**, 1027.
[52] Sorescu, D.C., Rice, B.M. and Thompson, D.L. (2000) "Theoretical studies of solid nitromethane", *J. Phys. Chem. B* **104**, 8406.
[53] Forester, T.R., Smith, W. and Clarke, J.H.R. (1994) "A molecular dynamics study of valinomycin and the potassium–valinomycin complex", *J. Phys. Chem.* **98**, 9422.
[54] Bordat, P. and Brown, R. (1999) "A molecular model of *p*-terphenyl and its disorder-order transition", *Chem. Phys.* **246**, 323.
[55] Bordat, P. and Brown, R. (1997) "Correspondence between electronic origins and substitution sites in pentacene/*p*-terphenyl mixed crystals by molecular modelling", *Chem. Phys. Lett.* **291**, 153.
[56] Bordat, P. and Brown, R. (2000) "Elucidation of optical switching of single guest molecules in terrylene/*p*-terphenyl mixed crystals", *Chem. Phys. Lett.* **331**, 439.
[57] Abu-Sharkh, B.F. and Hamad, E.Z. (2000) "Simulation and model development for the equation of state of self-assembling nonadditive hard chains", *Macromolecules* **33**, 1345.
[58] Abu-Sharkh (2000) "Equation of state and phase separation in binary mixtures of non-additive chains", *Macromolecules* **33**, 9437.
[59] Abu-Sharkh (2001) "Glass transition temperature of poly(vinylchloride) from molecular dynamics simulation: explict atom model versus rigid CH_2 and CHCl group models", *Comput. Theoret. Polymer Sci.* **11**, 29.
[60] Karatasos, K. and Adolf, D.B. (2000) "Slow modes in local polymer dynamics", *J. Chem. Phys.* **112**, 8225.
[61] Karatasos, K., Adolf, D.B. and Hotson, S. (2000) "Effects of density on the local dynamics and conformational statistics of polyethylene: a molecular dynamics study", *J. Chem. Phys.* **112**, 8695.
[62] Ryckaert, J.-P. and Bellemans, A. (1975) "Molecular dynamics of liquid *n*-butane near its boiling point", *Chem. Phys. Lett.* **30**, 123.
[63] Steele, D. (1985), *J. Chem. Soc. Faraday Trans.* **81**(2), 1077.
[64] Smith, P., Lynden-Bell, R.M., Earnshaw, J.C. and Smith, W. (1999) "The surface ordered phase of liquid heptadecane", *Mol. Phys.* **98**, 255.
[65] Smith, P., Lynden-Bell, R.M. and Smith, W. (2000) "The behaviour of liquid alkanes near interfaces: a simulation study", *Mol. Phys.* **98**, 255.
[66] Trachenko, K.O., Dove, M.T., Harris, M.J. and Heine, V. (2000) "Dynamics of silica glass: two-level tunnelling states and low energy floppy modes", *J. Phys. Condens. Matter* **12**, 8041.
[67] Smith, W., Forester, T.R., Greaves, G.N., Hayter, S. and Gillan, M.J. (1997) "Molecular dynamics simulation of alkali-metal diffusion in alkali-metal disilicate glasses", *J. Mater. Chem.* **7**, 331.

[68] Vessal, B., Amini, M., Leslie, M. and Catlow, C.R.A. (1990) "Potentials for molecular dynamics simulation of silicate glasses", *Mol. Simul.* **5**, 1.
[69] Montorsi, M., Menziani, M.C., Leonelli, C., Pellacani, G.C. and Cormack, A.N. (2000) "Molecular dynamics simulations of alumina addition in sodium silicate glasses", *Mol. Simul.* **24**, 157.
[70] Montorsi, M., Menziani, M.C., Leonelli, C. and Cormack, A.N. (1999) "The sodium-alumino silicate glasses: a molecular dynamics study", *Mol. Engng* **8**, 427.
[71] Leonelli, C., Lusvardi, G., Montorsi, M., Menziani, M.C., Menabue, L., Mustarelli, P. and Linati, L. (2001) "Influence of small additions of Al_2O_3 on the properties of $Na_2O-3SiO_2$ glass", *J. Phys. Chem.* **105**, 919.
[72] Gou, F., Greaves, G.N., Smith, W. and Winter, R. (2001) "Molecular dynamics simulation of sodium borosilicate glasses", *J. Noncryst. Solids* **293–295**, 539.
[73] Monteil, A., Bernard, C., Chaussedent, S., Ferrari, M., Balu, N. and Obriot, J. (2000) "Pressure effect on the structure and luminescence of rare-earth ions doped glasses: an investigation by molecular dynamics simulation", *J. Lumin.* **87–89**, 691.
[74] Chaussedent, S., Bernard, C., Monteil, A., Balu, N., Obriot, J., Ronchin, S., Tosello, C. and Ferrari, M. (2000) "Structural properties of erbium-activated silica–titania glasses: modeling by molecular dynamics method", *Rare-Earth-Doped Mater. Devices IV, Proc. SPIE* **3942**, 243.
[75] Feusten, B.P. and Garofalini, S.I.I. (1998) "Empirical three-body potential for vitreous silica", *J. Chem. Phys.* **89**, 5818.
[76] Bernard, C., Chaussedent, S., Monteil, A., Balu, N., Obriot, J., Duvererger, C., Ferrari, M., Bouazaoui, M., Kinowski, C. and Turrell, S. (2001) "Application of molecular dynamics techniques and luminescent probes to the study of glass structure:the SiO_2-GeO_2 case", *J. Non-Cryst. Solids* **284**, 68.
[77] Forester, T.R., Smith, W. and Clarke, J.H.R. (1997) "Antibiotic activity of valinomycin: molecular dynamics simulations involving the water/membrane interface", *J. Chem. Soc. Faraday Trans.* **93**, 613.
[78] Smondyrev, A.M. and Berkowitz, M.L. (1998) "United atom force fields for phospholipid membranes: constant pressure molecular dynamics simulation of dipalmitoylphosphatidylcholine/water system", *J. Comput. Chem.* **20**, 531.
[79] Smondyrev, A.M. and Berkowitz, M.L. (1999) "Molecular dynamics study of S_{n-1} and S_{n-2} chain conformations in dipalmitoylphosphatidylcholine membranes", *J. Chem. Phys.* **110**, 3981.
[80] Smondyrev, A.M. and Berkowitz, M.L. (1999) "Molecular dynamics simulation of DPPC bilayer in DMSO", *Biophys. J.* **76**, 2472.
[81] Smondyrev, A.M. and Berkowitz, M.L. (1999) "Structure of dipalmitoylphosphatidylcholine/cholesterol bilayer at low and high cholesterol concentrations: a molecular dynamics study", *Biophys. J.* **77**, 2075.
[82] Dominguez, H., Smondyrev, A.M. and Berkowitz, M.L. (1999) "Computer simulations of phosphatidylcholine monolayers at air/water and CCl4/water interfaces", *J. Phys. Chem.* **103**, 9582.
[83] Smondyrev, A.M. and Berkowitz, M.L. (2000) "Molecular dynamics simulation of dipalmitoylphosphatidylcholine membrane with cholesterol sulfate", *Biophys. J.* **78**, 1672.
[84] Smondyrev, A.M. and Berkowitz, M.L. (1999) "Molecular dynamics simulation of fluorination effects on a phospholipid bilayer", *J. Chem. Phys.* **111**, 9864.
[85] Smondyrev, A.M. and Berkowitz, M.L. (2000) "Determining why nature needs cholesterol", *Envision* **16**, 12.
[86] Schlenkrich, M., Brickmann, J., MacKerell, A.D. and Karplus, M. (1996) Biological Membranes (Birkhäuser, Berlin).
[87] Chiu, S., Clark, M., Balaji, V., Subramaniam, S., Scott, H. and Jacobsson, E. (1995) "Incorporation of surface tension into molecular dynamics simulation of an interface: a fluid phase lipid bilayer membrane", *Biophys. J.* **69**, 1230.
[88] Chau, P.L. (2001) "Process and thermodynamics of ligand-receptor interaction studied using a novel simulation method", *Chem. Phys. Lett.* **334**, 343.
[89] Melchionna, S., Falconi, M. and Desideri, A. (1998) "Effect of temperature and hydration on protein fluctuations: molecular dynamics simulation of Cu, Zn superoxide dismutase at six different temperatures. Comparison with neutron scattering data", *J. Chem. Phys.* **108**, 6033.

[90] Melchionna, S., Luise, A., Venturoli, M. and Cozzini, S. (1998). "DLPROTEIN: a molecular dynamics package to simulate biomolecules", Science and supercomputing at CINECA—1997 Report. Supercomputing Group, CINECA. Ed. Voli, M. 496.
[91] van Gunsteren, W.F. and Berendsen, H.J.C. (1987) The GROMOS Manual (University of Groningen, The Netherlands).
[92] Falconi, M., Melchionna, S. and Desideri, A. (1999) "Molecular dynamics simulations of Cu, Zn superoxide dismutase: effect of temperature on dimer asymmetry", *Biophys. J.* **81**, 197.
[93] Luise, M., Falconi, M. and Desideri, A. (2000) "Molecular dynamics simulation of solvated Azurin: correlation between surface solvent accessibility and water residence times", *Proteins Struct. Funct. Genet.* **39**, 56.
[94] Born, M. and Huang, K. (1954) Dynamical Theory of Crystal Lattices (Oxford University Press, Oxford).
[95] de Leeuw, N.H. and Parker, S.C. (1998) "Molecular-dynamics simulation of MgO surfaces in liquid water using a shell-model potential for water", *Phys. Rev. B* **58**, 13901.
[96] Mitchell, P.J. and Fincham, D. (1993) "Shell model simulations by adiabatic dynamics", *J. Phys. Condens. Matter* **5**, 1031.
[97] Dick, B.G. and Overhauser, A.W. (1958) "Theory of dielectric constants of alkali halide crystals", *Phys. Rev. B* **112**, 90.
[98] de Leeuw, N.H., Parker, S.C. and Harding, J.H. (1999) "Molecular dynamics simulation of crystal dissolution from calcite steps", *Phys. Rev. B* **60**, 13792.
[99] Warne, M.R., Allan, N.L. and Cosgrove, T. (2000) "Computer simulation of water molecules at kaolinite and silica surfaces", *Phys. Chem. Chem. Phys.* **2**, 3663.
[100] Sayle, D.C. and Watson, W. (2000) "Simulated amorphisation and recrystallisation: nanocrystallites within meso-scale supported oxides", *J. Mater. Chem.* **10**, 2241.
[101] Sayle, D.C. and Watson, G.W. (2000) "Dislocations, lattice slip, defects and rotated domains: the effect of a lattice misfit on supported thin-film metal oxides", *Phys. Chem. Chem. Phys.* **2**, 5491.
[102] Sayle, D.C. and Watson, G.W. (2001) "The Atomistic Structures of MgO/$SrTiO_3$ (001) and BaO/$SrTiO_3$ (001) using simulated amorphization and recrystallization", *J. Phys. Chem. B* **105**, 5506.
[103] San-Miguel, M.A. and Rodger, P.M. (2000) "The effect of corrosion inhibitor films on deposition of wax to metal oxide surfaces", *J. Mol. Struct. (Theochem)* **506**, 263.
[104] Duffy, D.M. and Rodger, P.M. (2000) "Modelling the interaction between the poly(octadecyl acrylate) inhibitor and an *n*-octacosane crystal", *Phys. Chem. Chem. Phys.* **2**, 4804.
[105] Tepper, H.L. and Briels, W.J. (2001) "Simulations of crystallization and melting of the fcc (100) interface: the crucial role of lattice imperfections", *J. Cryst. Growth* **230**, 270.
[106] Clarke, J.H.R., Smith, W. and Woodcock, L.V. (1986) "Short range effective potentials for ionic fluids", *J. Chem. Phys.* **84**, 2290.
[107] Kholmurodov, K., Puzynin, I., Smith, W., Yasuoka, K. and Ebisuzaki, T. (2001) "MD simulation of cluster-surface impacts for metallic phases: soft landing, droplet spreading and implantation", *Comput. Phys. Commun.* **141**, 1.
[108] Sutton, A.P. and Chen, J. (1990) "Long-range Finnis–Sinclair potentials", *Phil. Mag. Lett.* **61**, 139.
[109] Somasundaram, T., Lynden-Bell, R.M. and Patterson, C.H. (1999) "The passage of gases through the liquid water/vapour interface: a simulation study", *Phys. Chem. Chem. Phys.* **1**, 143.
[110] in het Panhuis, M., Patterson, C.H. and Lynden-Bell, R.M. (1998) "A molecular dynamics study of carbon dioxide in water: diffusion, structure and thermodynamics", *Mol. Phys.* **94**, 963.
[111] Somasundaram, T., in het Panhuis, M., Lynden-Bell, R.M. and Patterson, C.H. (1999) "A simulation study of the kinetics of passage of CO_2 and N_2 through the liquid/vapor interface of water", *J. Chem. Phys.* **111**, 2190.
[112] Somasundaram, T. and Lynden-Bell, R.M. (1999) "The velocity distribution of desorbing molecules: a simulation study", *Mol. Phys.* **97**, 1029.
[113] Fernandes, P.A., Cordeiro, M.N.D.S. and Gomes, J.A.N.F. (1999) "Molecular dynamics simulation of the water/1,2-dichloroethane interface", *J. Mol. Struct. (Theochem)* **463**, 151.
[114] Fernandes, P.A., Cordeiro, M.N.D.S. and Gomes, J.A.N.F. (1999) "Molecular dynamics simulation of liquid 2-heptanone, pure and saturated with water", *J. Phys. Chem. B* **103**, 1176.

[115] Fernandes, P.A., Cordeiro, M.N.D.S. and Gomes, J.A.N.F. (1999) "Molecular dynamics simulation of the water/2-heptanone liquid–liquid interface", *J. Phys. Chem. B* **103**, 6290.
[116] Fernandes, P.A., Cordeiro, M.N.D.S. and Gomes, J.A.N.F. (1999) "Molecular dynamics study of the transfer of iodide across two liquid/liquid interface", *J. Phys. Chem. B* **103**, 8930.
[117] Fernandes, P.A., Cordeiro, M.N.D.S. and Gomes, J.A.N.F. (2000) "Influence of ion size and charge in ion transfer processes across a liquid–liquid interface", *J. Phys. Chem. B* **104**, 2278.
[118] Catlow, C.R., Ackermann, L., Bell, R.G., Cora, F., Gay, D.H., Nygren, M.A., Pereira, J.C., Sastre, G., Slater, B. and Sinclair, P.E. (1997) "Computer modelling as a technique in solid state chemistry", *Faraday Discuss.* **106**, 1.
[119] Sastre, G., Corma, A. and Catlow, C.R.A. (1999) "Diffusion of para- and ortho-xylene mixture in CIT-1 zeolite: a molecular dynamics study", *Top. Catalysis* **9**, 215.
[120] Sastre, G., Corma, A. and Catlow, C.R.A. (1998) "Molecular diffusion processes in crystalline microporous materials", *Mat. Res. Soc. Symp. Proc.* **527**, 481.
[121] Sastre, G., Raj, N., Catlow, C.R.A., Roque-Malherbe, R. and Corma, A. (1998) "Selective diffusion of C8 aromatics in a 10 and 12 MR zeolite. A molecular dynamics study", *J. Phys. Chem. B* **102**, 3198.
[122] Forester, T. and Smith, W. (1997) "Bluemoon simulations of benzene in silicalite-1", *J. Chem. Soc. Faraday Trans.* **93**, 3249.
[123] Carter, E.A., Ciccotti, G., Hynes, J.T. and Kapral, R. (1989) "Constrained reaction coordinate dynamics for the simulation of rare events", *Chem. Phys. Lett.* **156**, 472.
[124] Sastre, G., Catlow, C.R.A. and Corma, A. (1999) "Diffusion of benzene and propylene in MCM-22 zeolite. A molecular dynamics study", *J. Phys. Chem. B* **103**, 5187.
[125] Corma, A., Catlow, C.R.A. and Sastre, G. (1998) "Diffusion of linear and branched C7 paraffins in ITQ-1 zeolite. A molecular dynamics study", *J. Phys. Chem. D* **102**, 7085.
[126] Raj, N., Sastre, G. and Catlow, C.R.A. (1999) "Diffusion of octane in silicalite: a molecular dynamics study", *J. Phys. Chem. B* **103**, 1007.
[127] Sastre, G., Catlow, G.R.A., Chica, A. and Corma, A. (1999) "Molecular dynamics of C7 hydrocarbon in ITQ-2. The benefit of zeolite structures containing accessible pockets", *J. Phys. Chem. B* **104**, 416.
[128] Sastre, G., Chica, A. and Corma, A. (2000) "On the mechanism of alkane isomerisation (isodewaxing) with unidirectional 10-member ring zeolites. A molecular dynamics and catalytic study", *J. Catalysis* **195**, 227.
[129] Cook, M.J. and Wilson, M.R. (1998) "Molecular dynamics simulations of liquid crystal phases using atomistic potentials", *Mol. Phys.* **93**, 955.
[130] Cook, M.J. and Wilson, M.R. (2000) "Simulation studies of dipole correlation in the isotropic liquid phase", *Liq. Cryst.* **27**, 1573.
[131] Cook, M.J. and Wilson, M.R. (2001) "Development of an all-atom force field for the simulation of liquid crystal molecules in condensed phases (LCFF)", *Mol. Cryst. Liq. Cryst.* **357**, 149.
[132] Cook, M.J. and Wilson, M.R. (2001) "A molecular dynamics simulation study of dipole correlation in the isotropic phase of the mesogens me5NF and GGP5Cl", *Mol. Cryst. Liq. Cryst.* **357**, 127.
[133] Cook, M.J. and Wilson, M.R. (2001) "The first thousand-molecule simulation of a mesogen at the fully atomistic level", *Mol. Cryst., Liq. Cryst.* **363**, 181.
[134] Ramirez-Cuesta, A.J., Mitchell, P.C.H. and Rodger, P.M. (1998) "Template-framework interaction's in chiral AlPOs", *J. Chem. Soc. Faraday Trans.* **94**, 2249.
[135] Ramirez-Cuesta, A.J., Mitchell, P.C.H., Wilkinson, A.P., Parker, S.F. and Rodger, P.M. (1998) "Dynamics of water molecules in a templated aluminophosphate: molecular dynamics simulation of inelastic neutron scattering spectra", *Chem. Commun.* **1998**, 2653.
[136] Ramirez-Cuesta, A.J., Mitchell, P.C.H., Parker, S. and Rodger, P.M. (1999) "Dynamics of water and template molecules in the interlayer space of a layered aluminophosphate. Experimental inelastic neutron scattering spectra and molecular dynamics simulated spectra", *Phys. Chem. Chem. Phys.* **1**, 5711.
[137] Rodger, P.M., Forester, T.R. and Smith, W. (1996) "Simulations of the methane hydrate/methane gas interface near hydrate forming conditions", *Fluid Phase Eq.* **116**, 326.
[138] Rodger, P.M. (2000) "Methane hydrate: melting and memory", *Ann. NY Acad. Sci.* **912**, 474.
[139] Phillips, S.C. and Essex, J.W. (2000) "Digitally filtered molecular dynamics: the frequency specific control of molecular dynamics simulations", *J. Chem. Phys.* **112**, 2586.

[140] Elliott, J.A. and Windle, A.H. (2000) "A dissipative particle dynamics method for modeling the geometrical packing of filler particles in polymer composites", *J. Chem. Phys.* **113**, 10367.
[141] Groot, R.D., Madden, T.J. and Tildesley, D.J. (1999) "On the role of hydrodynamic interactions in block copolymer microphase separation", *J. Chem. Phys.* **110**, 9739.
[142] Simdyankin, S.I., Taraskin, S.N., Dzugutov, M. and Elliot, S.R. (2000) "Vibrational properties of the one-component α-phase", *Phys. Rev. B* **62**, 3223.
[143] Yong, C.W., Smith, W. and Kendall, K. (2001) "Investigation of contact interaction of (001) MgO: molecular dynamics simulation studies", *J. Mater. Chem.*, accepted.
[144] Stuart, S.J., Zhou, R. and Berne, B.J. (1996) "Molecular dynamics with multiple timescales: the selection of efficient reference system propagators", *J. Chem. Phys.* **105**, 1426.
[145] Procacci, P. and Marchi, M. (1996) "Taming the Ewald sum in molecular dynamics simulations of solvated proteins via multiple timestep algorithm", *J. Chem. Phys.* **104**, 3003.
[146] Kholmurodov, K., Smith, W., Yasuoka, K. and Ebisuzaki, T. (2000) "A highly vectorised link-cell FORTRAN code for the DL_POLY molecular dynamics simulation package", *Comput. Phys. Commun.* **125**, 167.
[147] Narumi, T. (1997) "Special purpose computer for molecular dynamics simulations" PhD Thesis (University of Tokyo, Japan).
[148] Sherwood, P. and de Vries, A.H. (1999) "ChemShell, a shell for computational chemistry". CCLRC Daresbury Laboratory. See http://www.cse.clrc.ac.uk/Activity/ChemShell.